Analysis of sphingosine-1-phosphate receptor 1/5 modulator therapy in mechanistic mouse models by visual system readouts

Inaugural-Dissertation

zur Erlangung des Doktorgrades
der Mathematisch-Naturwissenschaftlichen Fakultät
der Heinrich-Heine-Universität Düsseldorf

vorgelegt von

Christina Hecker
aus Duisburg

Düsseldorf, Januar 2022

Aus der Klinik für Neurologie des
Universitätsklinikums Düsseldorf
und dem Institut für Neurobiologie
der Heinrich-Heine-Universität Düsseldorf

Gedruckt mit der Genehmigung der
Mathematisch-Naturwissenschaftlichen Fakultät der
Heinrich-Heine-Universität Düsseldorf

Berichterstatter:

1. Prof. Dr. Philipp Albrecht

2. Prof. Dr. Charlotte von Gall

Tag der mündlichen Prüfung: 28.04.2022

Abstract

In several neurological diseases, such as multiple sclerosis (MS), neuronal degeneration is the critical mechanism for permanent disability of the patients. In the early disease state, the pathology of MS is mostly driven by autoimmune inflammation. In about 70% of MS patients opticus neuritis (ON), an inflammatory optic neuropathy associated with demyelination and retinal ganglion cell loss, is diagnosed during the disease course. Despite decades of research, mainly immunomodulatory therapies have been developed, reducing inflammatory relapses, but effective strategies to prevent chronic neuronal degeneration are still missing. MS and ON can be investigated in the animal model of experimental autoimmune encephalomyelitis (EAE) which mimics the key pathological features of MS. To analyze neuronal degeneration in the central nervous system the anterior visual pathway, namely the retina and optic nerve, can be used. A great advantage of the retina is that it is accessible non-invasively, which allows time-saving strategies to perform structural (optic coherence tomography (OCT)) and functional (optomotor response (OMR)) measurements.

In this thesis, we first determined which OMR setting is best suited for the analysis of EAE mice. We therefore compared contrast sensitivity and spatial frequency measurements of MOG_{35-55} immunized mice, regarding the test-retest reliability and the correlation with other readouts such as clinical EAE Scores, OCT measurements, and infiltration of immune cells. Our results showed that for analysis of C57BL/6J mice undergoing EAE, spatial frequency is the superior readout.

In the second work of this thesis siponimod, a Sphingosine-1-phosphate receptor 1 and 5 modulator, was analyzed in different mechanistic models.
Its immunomodulatory capacities are well-known, however, the aim was to investigate if siponimod has additional neuroprotective capacities. To analyze remyelinating properties our collaborators from Basel and Paris used the cuprizone demyelination model and a conditional demyelination in *Xenopus laevis*. Additionally, we examined the effect of siponimod in EAE mice regarding disease course and retinal neurodegeneration over 3 months. Our results revealed increased remyelination in corpus callosum of cuprizone-treated mice, a pro-remyelinating potential in the Xenopus model, and strong prophylactic and therapeutic effects in MOG_{35-55} EAE mice.

Zusammenfassung

Bei einigen neurologischen Erkrankungen, darunter die Multiple Sklerose (MS), ist die neuronale Degeneration der entscheidende Faktor für die chronische Verschlechterung des Zustands der Patienten. Die Pathologie der MS wird größtenteils durch autoimmune Entzündungsreaktionen vorangetrieben. Bei etwa 70% der MS Patienten wird während des Krankheitsverlaufs eine Optikusneuritis (ON), eine entzündliche Optikusneuropathie, die mit Demyelinisierung und Degeneration der retinalen Ganglienzellen einhergeht, diagnostiziert. Trotz jahrzehntelanger Forschung gibt es bisher hauptsächlich immunmodulatorische Therapien, die entzündliche Schübe verhindern, es fehlen allerdings noch immer wirksame Strategien zur Behandlung der chronischen neuronalen Degeneration. MS und ON können im Tiermodell der experimentellen autoimmunen Enzephalomyelitis (EAE), welches die wichtigsten pathologischen Merkmale der MS darstellt, untersucht werden. Zur Analyse der neuronalen Degeneration im zentralen Nervensystem kann die anteriore Sehbahn, genauer gesagt die Retina und der Sehnerv, verwendet werden. Ein großer Vorteil der Retina ist, dass sie von außen zugänglich ist und zeitlich unaufwändige und nicht-invasive Möglichkeiten zur Durchführung struktureller (optische Kohärenztomographie (OCT)) und funktioneller (optomotorische Reaktion (OMR)) Messungen bietet.

In dieser Arbeit haben wir zunächst ermittelt, welcher OMR-Messwert besser für die Analyse von EAE-Mäusen geeignet ist. Dazu wurden die Messungen der Kontrastempfindlichkeit und die Ortsfrequenzmessungen von EAE-Mäusen hinsichtlich ihrer Test-Retest-Zuverlässigkeit und der Korrelation mit anderen Messwerten wie klinischen EAE-Scores, OCT-Messungen und der Infiltration von Immunzellen untersucht. Unsere Ergebnisse zeigten, dass für die Analyse von C57BL/6J-Mäusen in EAE-Versuchen die Ortsfrequenz als Messgröße besser geeignet ist.

Im zweiten Teil dieser Dissertation wurde Siponimod, ein Modulator des Sphingosin-1-Phosphat-Rezeptors 1 und 5, in verschiedenen mechanistischen Modellen analysiert. Es ist bekannt, dass Siponimod immunmodulatorische Fähigkeiten besitzt, das Ziel war es daher zu untersuchen, ob Siponimod zusätzliche neuroprotektive Eigenschaften hat. Um die potentielle Remyelinisierung durch Siponimod zu analysieren, wurde von unseren Kooperationspartnern in Basel und Paris das Cuprizone-Mausmodell und ein induzierbares Demyelinisierungsmodell in *Xenopus Laevis* verwendet. Zusätzlich haben wir die Wirkung von Siponimod in EAE-Mäusen hinsichtlich des Krankheitsverlaufs und der retinalen

Neurodegeneration untersucht. Unsere Ergebnisse zeigen eine erhöhte Remyelinisierung im Corpus Callosum von Cuprizon behandelten Mäusen, ein pro-myelinisierendes Potential im Xenopus-Modell und starke prophylaktische und therapeutische Effekte in EAE-Mäusen.

Contents

1 Introduction

1.1 Neurodegenerative diseases

Chronic neuronal degeneration is a critical mechanism in the progression of patients suffering from several neurological diseases such as Parkinson´s disease, Alzheimer´s disease and multiple sclerosis (MS). In contrast to Alzheimer's and Parkinson´s disease, which belong to the classical neurodegenerative diseases, the pathology in MS is primary driven by autoimmune inflammation and demyelination, followed by neuronal loss (Beitz, 2014; Soria Lopez et al., 2019; Thompson et al., 2018). Despite decades of research effective strategies to prevent chronic neuronal/axonal degeneration are still an unmet need. Difficulties are here manly I) the complexity of the pathophysiology of neurodegenerative diseases, II) the limited *in vivo* access to the brain, due to the blood-brain barrier (BBB) that prevents the delivery of therapeutic agents to the central nervous system (CNS), and III) the laborious evaluation of clinical outcomes after treatment (Piguet et al., 2017).

1.1.1 Multiple Sclerosis and treatment strategies

MS is an inflammatory autoimmune disorder involving demyelination, loss of oligodendrocytes with subsequent axonal damage and eventually degeneration of neurons in the CNS, which leads to the persisting clinical disability of MS patients. The characteristic pathological hallmarks are the perivenular inflammatory lesions, leading to oligodendrocyte damage and demyelination. Although axons are relatively preserved in the early stages of disease, upon further progression of the disease an irreversible axonal damage occurs (Dobson and Giovannoni, 2019). The reason for the initial immune response against CNS antigens is not understood yet. However, in the last years, a better understanding of the different parameters, like genetics as well as environmental and lifestyle factors, that contribute to the development of the disease was gained (Olsson et al., 2017). Depending on the phase and severity of disease progression MS is distinguished in four main types. These are: clinically isolated syndrome, relapse-remitting MS, secondary progressive MS (SPMS), and primary progressive MS (PPMS) (Lublin, 2014). Although therapeutic strategies for MS have been improved, they are still insufficient to prevent chronic neurodegeneration. Treatments for MS mainly target inflammation and aim to reduce relapses. New therapeutics, such as Bruton tyrosine kinase (BTK) inhibitors, that block B-cell activation and cytokine release, show promising results in patients with relapsing MS (Montalban et al., 2019) and even promotion of myelin repair in models of demyelination

and remyelination (Martin et al., 2020). However, the currently developed drugs rather show efficiency in treatment of relapse-remitting MS, but have little or no efficiency in patients with progressive forms of MS (Wingerchuk and Carter, 2014). But there are therapeutics that were approved for treatment of PPMS and SPMS in recent years. Some of those, namely ocrelizumab and ofatumumab, are monoclonal antibodies that target B-cells and showed efficiency in treatment of progressive forms of MS (Graf et al., 2021; Hauser et al., 2020; Montalban et al., 2017).

For SPMS a new disease-modifying therapy was approved (Al-Salama, 2019), namely siponimod, a selective sphingosine 1-phosphate receptor 1 and 5 modulator, that significantly reduced disability progression, cognitive decline and total brain volume loss in patients suffering from SPMS (Kappos et al., 2018).

1.1.2 Optic Neuritis

Optic neuritis (ON) is an inflammatory optic neuropathy associated with demyelination and retinal ganglion cell (RGC) degeneration. It characteristically manifests as an acute, unilateral and painful vision loss (Bennett, 2019; London et al., 2013). ON is frequently linked with MS as it is the initial manifestation in approximately 25% of MS patients. During MS disease course ON is diagnosed in about 70% of patients, predominantly in the early, relapse-remitting phase (Toosy et al., 2014). Additionally, ON occurs in the context of several other inflammatory disorders of the central nervous system including neuromyelitis optica spectrum disorders and chronic relapsing inflammatory optic neuropathy (Bennett, 2019). The pathology of ON reflects the processes of acute inflammation, demyelination and consecutive neuronal degeneration, reflecting most characteristics of MS pathology, which also occur in other parts of the CNS (Dietrich et al., 2019a). Therefore, ON is a suitable model to examine new neuroprotective therapies in neurodegeneration (Aktas et al., 2016).

1.2 The anterior visual pathway

Axonal and neuronal degeneration affects not only the brain and spinal cord, but also the anterior visual pathway. The anterior visual pathway consists of the retina, optic nerves, chiasm and optic tract (Galetta et al., 2011). Since the retina is still part of the CNS, but is accessible none-invasively, it is often referred to as ‘window to the brain’. The retina contains, amongst others, RGCs, the neurons of the optic nerve, and has a unique structure, since it contains axons and glia cells in the absence of myelin (Frohman et al., 2008). The axons of the RGCs form the optic nerve and are wrapped with myelin, which is expressed by oligodendrocytes. Damage to CNS axons such as to the optic nerve, results in retrograde

and anterograde degeneration of the damaged tissue (London et al., 2013). Furthermore, scar formation, myelin destruction, and the creation of a neurotoxic environment that involves oxidative stress, deprivation of neurotrophic factors, excitotoxic levels of neurotransmitters, and abnormal aggregation of proteins and debris occurs. Such a hostile milieu often results in the death of neighboring neurons that were spared initially - a phenomenon called secondary degeneration (London et al., 2013; Schwartz et al., 1996). It was also shown that retinal degeneration of MS patients mirrors the overall disability evaluated by the Expanded Disability Status Scale as well as the loss of visual function (Albrecht et al., 2012, 2007; Fisher et al., 2006). Thus, examination of the visual pathway can provide insight to the mechanisms occurring during neuroinflammatory and neurodegenerative diseases, making it a valuable tool to analyze new therapeutic approaches.

1.2.1 Optical coherence tomography

To study structural changes of the retina during disease course and therapeutical treatment optical coherence tomography (OCT) can be utilized. OCT is a fast, non-invasive, interferometric technique that allows cross sectional imaging of retinal structures (Huang et al., 1991). New, 3rd generation OCT devices can provide high resolution anatomic reconstructions of the retinal morphology in a fast and reproducible manner. Thereby they allow an objective analysis of the retinal nerve fiber layer and deeper retinal layers of human patients (Frohman et al., 2008). With some minor modifications those OCT devices are also able to obtain and quantify high resolution morphological sections of mouse and rat retinae (Dietrich et al., 2019b, 2017; Fischer et al., 2009). One big advantage of OCT imaging in comparison to histological analysis is the possibility to perform longitudinal investigations, enabling detection of dynamic changes, avoiding inter-subject variability and thereby largely reducing the amount of animals needed per study (Dietrich et al., 2018). Additionally, fixation artifacts such as changes in layer thickness depending on the fixation protocol do not occur with *in vivo* OCT imaging.

1.2.2 Optomotor response

In mice and rats the visual function can be investigated by measuring the optomotor response (OMR). OMR typically refers to involuntary compensatory head and/or body movements in direction of a stimulus that can be followed by a quick reset phase and are used for image stabilization during self-motion (Kretschmer et al., 2017). To analyze OMR, the animals are placed on a platform where they can move freely. The platform is surrounded

by a square of monitors that display a moving grid of black bars circulating in a virtual cylinder around the mice in varying directions. The mice involuntarily track the moving grate with reflexive head and neck movements. As animals track only in temporal-nasal direction, separate assessments can be performed for each eye by alternating the direction of rotation of the cylinder (Douglas et al., 2005). The head movements are detected by the experimenter or automatically. Additionally, the head of the mouse is tracked, so that the virtual cylinder can be readjusted and a constant distance between the animal's head and the virtual cylinder is guaranteed, even if the mouse moves its head away from the center of the arena. The distance between the black bars in cycles per degree or the contrast can be reduced until the mice cannot track the movements anymore and the threshold is reached (Prusky et al., 2004). The optomotor response is reduced or eliminated in case of reduced visual acuity, therefore the functional effect of the neurodegeneration measured by OCT can also be monitored *in vivo* (Dietrich et al., 2019b).

1.3 Mouse model of experimental autoimmune encephalomyelitis- Optic neuritis

There are several experimental approaches available that replicate major features of MS and are therefore used to explore pathomechanisms and analyze therapeutic strategies. The most common used models for human MS are experimental autoimmune encephalomyelitis (EAE) models. EAE can be induced in a multitude of species and strains and by several myelin antigens, such as myelin basic protein, proteolipid protein, and myelin oligodendrocyte glycoprotein (MOG) (Dietrich et al., 2019a). The models mimic the key pathological features of MS: inflammation, demyelination, axonal loss and gliosis (Constantinescu et al., 2011). In this study the MOG peptide, fragment 35-55 (MOG_{35-55}) EAE, was used, which results in high rates of ON when induced in C57Bl/6J mice (Shao et al., 2004). Former studies in our group confirmed this hypothesis and showed that MOG_{35-55} EAE is well suited for analysis of retinal neurodegeneration in context of ON (Cruz-Herranz et al., 2019). To induce EAE, we immunized 6-week-old, female C57Bl/6J mice with MOG_{35-55} peptide emulsified in complete Freund´s Adjuvant (CFA) with heat-killed *Mycobacterium tuberculosis* H37Ra. Additionally, injections with pertussis toxin were performed on the same day and on day 2 after immunization. CFA is a strong adjuvant that provides a slow release of the MOG-antigen from the inoculum and uses inactivated *mycobacterium tuberculosis* as strong booster of the immune response (Lassmann and Bradl, 2017). *Mycobacterium tuberculosis* and pertussis toxin are also important for EAE

induction as they increase the permeability of the BBB (Bjelobaba et al., 2018; Constantinescu and Hilliard, 2005).

1.4 Sphingosine-1-phosphate receptor modulators

As mentioned earlier, first therapies showing efficiency in treatment of SPMS are sphingosine-1-phosphate receptor modulators. Sphingosine-1-phosphate (S1P) is an signaling lipid produced by the phosphorylation of sphingosine by sphingosine kinase 1 or 2. S1P is recognized by S1P receptors (S1PR), which are coupled to G proteins that affect several cellular pathways (Bryan and Del Poeta, 2018). Vertebrates possess five S1P receptors (S1PR1-5) that respond to extracellular S1P and thereby contribute to the regulation of embryonic development, physiological homeostasis and pathogenic processes in multiple organ systems (Proia and Hla, 2015). S1PRs are widely expressed within the CNS and show a cell-specific distribution pattern. The endothelial cells of the BBB, for instance, express S1PR1, S1PR3, and S1PR5 which contribute to maintain BBB integrity and prevent vascular permeability (Roggeri et al., 2020). Dysregulated S1P signaling is known to disrupt the BBB, an early event that contributes to many CNS diseases including MS, Alzheimer´s disease and ischemic stroke (Cartier and Hla, 2019). Additionally, persistent macrophage and microglia activation is observed in the CNS of MS patients and is considered a significant contributor of secondary progressive MS (Prineas et al., 2001). S1PR1 is ubiquitously expressed in innate immunity and has been found to mediate functions in most innate immune cells (Bryan and Del Poeta, 2018). Furthermore, astrocytes and microglia express mainly S1PR1 and S1PR3, which seem to be upregulated during the reactive state of the cells and in neuroinflammation (Roggeri et al., 2020). While S1PR5 in the CNS parenchyma is exclusively expressed by oligodendrocytes, it also seems to be crucial for natural killer cells to egress from the lymph nodes and bone marrow (Roggeri et al., 2020). Moreover, recent studies showed the role of S1P gradients and S1PR signaling in the migration and retention of adaptive immune cells in resident tissues, thereby influencing the specificity and magnitude of immune responses (Cartier and Hla, 2019). Considering all above, compounds that target S1P and S1PR are of interest for treatment of autoimmune diseases, like MS. These modulators are designed to be structurally similar to endogenous S1P and are S1PRs agonists. They are considered to be functional antagonists, since they bind to S1PRs which causes receptors internalization, ubiquitylation and subsequently degradation (Martínez-Morales et al., 2018; O'Sullivan et al., 2016). As the S1P/S1PR1 axis is known to be crucial for lymphocytes migration from the secondary

lymphoid nodes, S1PR1 internalization leads to a general lymphopenia, that, in turn, reduces the T-cell infiltration in the CNS, the main reason for the immunomodulatory effect of the modulators (Chiba, 2005). The first of such therapeutics was FTY720 (fingolimod), a S1PR1, S1PR3, S1PR4 and S1PR5 modulator, that was approved in 2010 as a first line therapy in relapse-remitting MS (Brinkmann et al., 2010). One side effect of fingolimod is however, a transient and dose-dependent decrease in heart rate and atrioventricular block mainly attributed to the activation of the S1PR3 receptor subtype (Roggeri et al., 2020). To avoid this side effect a new generation of S1PR modulators have been developed that are more selective towards S1PR1 and S1PR5. One of those is BAF312 (siponimod) which was approved for treatment of clinically isolated syndrome, relapsing-remitting MS, and active SPMS (Al-Salama, 2019).

2 Aims of the thesis

Neuroprotective strategies to prevent or delay neurodegeneration are urgently needed. New substances and approaches can be investigated in animal studies via analysis of the anterior visual system. In EAE, a mouse model of MS, structure and function of the anterior visual pathway can be studied by OCT, OMR, and histological analyses. We already evaluated the best suited OCT parameters (Cruz-Herranz et al., 2019) but not the appropriate OMR setup. Therefore, the first aim of this thesis was to analyze which OMR parameter is best suited for the study of EAE mice. The second aim of this thesis was then the study of siponimod, a selective S1P1/5 modulator, on remyelination and microglial activation in several mechanistic models.

3 Publications as first/shared first author

3.1 Comparison of different optomotor response readouts for visual testing in experimental autoimmune encephalomyelitis- opticus neuritis

Christina Hecker, Michael Dietrich, Andrea Issberner, Hans-Peter Hartung, Philipp Albrecht

Department of Neurology, Medical Faculty, Heinrich-Heine University Düsseldorf, Moorenstr. 5, 40225 Düsseldorf, Germany

The present manuscript was published in Journal of Neuroinflammation, 2020

Contribution:

- First authorship
- Design of the study and experiments (30 %)
- Execution, analysis and statistics of the experiments (85 %)
- Writing and drafting of the manuscript (90 %)

Hecker et al. Journal of Neuroinflammation (2020) 17:216
https://doi.org/10.1186/s12974-020-01889-z

Journal of Neuroinflammation

SHORT REPORT Open Access

Comparison of different optomotor response readouts for visual testing in experimental autoimmune encephalomyelitis-optic neuritis

Christina Hecker, Michael Dietrich, Andrea Issberner, Hans-Peter Hartung and Philipp Albrecht*

Abstract

Optomotor response is increasingly used in preclinical research for evaluating the visual function in rodents. However, the most suitable measuring protocol for specific scientific questions is not always established. We aimed to determine the optimal parameters for visual function analysis in experimental autoimmune encephalomyelitis optic neuritis (EAEON), an animal model for multiple sclerosis. Contrast sensitivity as well as spatial frequency both had a low variance and a good test-retest reliability. Also, both parameters were able to differentiate between the EAEON and the control group. Correlations with the retinal degeneration, assessed by optical coherence tomography, the infiltration of immune cells, and the clinical disability score revealed that spatial frequency was superior to contrast sensitivity analysis. We therefore conclude that spatial frequency testing is better suited as visual acuity assessment in C57Bl/6 J EAEON mice. Furthermore, contrast sensitivity measurements are more time consuming, possibly leading to more stress for the animals.

Keywords: Optomotor response, EAEON, Spatial frequency, Contrast sensitivity, Neurodegeneration

Introduction

Optic neuritis (ON) is a major source of disability in patients with inflammatory central nervous system diseases such as multiple sclerosis, and trials on optic neuritis are increasingly being applied to evaluate neuroprotective strategies [1]. Myelin oligodendrocyte glycoprotein-induced experimental autoimmune encephalomyelitis is reportedly associated with strong optic neuritis (EAEON) resulting in demyelination and axonal damage of the optic nerve and in the following degeneration of the inner retinal layers: retinal nerve fiber layer (axons), ganglion cell layer (neurons), and inner plexiform layer (dendritic arbor) [2–6]. Studies on preclinical models of experimental autoimmune encephalomyelitis optic neuritis (EAEON) are ideally suited to translationally evaluate the promise of clinical ON trials especially since more and more in vivo clinical readouts are being adapted to the preclinical setting [7]. To investigate the visual function in rodents, the optomotor response (OMR) can be used. The technique takes advantage of the optokinetic nystagmus, an involuntary tracking of a moving pattern. In rodents, the optokinetic nystagmus leads to reflexive movements of the head and neck, and therefore does not need any training of the animal. Nevertheless, mice need time to adapt to the experimental setting. In case of reduction or loss of visual function, the optomotor response is reduced or eliminated. Although the OMR is already used for visual function testing in rodents, the most sensitive and reliable OMR parameters are not well established. Spatial frequency

* Correspondence: phil.albrecht@gmail.com
Department of Neurology, Medical Faculty, Heinrich-Heine University Düsseldorf, Moorenstr. 5, 40225 Düsseldorf, Germany

(SF) and contrast sensitivity (CS) are often used as readouts to determine the thresholds of visual function.

In this study, we investigated if spatial frequency or contrast sensitivity analysis is better suited for the examination of visual function loss in myelin oligodendrocyte glycoprotein, fragment 35-55 (MOG_{35-55}) induced EAEON in C57BL/6 J mice.

Methods

Induction of EAEON

Female, 6-weeks old C57Bl/6 J mice were purchased from Janvier Labs (Le Genest-Saint-Isle, France). To induce EAEON, the mice were subcutaneously immunized (distributed over four spots on the hind and front flanks) with 200 µg of MOG_{35-55} peptide (Biotrend, Cologne, Germany) in complete Freund's adjuvant (CFA) (Becton Dickinson, Franklin Lakes, USA) containing 800 µg *Mycobacterium tuberculosis* H37Ra (Becton Dickinson, Franklin Lakes, USA). Additionally, the mice were intraperitoneally injected with 200 ng pertussis toxin (PT) (Sigma-Aldrich, St. Louis, USA) at the time of immunization and after 48 h. The sham control animals were immunized with phosphate-buffered saline in CFA and injected with the same PT doses. Clinical EAE scores were rated daily according to the following criteria: (0) no disease; (0.5) mild tail paresis; (1) obvious tail paresis or plegia; (1.5) tail plegia and no righting reflex; (2) mild signs of hind limb paresis with clumsy gait; (2.5) obvious signs of hind limb paresis; (3) hind limb plegia, mouse drags one leg behind; (3.5) hind limb plegia, mouse drags both legs behind; (4) mild signs of quadriparesis; (4.5) quadriplegia; and (5) death or moribund.

All performed animal procedures were done in compliance with the experimental guidelines approved by the regional authorities (State Agency for Nature, Environment and Consumer Protection; AZ 84-02.04.2016.A137)

Analysis of visual function using optomotor response

Optomotor response was analyzed using a testing chamber and the OptoMotry™ software from CerebralMechanics™ (Canada) [8]. The mice were placed on a platform surrounded by four screens creating a box. The screens displayed a moving grid creating a virtual cylinder with varying frequencies at 100% contrast or varying contrasts at 5 different given frequencies (0.064, 0.092, 0.103, 0.192, and 0.272 c/d (cycles/degree)). The examination times differed substantially between contrast sensitivity and spatial frequency testing, the former taking about 60 min and the latter 15 min for a single exam. Monitoring was performed using a camera at the top of the box filming the head movements (tracking), which were evaluated by a blinded researcher. Visual acuity was determined using the threshold of the highest spatial frequency respectively the lowest contrast at which the mice still tracked the moving grid. Clockwise rotation of the grid and tracking represents the left eye while counterclockwise rotation and tracking represents the right eye. The baseline was analyzed before immunization and follow-up measurements were performed 1, 2, 3, 4, 6, 8, 10, 12, and 16 weeks post-immunization. A more detailed description of the device and methodology is given elsewhere [8–10].

Optical coherence tomography

OCT measurements were performed under ambient light conditions using the Spectralis™ HRA + OCT device (Heidelberg Engineering, Heidelberg, Germany), and the methodology is reported in line with the APOSTEL recommendations [11]. The mice were anesthetized with isoflurane (Piramal critical care, Mumbai, India) vaporized at a concentration of 2.5% (2 L/min O_2) and positioned in a custom OCT holder described elsewhere [12]. Pupils were dilated with 2.5% phenylephrine-0.5% tropicamide ophthalmic solution (pharmacy of the university hospital Düsseldorf). For imaging of the mouse retina, Visc-Ophtal eye gel (Dr. Winzer, Berlin, Germany) and a custom contact lens was used to keep the eyes moist and to ensure a constant and homogenous refraction during the examination. To adapt the focus to the mouse eye and retina, a 25-diopter adaptor lens was placed on the objective lens of the OCT device. OCT imaging was carried out with the software integrated TruTrack™ eye tracking to diminish breathing artifacts and to achieve consistent ocular orientations. OCT measurements were performed at the same time points as OMR analysis.

In order to analyze the thickness of the retinal layers, volume scans were performed. The scans were acquired with an initial focus of 37.75 diopters followed by manual correction. Each volume scan consisted of 25 B-Scans recorded in high-resolution mode at 50 automatic real time (ART, rasterized from 50 average A-Scans). The automated segmentation by the Heidelberg Eye Explorer™ software version 1.9.10.0 was followed by manual correction of obvious segmentation errors by a blinded investigator. Thickness measurements were derived from the circular 1, 2, and 3 mm early treatment of diabetic retinopathy study grid centered on the optic disc, excluding the central part. We calculated the thickness of the inner retinal layers (IRL), consisting of the retinal nerve fiber layer, ganglion cell layer, and inner plexiform layer by averaging each sector of the grid, excluding the center, which corresponded to the optic nerve head.

Tissue sampling and histological analysis

One hundred ten days after immunization, mice were sacrificed with an overdose of isoflurane (Piramal critical care, Mumbai, India), and cardiac perfusion using phosphate-buffered saline (Gibco, Carlsbad, USA) was performed. Optic nerves were isolated and fixated with 4% paraformaldehyde (Carl Roth, Karlsruhe, Germany) overnight. Afterwards, the optic nerves were dehydrated in sucrose solutions with increasing concentrations and embedded in O.C.T. compound (Sakura™ Finetek, Alphen aan den Rijn, The Netherlands). Five micrometer longitudinal sections were cut, and hematoxylin and eosin staining was performed. Rating of infiltrating immune cells in optic nerves was performed by an investigator blinded to the experimental groups using a previously published score [13]: 0, no infiltration; 1, mild cellular infiltration; 2, moderate infiltration; 3, severe infiltration; and 4, massive infiltration.

Statistics

Statistical analysis was performed using Prims 5.0 (Graphpad, San Diego, USA) and SPSS version 20 (IBM, Endicott, USA). Area under the curve of EAE daily scores was calculated for both groups and compared by *t* test analysis. Test-retest reliability was examined for spatial frequency and contrast sensitivity OMR measurements by interclass correlation coefficient (ICC) calculation using SPSS. Differences in retinal thickness and OMR measurements were analyzed using generalized estimating equations (GEE) with an exchangeable correlation matrix to adjust for intrasubject inter-eye correlations using SPSS. *P* values are selected as follows: $^{*}P \leq 0.05$, $^{**}P \leq 0.01$, and $^{***}P \leq 0.001$.

Results

Test-retest reliability

As a first step, the test-retest reliability of spatial frequency and contrast sensitivity measurements were investigated. Twenty eyes of 10 mice were tested on two consecutive days at the same day time by the same researcher 15 weeks post-immunization. Results showed that both measurements have a low variance and a good reproducibility with ICC values of 0.964 for spatial frequency (Fig. 1a) and 0.889–0.955 for contrast sensitivity (Fig. 1b–f).We were

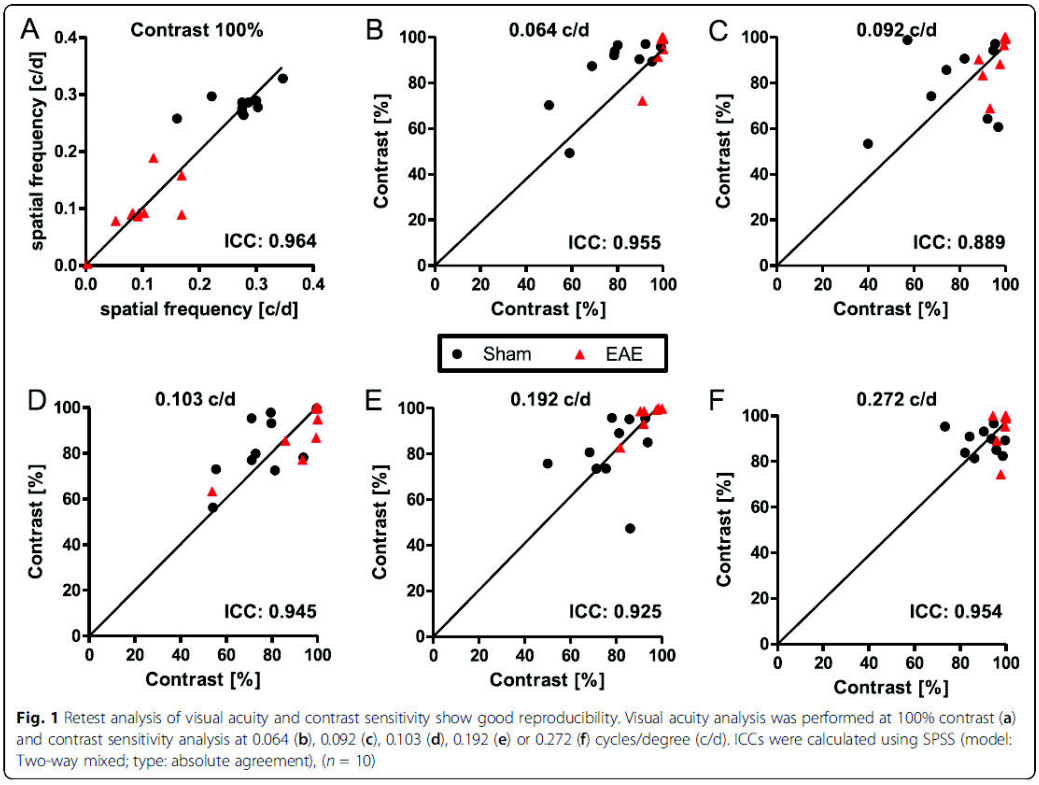

Fig. 1 Retest analysis of visual acuity and contrast sensitivity show good reproducibility. Visual acuity analysis was performed at 100% contrast (**a**) and contrast sensitivity analysis at 0.064 (**b**), 0.092 (**c**), 0.103 (**d**), 0.192 (**e**) or 0.272 (**f**) cycles/degree (c/d). ICCs were calculated using SPSS (model: Two-way mixed; type: absolute agreement), ($n = 10$)

able to demonstrate that the best reproducibility to analyze contrast sensitivity is at a spatial frequency of 0.064 c/d. Although all readouts show good reproducibility, the animals present a considerable inter subject variability suggesting that longitudinal investigations analyzing changes from baseline are better suited to detect subtle changes than cross-sectional end point measurements. This is similar to the findings for OCT imaging and highlights the advantage of these in vivo assessments over other techniques like histology that are only possible post-mortem. The test-retest analysis revealed that spatial frequency testing is better suited to differentiate between control and EAE animals (Fig. 1a). Since in the context of EAEON the spatial frequency often drops below a value of 0.1 c/d (Fig. 1a), we decided to proceed with the contrast sensitivity analysis at 0.064 c/d for the following experiments.

We continued by testing both readouts in the EAEON mouse model with eight eyes of two sham/control and two EAEON mice. In general, spatial frequency and contrast sensitivity analysis were able to differentiate between sham/control and EAEON mice. However, spatial frequency showed not only a clearer separation of

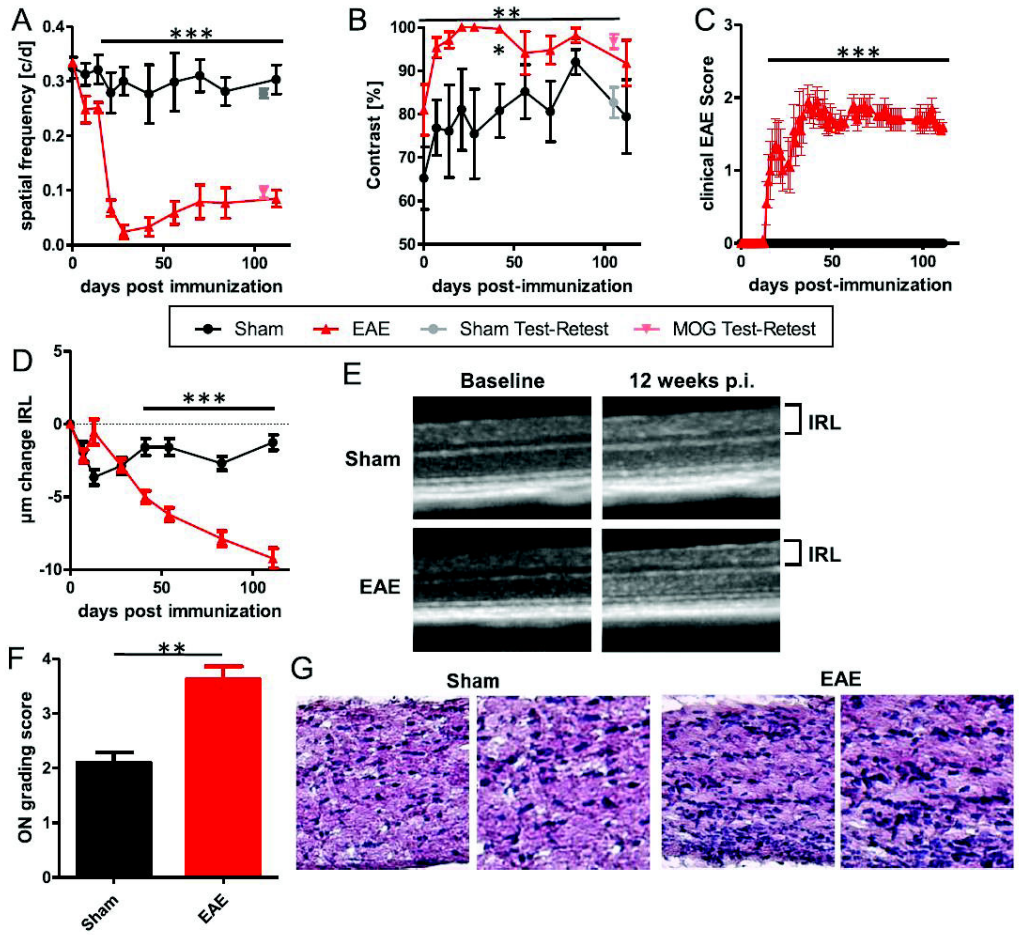

Fig. 2 Analysis of visual function using OMR, thinning of the inner retinal layers and infiltration of immune cells in the inflammatory EAEON-model over a period of 110 days. Visual acuity tested by spatial frequency (**a**) and contrast sensitivity (**b**) at 0.064 c/d (n = 4, note that a higher contrast equals worse visual acuity; compared by GEE analysis). **c** Clinical EAE score (area under the curve compared by t-test), **d** change of inner retinal layers (compared using GEE analysis), **e** representative OCT images (p.i. post-immunization), **f** infiltrating immune cells in the optic nerve (*n* = 5), and **g** representative histological images of optic nerves (H&E staining). The time courses present the results of an EAE experiment with at least four mice per group (*$p < 0.05$; **$p < 0.01$; ***$p < 0.001$)

the two groups (Figs. 1a and 2a + b), but also a better correlation with the degeneration of the IRL, assessed by OCT (Fig. 2d + e) (SF, $p < 0.001$ vs CS, $p < 0.001$; GEE), infiltrating immune cells (Fig. 2f + g) (SF, $r = -0.78$; $p = 0.028$ vs CS, $r = 0.42$; $p = 0.354$; Spearman), and the EAE score (Figure 2c) (SF, $r = -0.76$; $p < 0.001$ vs CS, $r = 0.38$; $p = 0.059$; Spearman) than contrast sensitivity.

Discussion

In this study, spatial frequency and contrast sensitivity analysis were compared as readout methods to examine visual acuity in EAEON mice. Furthermore, correlation with clinical EAE-scores, thinning of inner retinal layers, and infiltrating immune cells in the optic nerve was studied. Even though OMR is a reflex and therefore training is not mandatory, mice still need time to adapt to the experimental setting. During long-time measurements, such as measurements of all five frequencies for contrast sensitivity analysis, animals sometimes need to be animated to differentiate if loss of tracking is due to reaching the threshold or due to decreasing attention of the animal. Furthermore, experimenters should be blinded for the experimental groups and need training to reliably distinguish between tracking and normal behavioral movements. Choosing the right spatial frequency for contrast sensitivity testing is crucial. Visual function is continuously being lost during EAEON, and in order to assure reliable results over the whole course of the disease, we decided to perform the test-retest analysis with mice that were in a chronic stage. This may account for the worse separation of EAE, and sham-immunized mice in the contrast measurements at the higher spatial frequencies testing spatial frequencies between 0.064 c/d and 0.272 c/d for test-retest reproducibility and during EAEON revealed that 0.064 c/d was the most reproducible and was still detectable by mice even at lower contrast during EAEON. Testing at lower spatial frequencies was not possible for contrast sensitivity assessments due to the specifications of the device. Although other groups found that in rhodopsin knockout mice contrast sensitivity analysis was more sensitive for visual decline than spatial frequency [14], we conclude that for EAEON mice the opposite is true. These different conclusions highlight the fact that different models and reasons for visual deficits may need different algorithms for testing visual function. While rhodopsin knockout mice show decrease of cone density and retinal thinning of the outer retinal layers, our EAEON mice present neuroaxonal degeneration and thinning of the inner retinal layers and the optic nerve. It is therefore important to evaluate the sensitivity of different testing algorithms before starting visual testing in new experimental models. To this end, our data suggest that spatial frequency testing at 100% contrast and contrast sensitivity testing at 0.064 c/d seem to be good starting points, in line with results from other researchers [8, 15].

Conclusions

We demonstrate that, in EAEON mice, spatial frequency measurement is better suited for the analysis of the optokinetic response than contrast sensitivity testing. Apart from the superior results for spatial frequency, analysis of contrast sensitivity is also more time-consuming and therefore leads to more stress for the mice and a lower throughput for experiments.

Abbreviations

CFA: Complete Freund's adjuvant; CS: Contrast sensitivity; EAEON: Experimental autoimmune encephalomyelitis/optic neuritis; GEE: Generalized estimated equation; ICC: Intraclass correlation coefficient; IRL: Inner retinal layers; MOG_{35-55}: Myelin oligodendrocyte glycoprotein fragment 35-55; OCT: Optical coherence tomography; OMR: Optomotor response; ON: Optic neuritis; p.i.: Post-immunization; PT: Pertussis toxin; SF: Spatial frequency

Acknowledgements

Not applicable.

Authors' contributions

CH, MD, and AI performed the experiments and analyzed the date; CH and PA wrote the manuscript; MD and HPH were involved in revising the manuscript critically for important intellectual content and made substantial contributions to interpretation of data. PA conceived the study and supervised experiments. All authors read and approved the final manuscript.

Funding

This work was supported by grants from the charitable Ilselore-Luckow Foundation to PA.

Availability of data and materials

The dataset obtained and analyzed in this study is available from the corresponding author on a reasonable request.

Ethics approval and consent to participate

All protocols involving animals were in compliance with the experimental guidelines approved by the regional authorities (State Agency for Nature, Environment, and Consumer Protection) and conform to the Association for Research in Vision and Ophthalmology (ARVO) Statement for the Use of Animals in Ophthalmic and Vision Research.

Consent for publication

Not applicable.

Competing interests

The Optomotry device was funded by a grant from the charitable Iselore Luckow Foundation to PA and HPH. Other than that, the authors declare that they have no conflict of interest related to the work presented. The following financial disclosures are unrelated to the work: MD received speaker honoraria from Novartis and Merck. AI declares no financial disclosures. HPH has received fees for serving on steering committees from Biogen Idec, GeNeuro, Sanofi Genzyme, Merck, Novartis Pharmaceuticals, Octapharma, Opexa Therapeutics, Teva Pharmaceuticals, MedImmune, Bayer HealthCare, Forward Pharma, and Roche; fees for serving on advisory boards from Biogen Idec, Sanofi Genzyme, Merck, Novartis Pharmaceuticals, Octapharma, Opexa Therapeutics, Teva Pharmaceuticals, and Roche; and lecture fees from Biogen Idec, Sanofi Genzyme, Merck, Novartis Pharmaceuticals, Octapharma, Opexa Therapeutics, Teva Pharmaceuticals, MedImmune, and Roche. PA received compensation for serving on Scientific Advisory Boards for Ipsen, Novartis, and Biogen; he received speaker honoraria and travel support from Novartis, Teva, Biogen, Merz Pharmaceuticals, Ipsen, Allergan, Bayer HealthCare, Esai, UCB, and Glaxo Smith Kline; he received research support from Novartis, Biogen, Teva, Merz Pharmaceuticals, Ipsen, and Roche.

Received: 17 April 2020 Accepted: 6 July 2020
Published online: 18 July 2020

References

1. Aktas O, Albrecht P, Hartung H-P. Optic neuritis as a phase 2 paradigm for neuroprotection therapies of multiple sclerosis: update on current trials and perspectives. Curr Opin Neurol. 2016;29:199–204.
2. Cruz-Herranz A, Dietrich M, Hilla AM, Yiu HH, Levin MH, Hecker C, et al. Monitoring retinal changes with optical coherence tomography predicts neuronal loss in experimental autoimmune encephalomyelitis. J Neuroinflammation. 2019;16:203.
3. Dietrich M, Helling N, Hilla A, Heskamp A, Issberner A, Hildebrandt T, et al. Early alpha-lipoic acid therapy protects from degeneration of the inner retinal layers and vision loss in an experimental autoimmune encephalomyelitis-optic neuritis model. J Neuroinflammation. 2018;15:71.
4. Dietrich M, Koska V, Hecker C, Göttle P, Hilla AM, Heskamp A, et al. Protective effects of 4-aminopyridine in experimental optic neuritis and multiple sclerosis. Brain J Neurol. 2020;143:1127–42.
5. Knier B, Rothhammer V, Heink S, Puk O, Graw J, Hemmer B, et al. Neutralizing IL-17 protects the optic nerve from autoimmune pathology and prevents retinal nerve fiber layer atrophy during experimental autoimmune encephalomyelitis. J Autoimmun. 2015;56:34–44.
6. Manogaran P, Samardzija M, Schad AN, Wicki CA, Walker-Egger C, Rudin M, et al. Retinal pathology in experimental optic neuritis is characterized by retrograde degeneration and gliosis. Acta Neuropathol Commun. 2019;7:116.
7. Dietrich M, Aktas O, Hartung H-P, Albrecht P. Assessing the anterior visual pathway in optic neuritis: recent experimental and clinical aspects. Curr Opin Neurol. 2019;32:346–57.
8. Prusky GT, Alam NM, Beekman S, Douglas RM. Rapid quantification of adult and developing mouse spatial vision using a virtual optomotor system. Invest Ophthalmol Vis Sci. 2004;45:4611–6.
9. Douglas RM, Alam NM, Silver BD, McGill TJ, Tschetter WW, Prusky GT. Independent visual threshold measurements in the two eyes of freely moving rats and mice using a virtual-reality optokinetic system. Vis Neurosci. 2005;22:677–84.
10. Dietrich M, Hecker C, Hilla A, Cruz-Herranz A, Hartung H-P, Fischer D, et al. Using optical coherence tomography and optokinetic response as structural and functional visual system readouts in mice and rats. J Vis Exp JoVE. 2019.
11. Cruz-Herranz A, Balk LJ, Oberwahrenbrock T, Saidha S, Martinez-Lapiscina EH, Lagreze WA, et al. The APOSTEL recommendations for reporting quantitative optical coherence tomography studies. Neurology. 2016;86:2303–9.
12. Dietrich M, Cruz-Herranz A, Yiu H, Aktas O, Brandt AU, Hartung H-P, et al. Whole-body positional manipulators for ocular imaging of anaesthetised mice and rats: a do-it-yourself guide. BMJ Open Ophthalmol. 2017;1:e000008.
13. Shindler KS, Guan Y, Ventura E, Bennett J, Rostami A. Retinal ganglion cell loss induced by acute optic neuritis in a relapsing model of multiple sclerosis. Mult Scler Houndmills Basingstoke Engl. 2006;12:526–32.
14. Xiao J, Adil MY, Chang K, Yu Z, Yang L, Utheim TP, et al. Visual contrast sensitivity correlates to the retinal degeneration in rhodopsin knockout mice. Invest Ophthalmol Vis Sci. 2019;60:4196–204.
15. Lehmann K, Schmidt K-F, Löwel S. Vision and visual plasticity in ageing mice. Restor Neurol Neurosci. 2012;30:161–78.

Publisher's Note

3.2 Increased remyelination and pro-regenerative microglia under siponimod therapy in mechanistic models

Michael Dietrich[1]*, **Christina Hecker[1]***, Elodie Martin[2], Dominique Langui[2], Michael Gliem[1], Bruno Stankoff[2,3], Catherine Lubetzki[2,4], Joel Gruchot[1], Peter Göttle[1], Andrea Issberner[1], Milad Nasiri[1], Pamela Ramseier[5], Christian Beerli[5], Sarah Tisserand[5], Nicolau Beckmann[5], Derya Shimshek[5], Patrick Petzsch[6], David Akbar[2], Bodo Levkau[7], Holger Stark[8], Karl Köhrer[6], Hans-Peter Hartung[1,9,10], Patrick Küry[1], Sven G. Meuth[1], Marc Bigaud[5], Bernard Zalc[2]*, Philipp Albrecht[1]*‡

*Equally contributing first/last authors

[1]Heinrich-Heine University Düsseldorf, Medical Faculty, Department of Neurology, Düsseldorf, Germany

[2]Sorbonne Université, Inserm, CNRS, Institut du Cerveau, Pitié-Salpêtrière Hospital, F-75013 Paris, France

[3]AP-HP, Saint-Antoine Hospital, F-75012 Paris, France

[4]AP-HP, Pitié-Salpêtrière Hospital, F-75013 Paris, France

[5]Novartis Institutes for BioMedical Research, Basel, Switzerland

[6]Biological and Medical Research Center (BMFZ), Medical Faculty, Heinrich-Heine-University, Duesseldorf, Germany

[7]Institute for Molecular Medicine III, University Hospital Düsseldorf and Heinrich-Heine University Düsseldorf, Düsseldorf, Germany.

[8]Institute of Pharmaceutical and Medicinal Chemistry, Heinrich Heine University Düsseldorf, Duesseldorf, Germany.

[9]Brain and Mind Center, University of Sydney, Australia;

[10]Medical University of Vienna, Austria

The presented manuscript was accepted in Neurology Neuroimmunology and Neuroinflammation, 2022

Contribution:

- Shared first authorship
- Execution, analysis and statistics of the following methods: OCT measurements (90 %), OKR measurements (90%), EAE experiments (50 %), histology of optic nerve (40 %) and retina (50 %), blood FACS analysis (50 %)
- Writing and drafting of the manuscript (30%)

Title: Increased remyelination and pro-regenerative microglia under siponimod therapy in mechanistic models.

Authors: Michael Dietrich[1]*, Christina Hecker[1]*, Elodie Martin[2], Dominique Langui[2], Michael Gliem[1], Bruno Stankoff[2,3], Catherine Lubetzki[2,4], Joel Gruchot[1], Peter Göttle[1], Andrea Issberner[1], Milad Nasiri[1], Pamela Ramseier[5], Christian Beerli[5], Sarah Tisserand[5], Nicolau Beckmann[5], Derya Shimshek[5], Patrick Petzsch[6], David Akbar[2], Bodo Levkau[7], Holger Stark[8], Karl Köhrer[6], Hans-Peter Hartung[1,9,10], Patrick Küry[1], Sven G. Meuth[1], Marc Bigaud[5], Bernard Zalc[2]*, Philipp Albrecht[1]*‡

Affiliations:

*Equally contributing first/last authors

[1]Department of Neurology, Heinrich-Heine University Düsseldorf, Medical Faculty, 40225 Düsseldorf, Germany

[2]Sorbonne Université, Inserm, CNRS, Institut du Cerveau, Pitié-Salpêtrière Hospital, 75013 Paris, France

[3]AP-HP, Saint-Antoine Hospital, 75012 Paris, France

[4]AP-HP, Pitié-Salpêtrière Hospital, 75013 Paris, France

[5]Novartis Institutes for BioMedical Research, 4056 Basel, Switzerland

[6]Biological and Medical Research Center (BMFZ), Heinrich-Heine-University Düsseldorf, Medical Faculty, 40225 Duesseldorf, Germany

[7]Institute for Molecular Medicine III, University Hospital Düsseldorf and Heinrich-Heine University Düsseldorf, 40225 Düsseldorf, Germany

[8]Institute of Pharmaceutical and Medicinal Chemistry, Heinrich Heine University Düsseldorf, 40225 Duesseldorf, Germany

[9]Brain and Mind Center, University of Sydney, NSW 2006, Australia

[10]Medical University of Vienna, 1090 Vienna, Austria

‡Corresponding Author: Philipp Albrecht, M.D., Professor of Neurology, Consultant Neurologist

phone: +49(0)211-8108475, fax: +49(0)211-8106183

Email: phil.albrecht@gmail.com

Abstract

Background and Objectives: Siponimod is an oral, selective sphingosine 1-phosphate receptor-1/5 modulator, approved for treatment of multiple sclerosis.

Methods: Mouse MRI was used to investigate remyelination in the cuprizone model. We then used a conditional demyelination Xenopus laevis model, to assess the dose-response of siponimod on remyelination. In experimental autoimmune encephalomyelitis-optic neuritis (EAEON) in C57Bl/6J mice, we monitored the retinal thickness and the visual acuity using optical coherence tomography and optomotor response. Optic nerve inflammatory infiltrates, demyelination, as well as microglial and oligodendroglial differentiation were assessed by immunohistochemistry, quantitative realtime PCR and bulk RNA sequencing

Results: An increased remyelination was observed in the cuprizone model. Siponimod treatment of demyelinated tadpoles improved remyelination in comparison to control in a bell-shaped dose-response curve. Siponimod in the EAEON model attenuated the clinical score, reduced the retinal degeneration and improved the visual function after prophylactic and therapeutic treatment, also in a bell-shaped manner. Inflammatory infiltrates and demyelination of the optic nerve were reduced, the latter even after therapeutic treatment, which also shifted microglial differentiation to a pro-myelinating phenotype.

Discussion: These results confirm the immunomodulatory effects of siponimod and suggest additional regenerative and promyelinating effects, which follow the dynamics of a bell-shaped curve with high- being less efficient than low concentrations.

Glossary

ANOVA = analysis of variance, Arg-1 = Arginase-1, BAF312/Sip = siponimod, BW = bodyweight, CC = corpus callosum, c/d = cycles per degree, DEG = differentially expressed genes, dpi = days post immunization, EAE(ON) = experimental autoimmune encephalomyelitis (optic neuritis), GCL = ganglion cell layer, GEE = generalized estimating equations, GFAP = glial fibrillary acidic protein, IPL = inner plexiform layer, IRL = inner retinal layer, LC/MS/MS = liquid chromatography/tandem mass spectrometry, MBP = myelin basic protein, MS = multiple sclerosis, MTR = magnetization transfer ratio, MTZ = metronidazole, MOG35-55 = myelin oligodendrocyte glycoprotein fragment 35-55, NTR = nitroreductase OCT = optical coherence tomography OMR = optomotor response, OPC = oligodendrocyte precursor cell, PDGRFα = platelet-derived growth factor receptor A, RGCs = retinal ganglion cells, RNFL = retinal nerve fiber layer, S1P1/5 = sphingosine 1-phosphate receptor 1 and 5, T2-WSI = T2-weighted signal intensity, TNF-α = tumor necrosis factor alpha, Ym1/Chi3l3 = Chitinase 3-like-3.

Introduction

Siponimod, a potent and highly selective sphingosine 1-phosphate receptor 1 and 5 (S1P1/5) modulator, is the first disease-modifying therapy that significantly reduced disability progression, cognitive decline and total brain volume loss versus placebo in patients with secondary progressive multiple sclerosis (SPMS), as demonstrated in the phase III EXPAND study.[1] It has beneficial effects in the central nervous system of experimental autoimmune encephalomyelitis (EAE) mice that are independent of peripheral immune effects, suggesting that, in addition to its anti-inflammatory effects, siponimod may be effective in limiting neurodegenerative pathological processes in SPMS.[2]

Promoting remyelination is another key therapeutic strategy to limit disability progression, and represents one of the major therapeutic challenges in MS. Therefore, experimental models to investigate substances promoting remyelination *in vivo* are of paramount interest.[3,4] The cuprizone-intoxication mouse model is a well-established mechanistic model to study remyelination processes.[5] As oligodendrocyte precursor cells (OPCs) are not affected by cuprizone they readily proliferate, migrate, differentiate and integrate again into the circuitry resulting in remyelination after withdrawal. Novel data from a *Xenopus laevis* demyelination model indicated a remyelinating potential of siponimod. Optic neuritis (ON) presenting with reduction of visual function is frequent in MS and accompanied by retinal nerve fiber layer thinning and retinal ganglion cell (RGC) loss, which can be used as an outcome parameter for neuroprotection studies investigating ON as a model for acute inflammatory relapses. [6–9] Therefore, in this innovative approach investigating the visual pathway of siponimod treated EAE-associated ON (EAEON) mice, we used longitudinal visual system readouts, namely optical coherence tomography (OCT) and optomotor response (OMR), which are ideally suited to evaluate CNS degeneration in preclinical studies and clinical approaches.[10–13]

In this study, we assessed the impact of siponimod in three different animal models of demyelination i) a toxic cuprizone-induced demyelination mouse model, ii) a conditional demyelination of optic nerve in transgenic *Xenopus laevis* and iii) a myelin oligodendrocyte glycoprotein fragment 35-55 (MOG_{35-55})-induced EAEON by visual system readouts, revealing yet unknown mechanisms on the shift of the microglial cell population towards a regenerative phenotype.

Materials and Methods

Cuprizone-intoxication model and measurement of C57Bl/6J mice

Cuprizone preparation and randomization is described in the eMethods. In brief, female C57BL/6J mice (8-10 weeks old from Charles River, Germany) received normal diet over 7 weeks (control group) or were fed with cuprizone-loaded pellets (2 g/kg food) for 5 weeks and then switched either to siponimod-loaded pellets (10 mg/kg food) over 2 weeks (cuprizone/siponimod group) or to drug-free pellets (cuprizone/sham group). MRI measurements were performed at week 5, 6 and 7 and histology on week 7 with LFB and GST-π as described in the eMethods.

Xenopus laevis demyelination model

To test the effect of siponimod on remyelination, *in vivo*, we used a conditional demyelination transgenic model, Tg(*mbp:GFP-NTR*), developed in *Xenopus laevis* as described before[14–16] and in the eMethods. Prior to the quantification of GFP+ cells, we anesthetized the tadpoles of either sex in 0.05% MS-222 (ethyl-3-aminobenzoate methanesulfonate; Sigma-Aldrich) and returned them to standard water conditions for recovery. Tadpoles were euthanized in 0.5% MS-222 before the optic nerve was dissected.

For regeneration experiments, metronidazole (MTZ)-exposed animals (MTZ preparation described in the eMethods) were allowed to recover for 3 days in either normal water (control) or water containing siponimod at increasing concentrations in ambient laboratory lighting (12h light/12h dark).

Induction of EAEON and treatment of C57Bl/6J mice

EAEON was induced in female, 6-weeks old C57Bl/6J by 200 µg MOG_{35-55} (Biotrend, Germany) immunization followed by intraperitoneal injections of 200 ng of pertussis toxin (Sigma-Aldrich, Germany) at day 0 and 2 as previously described.[17]

Mice were fed with siponimod-loaded pellets at 0.01 or 0.03 g/kg of food, leading to a daily drug-intake of approximately 2 and 6 mg/kg bodyweight, respectively (considering a mean daily food intake of 3 g/mouse).[18–21] Treatment was started at the same day (d0), 14 days (d14) or 30 days (d30) after MOG_{35-55} immunization. The clinical EAE score was graded daily as described previously.[17]

OCT and OMR in mice

The measurements of retinal layers were performed using a Spectralis™ HRA+OCT device (Heidelberg Engineering, Germany) with several adaptions for rodents.[22] The analysis and scanning protocols are described elsewhere[11,23] and in the eMethods, in line with the APOSTEL recommendations.[24]

Visual function analysis was carried out with a testing chamber and the OptoMotry™ software from CerebralMechanics™, Canada, as previously described-[23,25] and explained in detail in the eMethods.

Histological analysis

Wholemount of Xenopus optic nerve and analysis

Tadpoles were fixed by immersion in 4% paraformaldehyde for 1h at room temperature. Fixed optic nerves were carefully dissected out and processed as described in the eMethods. In brief, oligodendrocytes were stained with anti-GFP (1:1000, Aves Lab, USA) and microglial cells with *Bandeiraea Simplicifolia isolectin* B4

(Alexa Fluor594-conjugated IB4, 1:1000, Invitrogen), images were acquired using Olympus FV-1200 upright confocal microscope (Obj 20X-zoom 1.6).

Electron microscopy of Xenopus tadpole optic nerve

Xenopus larvae were fixed in a mixture of 2% paraformaldehyde, 2% glutaraldehyde, in 0.1 M cacodylate buffer pH 7.4 and 0.002% calcium chloride overnight at 4°C and processed as described in the eMethods. Ultrathin sections were examined on an HT7700 electron microscope (Hitachi) operated at 70 kV. Electron micrographs were taken using the integrated AMT XR41-B camera (2048X2048 pixels).

Quantification of GFP$^+$ cells in Xenopus optic nerve

As described previously,[16] GFP-fluorescence was analyzed directly *in vivo* in Xenopus embryos using an AZ100 Nikon Multizoom Macro-Microscope. From the emergence of the optic nerve, directly after the chiasm, to the retinal end, the total number of GFP+ cells were counted independently by two researchers in a double-blinded manner. The counts were compared to control untreated animals of the same developmental stage.

Wholemounts and histological optic nerve analysis of C57Bl/6J EAEON mice

After 21, 35 or 90 days of EAEON, mice were sacrificed and eyes and optic nerves were extracted and processed as described in the eMethods. Wholemounts were stained with anti-Bnr3a (1:200, Santa Cruz Biotechnology, USA).

Optic nerves slices were incubated with antibodies directed against CD3- (1:400, Dako), Iba1- (1:500, Wako chemicals), myelin basic protein (MBP) (1:500, Millipore), Ym1/Chi3l3: Chitinase 3-like-3 (Ym1) (1:100, Stem Cell Technology), Arginase-1 (Arg-1) (Abcam, 1:500), tumor necrosis factor alpha (TNF-α) (1:20, Invitrogen), Olig2 (1:250, Millipore), platelet-derived growth factor receptor A (PDFGRα) (1:250, Neuromics) and glial fibrillary acidic protein (GFAP) (1:1000, Neuromab). Cy5 anti-rat, Cy5 anti-rabbit (1:500, Millipore) and Alexa Fluor™ 488 anti-rabbit (1:500, Invitrogen) were used as secondary antibodies.

The CD3 and MBP staining results were rated by an investigator blinded to the experimental groups by scores described previously.[17]

Fluorescence stained longitudinal optic nerve sections were acquired with a Leica HyD detector attached to a Leica DMi8 confocal microscope (63x objective lens magnification). At least four sections of the optic nerve from one eye of each mouse were analyzed per staining.

Bulk RNA sequencing of optic nerve from EAEON mice

RNA extraction was performed as previously described.[26] RNA was stored at -80°C until analysis. Total RNA samples used for transcriptome analyses were quantified (Qubit RNA HS Assay, Thermo Fisher Scientific) and quality measured by capillary electrophoresis using the Fragment Analyzer and the 'Total RNA High Sensitivity Assay' (Agilent Technologies, Inc. Santa Clara, USA). All samples in this study showed high quality RNA Quality Numbers (RQN; mean = 8.5). The library preparation was performed according to the manufacturer's protocol using the 'SMART-Seq® Stranded Kit' (Takara Bio Inc. Kusatsu, Shiga, Japan) for Illumina®. Briefly, 10 ng total RNA were used for reverse transcription of total RNA, addition of Illumina adapters with barcodes via PCR, cleavage of ribosomal cDNA and library amplification. Bead purified libraries were normalized and finally sequenced on the NextSeq 550 system (Illumina Inc. San Diego, USA) with a read

setup of 1x75 bp. The bcl2fastq tool was used to convert the bcl files to fastq files as well for adapter trimming and demultiplexing.

qPCR analysis of optic nerve of EAEON C57Bl/6J mice

RNA extraction, reverse transcription, and quantitative real-time PCR were performed as previously described[26] using Fam/Dark quencher probes from the Universal Probe Library (Roche, Switzerland) or individually designed Fam/Tamra probes (Eurofins Genomics, Germany). HPRT and GAPDH served as endogenous control genes. Primer sequences can be found in eTable 1.

Statistics

Statistical analysis was performed using Prism 5 (version 5.00, Graphpad Software, Inc., USA) and IBM SPSS Statistics (version 20, IBM Corporation, USA). A two tailed analysis of variance (ANOVA) with Dunnett's post hoc test was used to compare the area under the curve for the EAE scores and blood siponimod concentration time courses. qPCRs were analyzed using two-way ANOVA with Bonferroni post hoc test. Group means were compared by one-way ANOVA with Dunnett's post hoc test using one eye per animal for the histological investigations. Differences in retinal thickness and visual function were analyzed using generalized estimating equations (GEE) with an exchangeable correlation matrix in order to adjust for intrasubject inter-eye correlations.

MRI data were analyzed using Anova with random effects (Systat version 13; Systat Software Inc., San Jose, California, USA) to take into account the longitudinal structure of the data. A value of $p < 0.05$ was considered significant.

For the RNAseq, the analysis on the fastq files was performed with CLC Genomics Workbench (version 20.0.4, QIAGEN, Venlo. NL). The reads of all probes were adapter trimmed (Illumina TruSeq) and quality trimmed (using the default parameters: bases below Q13 were trimmed from the end of the reads, ambiguous nucleotides maximal 2). We performed mapping against the Mus musculus (mm10; GRCm38.86) (March 24, 2017) genome sequence. Multi-group comparisons were made and statistically determined using the Empirical Analysis of DGE (version 1.1, cutoff = 5) after grouping of the samples (n=5 for each group). The Resulting p -values were corrected for multiple testing by FDR. A p-value of ≤0.05 was considered significant.

Study approval

C57Bl/6J mice: The procedures were performed in accordance with the "Animal Research: Reporting of In Vivo Experiments" (ARRIVE) guidelines, approved by the regional authorities (State Agency for Nature, Environment and Consumer Protection; AZ 84-02.04.2016.A137) and conform to the Association for Research in Vision and Ophthalmology (ARVO) Statement for the Use of Animals in Ophthalmic and Vision Research. Cuprizone studies were approved by the Swiss Cantonal Veterinary Authority of Basel City, Switzerland (license BS-2711).

Xenopus laevis tadpoles: Animal care was in compliance with institutional and national guidelines. All animal experiments conformed to the European Community Council directive (86/609/EEC) as modified (2010/603/UE) and have been approved by the ethical committee of the French Ministry of Higher Education and Research (APAFIS#5842-2016101312021965).

Data Availability

Data not provided in the article because of space limitations may be shared at the request of any qualified investigator for purposes of replicating procedures and results.

Results

Siponimod promotes remyelination after cuprizone-intoxication

We employed the cuprizone model of toxic demyelination to study siponimod's effects on remyelination in vivo. During the 5 week-intoxication phase, no particular health issue could be detected in cuprizone-treated vs control mice and similar longitudinal bodyweight changes vs baseline were observed in the 3 study groups (Figure 1A). Hence, at the start of the treatment, all 3 groups presented similar mean bodyweights (21.9 ± 0.4 g; 21.4 ± 0.4 g; 22.2 ± 0.3 g).

Over the following 2 weeks, the mice that received drug free pellets (cuprizone/sham group) showed a slight but significant loss in bodyweight vs controls. This was not observed in mice that received siponimod-loaded pellets (cuprizone/siponimod group) (Figure 1A). In this group, the mean siponimod concentrations measured in blood and brain homogenates were within the expected ranges, i.e. 0.41 ± 0.01 µM and 2.7 ± 0.7 nmol/g (equivalent to 2.7 ± 0.7 µM), confirming the success of the treatment.

As expected, cuprizone-intoxicated mice showed marked demyelination within their CC, at week-5, as suggested by significantly decreased magnetization transfer ratio (MTR) in these regions when compared to values in control mice (Figure 1C). Upon cuprizone washout in weeks 5 to 7, MTR in mice fed with drug-free pellets increased in the CC (Figure 1C), suggesting spontaneous partial remyelination. This effect was particularly evident when calculating the area-under-the-curve (AUC) (Figure 1D). Five weeks of cuprizone intoxication resulted also in T2-weighted CC signal increases by 53% (Figure 1B). After cuprizone withdrawal at week 5, the T2-weighted signal intensity (T2-WSI) was reduced in the CC at week 5 to 7 (Figure 1E), consistent with spontaneous partial remyelination and reduction of neuroinflammation in these areas.[27] Addition of siponimod to food pellets increased this reduction of T2-WSI (Figure 1E) with a significant difference to siponimod-free pellet treated mice in the CC. This effect was again particularly evident when analyzing the AUC (Figure 1F). T2-WSI in the CC of control mice remained unaltered. Both MTR and T2-WSI data of the CC indicate the beneficial effects of siponimod treatment in the cuprizone model. Terminal qIHC for LFB density and oligodendrocyte numbers (GST-π) revealed a degree of myelination in the CC reduced by about half in cuprizone-challenged mice receiving drug-free food pellets vs controls. A trend towards a lower degree of CC demyelination was observed in siponimod-treated mice, with changes in LFB density and oligodendrocyte numbers reduced by about 25-45% vs siponimod-free mice (eFigure 1).

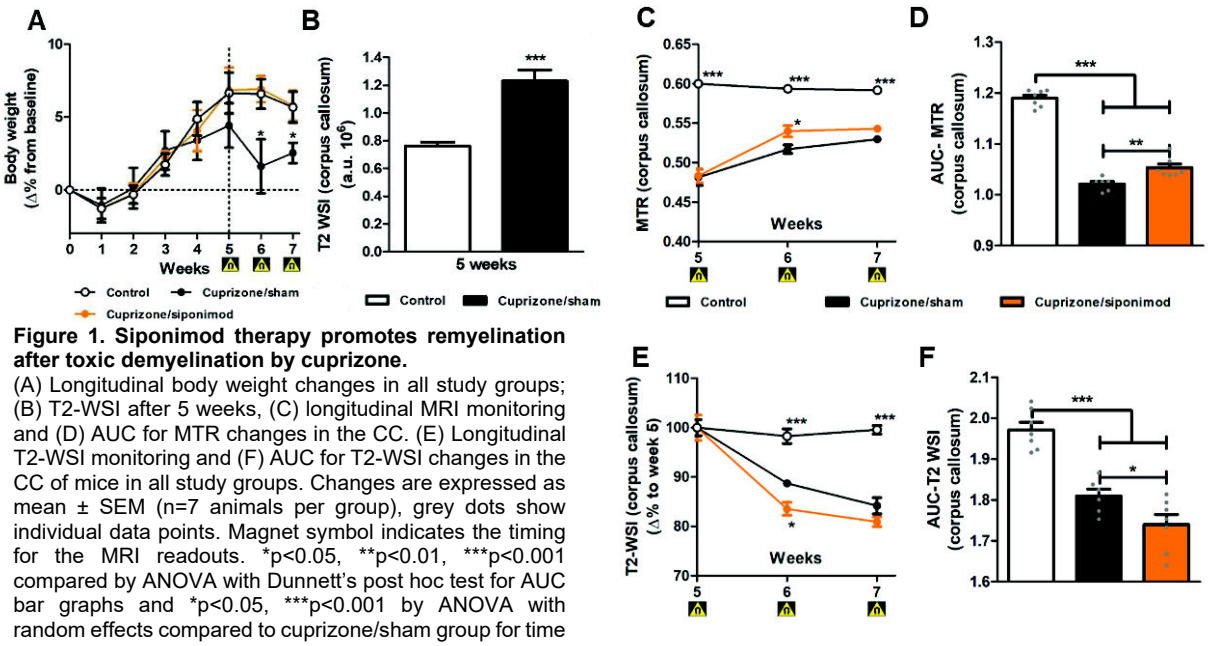

Figure 1. Siponimod therapy promotes remyelination after toxic demyelination by cuprizone.
(A) Longitudinal body weight changes in all study groups; (B) T2-WSI after 5 weeks, (C) longitudinal MRI monitoring and (D) AUC for MTR changes in the CC. (E) Longitudinal T2-WSI monitoring and (F) AUC for T2-WSI changes in the CC of mice in all study groups. Changes are expressed as mean ± SEM (n=7 animals per group), grey dots show individual data points. Magnet symbol indicates the timing for the MRI readouts. *p<0.05, **p<0.01, ***p<0.001 compared by ANOVA with Dunnett's post hoc test for AUC bar graphs and *p<0.05, ***p<0.001 by ANOVA with random effects compared to cuprizone/sham group for time courses.

Siponimod driven activation of S1P1/5 receptor promotes remyelination

Conditional oligodendrocyte ablation and demyelination followed by spontaneous remyelination was investigated in the Tg(*mbp:GFP-NTR)* Xenopus laevis model and the dynamics are reported in the eAppendix 1 and eFigure 2. Demyelination and remyelination was analyzed by counting the number of GFP+ cells per optic nerve in vivo before (D0), at the end of MTZ treatment (D10), and then on day 3 (R3) of the repair period. To assess remyelination potency upon stopping MTZ exposure, siponimod was added in the swimming water at nominal doses ranging from 0.1 nM to 1 µM. Under these conditions, siponimod accumulated over time in tadpole tissues in a dose-proportional manner reaching mean levels of 30-60 pmol/g (equivalent to 30-60 nM) at nominal doses ≤ 3 nM whereas mean tissues exposures equivalent to 0.6, 1.7 and 36 µM were achieved at the nominal dose of 0.03, 0.1 and 1 µM, respectively. Interestingly, at all nominal doses tested, similar siponimod levels were measured in "Brain" vs "Body" samples, with a mean Brain/Body ratio of 0.9 ± 0.3.

Siponimod treatments, at nominal doses from 0.1 to 3 nM, improved remyelination in a dose-dependent manner, with a maximal and significant 2.3 ± 0.2 fold increase vs control observed at the nominal dose of 1 nM (i.e. achieving about 60 nM accumulated in tissues over 3 days). At nominal doses >3 nM (i.e. > 60 nM in tissues), the pro-myelination effect of siponimod reduced markedly in a dose-dependent manner, with nearly no trend observed at nominal doses ≥30 nM (i.e. 600 nM accumulated in tissues), revealing an unclassical "bell-shaped" overall dose-response curve for siponimod in this remyelination model (Figure 2A).

In addition to S1P5, siponimod acts also on S1P1, a receptor expressed by microglia. To explore the effect of siponimod treatment on microglial cells transgenic Tg(*mbp:GFP-NTR)*Xenopus were demyelinated by 10 days exposure to metronidazole (10mM) and then returned to either normal water or water containing siponimod (1nM) for 3 days. Optic nerves were dissected and doubly labeled with IB4 isolectin and anti-GFP (Figure 2, B-E). In addition to the expected increase (2.04 fold vs ctrl p= 0.017) in the number of GFP+ cells (Figure 2D) we also observed a 1.81 fold increase (p<0.0001) in the number of IB4-labeled microglial cells (Figure 2E). After 3 days of recovery, microglial cells presented with an elongated morphology, extending their processes along the optic nerve and we did not notice a change in the morphology of microglia upon siponimod treatment (Figure 2, B and C).

To verify that the siponimod-induced increased number of oligodendrocyte (GFP+ cells) translated into increased myelination, optic nerves were dissected and processed for electron microscopy. The number of myelinated axons quantified on semi-thin sections was nearly doubled (1.97 ± 0.14 fold vs ctrl; p =0.042) (Figure 2I) and there was no noticeable morphological changes compared to control conditions (Figure 2, F-H).

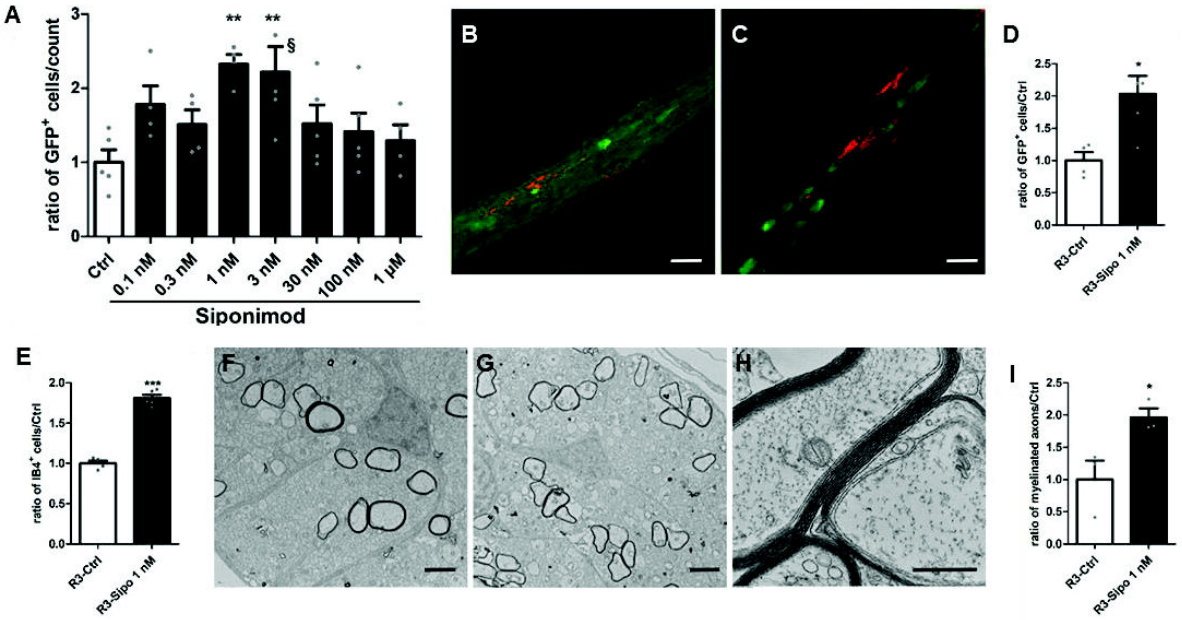

Figure 2. Spontaneous remyelination of transgenic Xenopus laevis with siponimod treatment; effects on microglia, oligodendrocytes and remyelination.
Stage 52-53 transgenic Tg(mbp:GFP-NTR) Xenopus laevis tadpoles were exposed for 10 days in metronidazole (10 mM) before being returned in normal water or water containing increasing concentrations of siponimod. (A) Remyelination was assayed by counting the number of GFP+ oligodendrocytes per optic nerve in vivo on day 3 (R3) of the repair period (n = 5-8 tadpoles per group). (B, C) After demyelination, animals were returned for 3 days to either normal water (Ctrl) or water containing siponimod (1nM). Confocal images of oligodendrocytes (GFP+ green) and microglia (IB4+ red) in the optic nerve following spontaneous recovery (B) or siponimod treatment (C). Quantification of the effects of siponimod treatment on the number of myelin forming (D) oligodendrocytes and (E) microglia (ctrl n=4; siponimod n=6). Electron micrograph of transversally cut optic nerve 3 days after either (F) spontaneous recovery or (G) siponimod treatment. (H) Higher magnification of ongoing remyelination under siponimod treatment showing axons ensheathed with increasing number of myelin wraps. (I) Quantification of the number of myelinated axons per optic nerve following siponimod treatment vs control of spontaneous remyelination (n=5). Data are expressed as mean ± SEM, grey dots show individual data points). **p<0.01 calculated using 1-way ANOVA followed by Dunn's post-hoc test for (A) compared to control (Ctrl) condition. For D, E, I with *p < 0.05, ***p < 0.001 (Student's two-tailed unpaired t test). Scale bars: B+C = 20µm; F-H = 2 µm. §One data points out of axis limits.

Siponimod reduces the disability score and retinal degeneration in an EAEON model

Prior to investigating the effects of siponimod on EAEON we performed a pharmacokinetics study, which demonstrated that treatment by loaded food pellets was superior to supply by drinking water and showed a robust effect on circulating blood cell counts in flow cytometry (eAppendix 1, eFigure 3 and eFigure 4). After observing these promising data in the cuprizone and the *Xenopus laevis* demyelination models, we longitudinally investigated retinal neurodegeneration in MOG_{33-55} peptide induced EAEON in C57BL/6J mice over 90 days in order to test the potential of siponimod to protect from acute inflammatory relapses, as well as chronic degeneration, similar to the progression of SPMS. In this model, prophylactic siponimod treatment acted beneficially on clinical EAE scores with more pronounced effects compared to therapeutic treatment. Siponimod prophylactic diet treatments at 2 and 6 mg/kg BW attenuated the clinical EAE scores by approximately 80% and 95%, respectively. The therapeutic effect was significant with the lower dose (2 mg/kg) at both time points, and when started at d14 almost similar to the prophylactic treatment (Figure 3A). Analyzing the structural changes by OCT, untreated sham control mice showed a nearly constant IRL thickness, while MOG peptide immunized animals presented a prominent loss of IRL thickness until day 90. Prophylactic

siponimod therapy at 2 and 6 mg/kg BW reduced the OCT-measured degeneration of the IRL by approximately 50%. Beneficial effects were observed with therapeutic diet treatments starting at day 14 with 2 mg/kg BW being superior over 6 mg/kg BW ($p<0.01$), but not at day 30 (Figure 3B). Analyzing the visual acuity, a strong decrease of spatial frequency over 90 days of vehicle treated MOG EAE mice was revealed. This was significantly prevented by almost all therapeutic interventions, despite the late treatment (d30) with the higher dose (6 mg/kg) of siponimod (Figure 3C). These effects, measured longitudinally *in vivo,* were well reflected by the investigation of retinal ganglion cell (RGC) survival 90 days post immunization (dpi). Prominent RGC loss of untreated EAE animals was diminished by siponimod prophylactic diet, as well as therapeutic treatment with 2 mg/kg, but not 6 mg/kg starting 14 dpi (Figure 3, D and E).

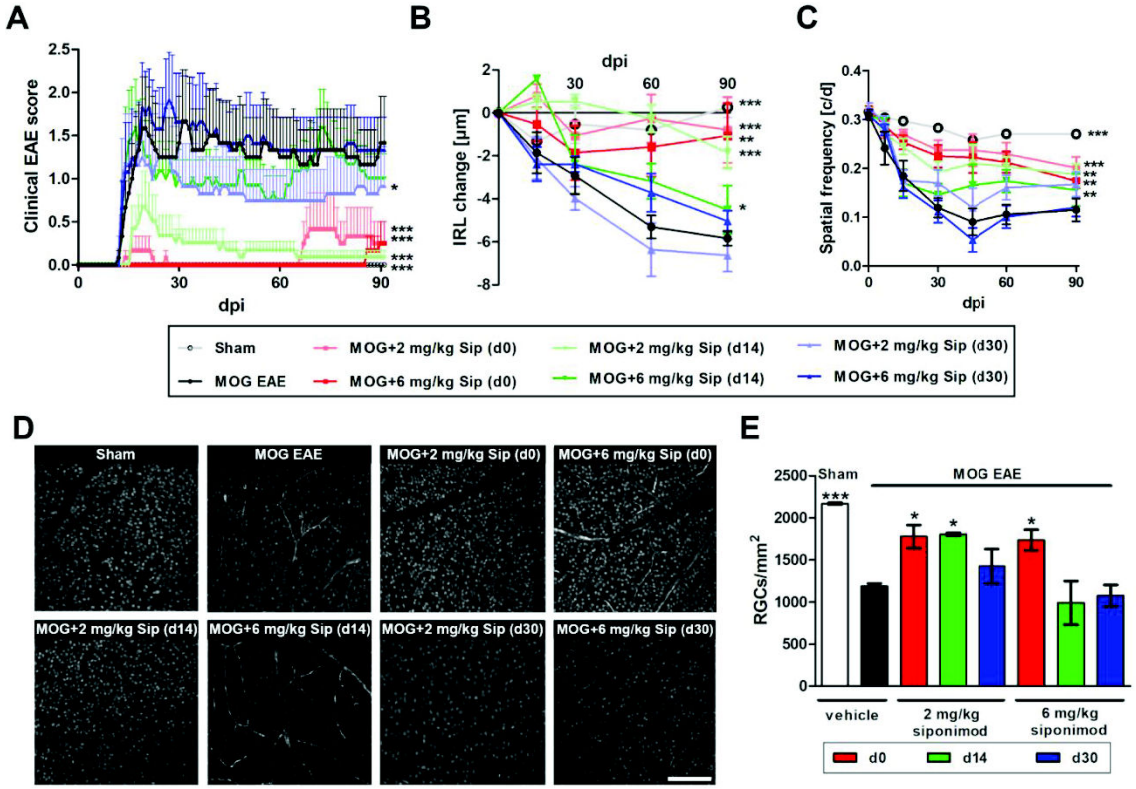

Figure 3. Siponimod attenuates MOG35-55-induced EAE in C57BL/6J mice in a dose and time dependent manner. (A) Clinical EAE score, (B) degeneration of the inner retinal layers and (C) visual function by spatial frequency in cycles per degree (c/d) of female C57BL/6J EAE mice over 90 days of EAE. (D) Brn3a stained RGCs after 90 days of EAE of Sham, MOG EAE and siponimod treated mice, scale bar=200 µm. (E) The bar graph shows the RGC density 90 days after immunization. Siponimod was administered either on the day of immunization (d0), 14 days (d14) or 30 days (d30) post immunization (dpi). All graphs represent the pooled mean ± SEM, grey dots show individual data points (out of two independent experiments each with n = 6 animals per group) with *p<0.05; **p<0.01; ***p<0.001, area under the curve compared by GEE or ANOVA with Dunnett's post hoc test for time courses compared to untreated MOG EAE. *p<0.05, ***p<0.001, by ANOVA with Dunnett's post hoc test compared to MOG EAE untreated mice for the bar graph.

Siponimod prevents inflammation and demyelination of the optic nerve

To assess the effects of siponimod on immune cell infiltration into the CNS during EAE, we performed histological analyses of Iba1$^+$ microglia/macrophages and CD3$^+$ T-cells in longitudinal optic nerve sections (Figure 4A). A significant reduction of microglia/macrophage activity as well as T-cell infiltration was observed in the optic nerves of mice after prophylactic (d0) siponimod treatment compared to untreated EAE mice. Interventions at later time points did not diminish the infiltrating Iba1$^+$ cells. Nevertheless, a therapeutic siponimod treatment at the peak of disease (d14) led to a less severe infiltration of CD3$^+$ lymphocytes compared to MOG EAE vehicle treated mice. When the mice were fed with siponimod loaded pellets from 30 days after MOG immunization, the number of immune cells could not be reduced at 2 or 6 mg/kg BW (Figure 4B). To test the capacity of siponimod to prevent from demyelination, we analyzed the myelin status of the

optic nerve by performing immunohistological stainings against the myelin basic protein (MBP) protein. The axonal tissue of MOG immunized mice presented large areas of demyelination while the optic nerves from untreated sham mice showed a homogeneous myelin structure. The MBP stained lesions in the optic nerve were significantly reduced after a prophylactic siponimod therapy, showing almost the same uniform pattern as sham control animals. Even late siponimod therapy (d14) showed a beneficial effect at 2 mg/kg BW, while a treatment starting at day 30 had no significant effect on the myelin loss during EAEON in C57Bl/6J mice until 90 days after immunization (Figure 4, A and B).

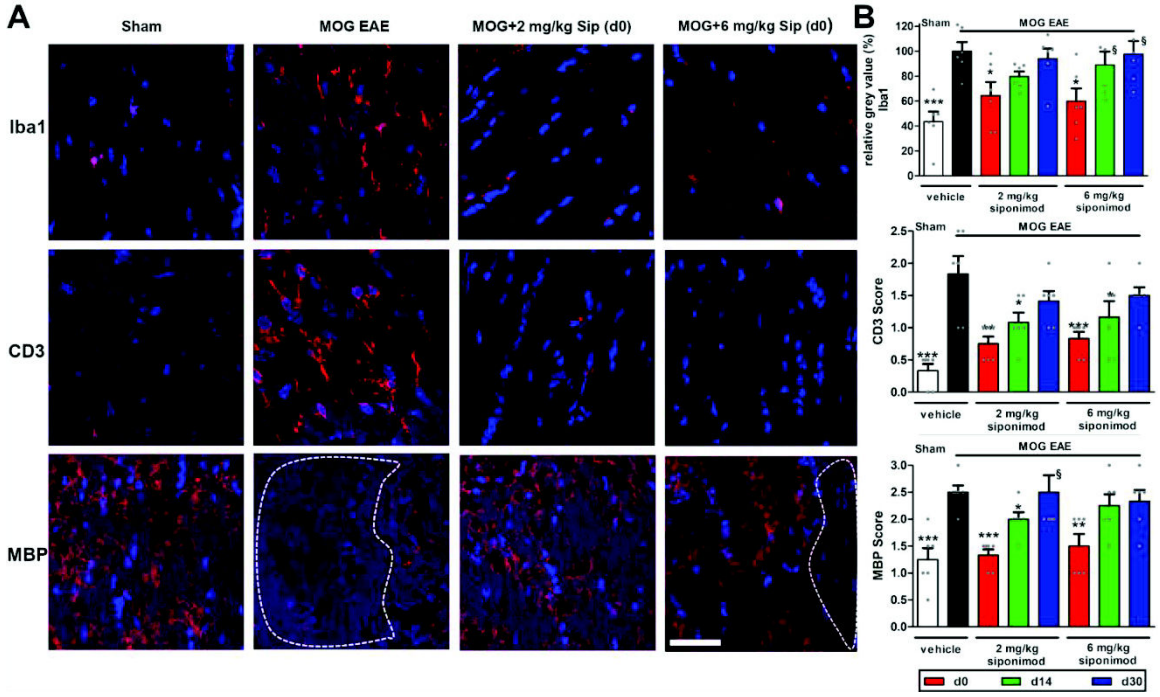

Figure 4. Prophylactic siponimod therapy reduces immune cell infiltration and prevents demyelination.
(A) Longitudinal sections of optic nerves of C57Bl/6J mice were stained for Iba1, CD3 and MBP 90 days after MOG35-55 immunization; dotted lines indicate areas of demyelination, scale bar=50 µm. (B) Quantitative analyses of microglial activation (Iba1) by fluorescence intensity measurement, T-cell infiltration (CD3 score) and myelin status (MBP score). One optic nerve per mouse was included. All graphs represent the pooled mean ± SEM, grey dots show individual data points (n = 6 animals per group out of two independent experiments), with *p<0.05, **p<0.01, ***p<0.001 by ANOVA with Dunnett's post hoc test compared to MOG untreated mice. §Few data points out of axis limits.

Extended analysis of oligodendrocyte populations (Figure 5A) revealed, that siponimod (d14) improved survival of Olig2+ cells in the optic nerve after 35 dpi compared to untreated MOG EAE mice. As a marker for OPCs, PDGRFα stained cells showed no difference in cell number when we compared untreated and siponimod treated EAE mice at 2 and 6 mg/kg BW, while sham control mice had higher OPC numbers at 21 and 35 dpi. Similar as after 90 dpi, early demyelination was reduced after siponimod therapy for both doses (Figure 5B). Increased astrocytosis in the optic nerve, analyzed by GFAP staining, was observed in MOG EAE mice after 21 and 35 dpi while no effect of siponimod was observed (eFigure 5).

In the retina of the mice, we assessed microglia (Iba1) and astrocyte/Mueller cell (GFAP) appearance also 90 days after MOG immunization. We found an increased number of Iba1+ cells in untreated EAEON animals compared to sham mice, but only observed a significant decrease for microglia numbers at the 2 mg/kg BW siponimod dose (d0) (eFigure 6).

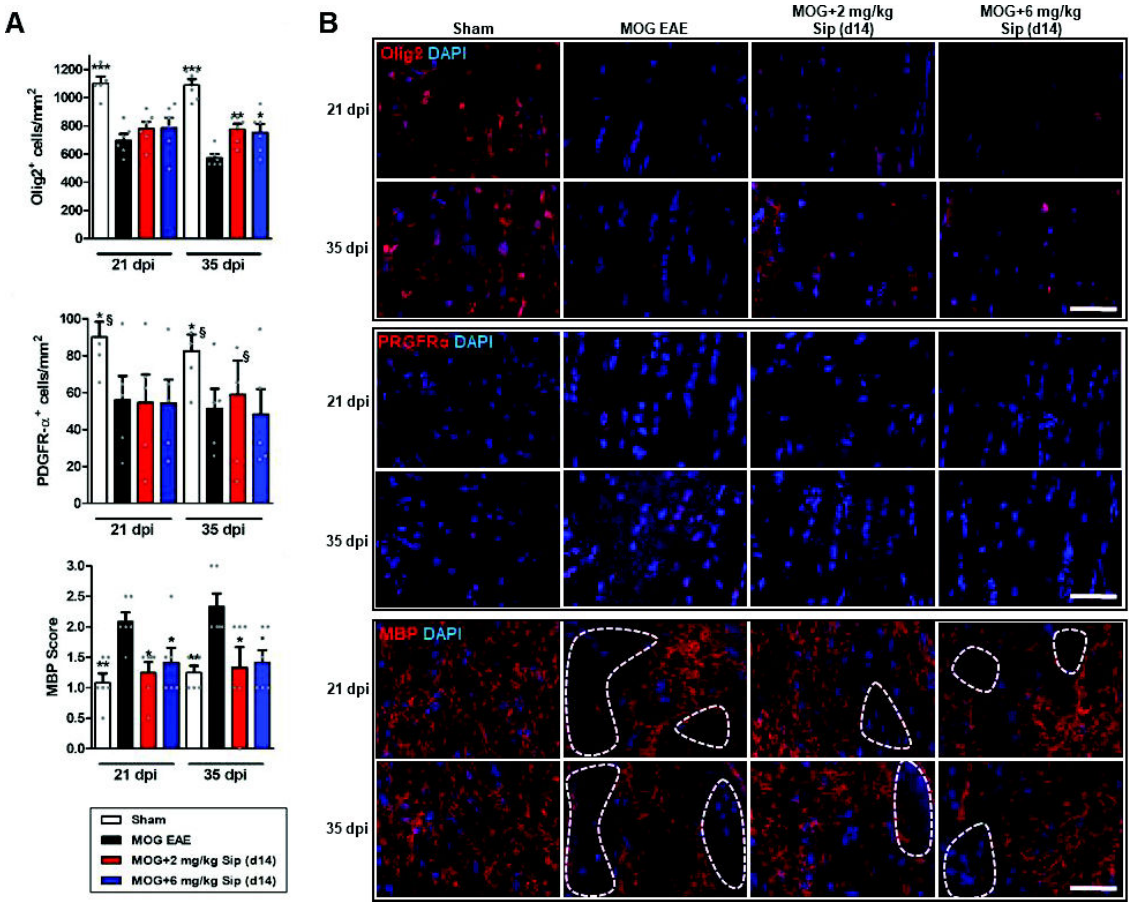

Figure 5. Siponimod also reduces early demyelination but does not alter OPC survival.
(A) Quantitative analysis of longitudinal sections of optic nerves of C57Bl/6J mice, stained for (B) Olig2, PDGFRα and MBP at 21 and 35 days after MOG35-55 immunization, dotted lines indicate areas of demyelination, scale bar=50 µm. One optic nerve per mouse was included histological examination. All graphs represent the pooled mean ± SEM, grey dots show individual data points (n = 6 animals per group out of two independent experiments), with *p<0.05, **p<0.01, ***p<0.001 by ANOVA with Dunnett's post hoc test compared to untreated MOG EAE. §Few data points out of axis limits.

Siponimod shifts microglia to a pro-myelinating phenotype

As siponimod still had beneficial effects on the MBP level even in the therapeutic approach (d14), we expanded the expressional and histological analysis in the optic nerve, testing genes involved in oligodendrocyte as well as microglia regulation. After siponimod treatment (2 mg/kg BW), we found significant upregulation in the optic nerve mRNA expression level 35 dpi of genes marking oligodendrocyte precursor cells NG2 and PDGFR-α, as well as for the markers for resting microglia CD206 and TMEM 119 (eFigure 7), which could however not be corroborated on the protein level by histological examinations. Chitinase 3-like-3 (Chi3l3/Ym1) and arginase-1 (Arg-1) mRNA levels were significantly upregulated 21 and 35 dpi, especially after treatment with 2 mg/kg BW siponimod compared to MOG EAE untreated mice (Figure 6A). Both are markers for regeneration-supporting microglia. Similar results were observed in BV2 cells, a microglial cell line, where Ym1 and Arg-1 mRNA levels were upregulated after siponimod treatment (eFigure 8). Additionally, mRNA levels of TNF-α, a cytokine expressed by activated, pro-inflammatory microglia, was significantly reduced after siponimod therapy compared to untreated EAE mice (Figure 6A). The transcriptional regulation was mirrored by the histological examination of the optic nerve, where Ym1 and Arg-1 were found upregulated 21 and 35 dpi after siponimod treatment with a trend towards a more potent effect of the lower siponimod dose (2 mg/kg BW). TNF-α was significantly upregulated in the optic nerve of EAE animals with a peak at 35 dpi, while mice under siponimod therapy showed a significantly lower expression of TNF-α (Figure 6, B and C).

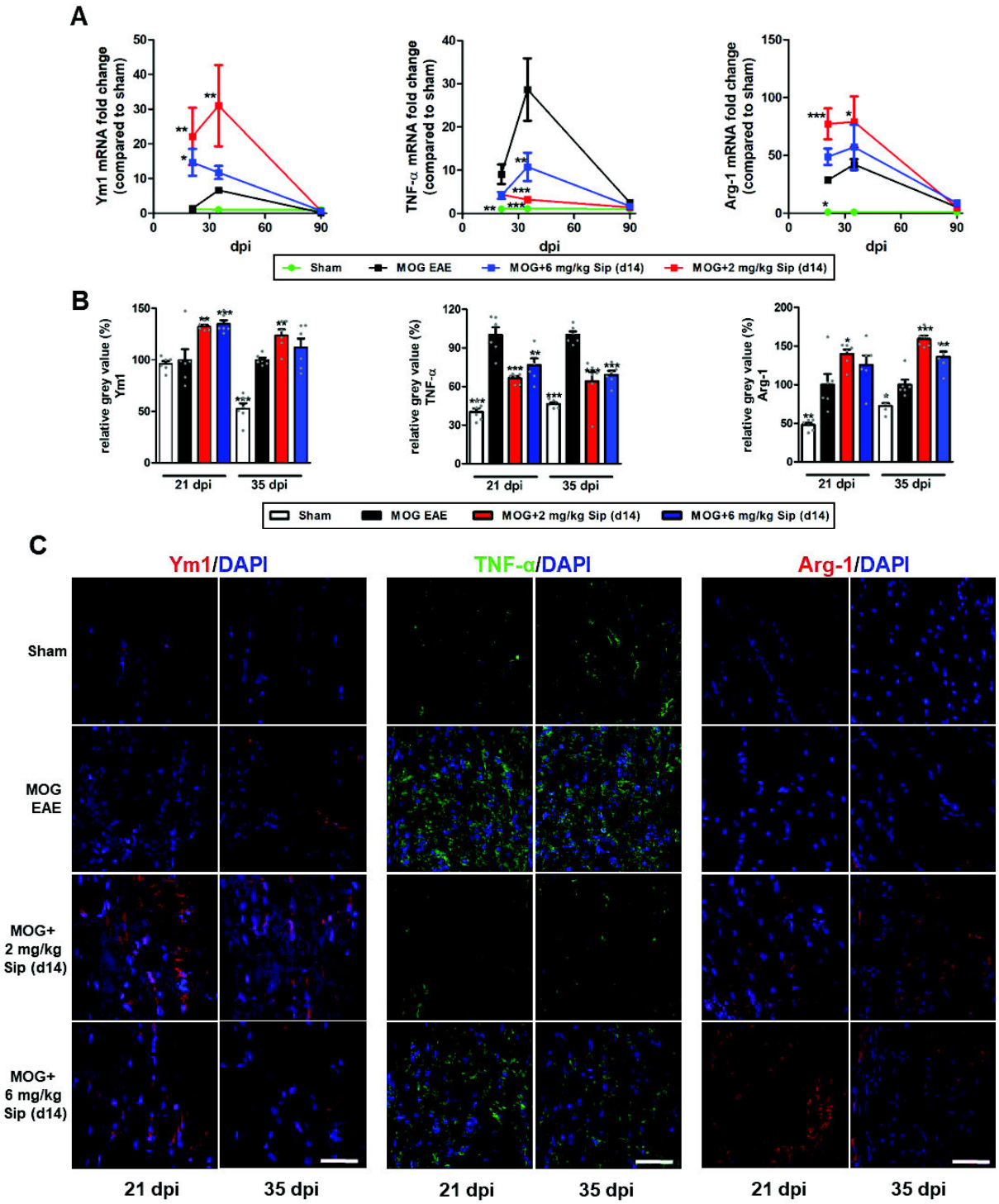

Figure 6. Siponimod therapy shifts microglia to a regenerative phenotype.
(A) qPCR analysis of optic nerve tissue of the microglia related genes Ym1, TNF-α and Arg-1 at 21, 35 and 90 dpi. (B) Quantitative analysis of longitudinal sections of optic nerves of C57Bl/6J mice, stained for (C) Ym1, TNF-α and Arg-1 at 21 and 35 days after MOG35-55 immunization, scale bar=50 µm. One optic nerve per mouse was included for qPCR and histological examination. All graphs represent the pooled mean ± SEM, grey dots show individual data points (n = 6 animals per group out of two independent experiments), with *p<0.05, **p<0.01, ***p<0.001 by area under the curve for time course compared by ANOVA with Dunnett's post hoc test compared to untreated MOG EAE.

RNA sequencing analysis of the EAEON optic nerve reveals downregulation of genes associated to inflammation after siponimod treatment.

In a completely unbiased approach, we used bulk RNA sequencing of the optic nerve of EAEON animals with and without siponimod treatment at 21 dpi, starting the therapy 14 days after immunization (d14). P-values were adjusted for multiple testing to control the false discovery rate (FDR) (pFDR<0.05), fold change (FC) was

set to 1.5. In a heat map, showing the differentially expressed genes (DEGs), sham and MOG EAE animals show a fully altered expression profile, while the DEGs of MOG and siponimod treated mice (2 mg/kg) are more similar (Figure 7A).

Comparing sham to MOG EAE animals, an upregulation of 2109 gens and a downregulation of 623 genes was observed, displayed in a volcano plot (Figure 7B). After the siponimod treatment, we found a downregulation of 129 genes and an upregulation of one gene after treatment with 2 mg/kg BW siponimod (Figure 7C) and a downregulation of 106 genes with 6 mg/kg BW siponimod compared to untreated MOG EAE control. The five most differentially expressed genes associated to inflammation are summarized in eTable 2.

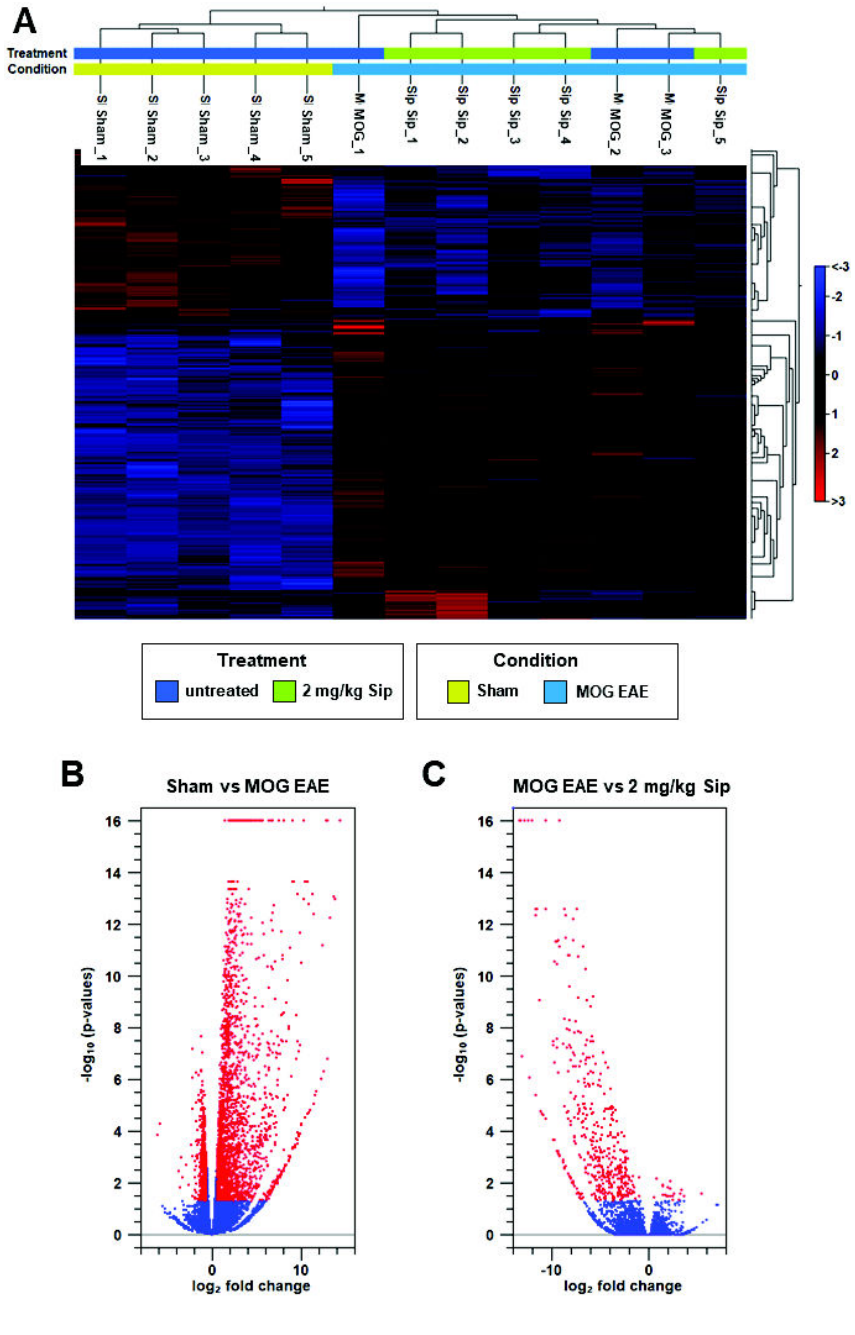

Figure 7. Gene expression profile of optic nerves of MOG EAE and siponimod treated mice 21 dpi.
(A) Hierarchical clustering of DEGs after sham, MOG EAE and MOG with 2 mg/kg BW siponimod treatment. Red indicates increased expression and blue indicates decreased expression. Differences in expression were set to FC ≥ 1.5 with p(FDR)<0,05. Volcano plot showing differentially expressed genes 21 dpi for (B) sham compared to MOG EAE animals and (C) MOG EAE compared to MOG with 2 mg/kg siponimod. For each plot, the X-axis represents log2 FC and the Y-axis represents -log10 (p-values). DEGs are shown as red dots.

Discussion

While the early disease progression in MS can be effectively prevented or mitigated by immunomodulatory therapy, there is still an unmet need for remyelinating strategies and substances to attenuate or inhibit the degeneration occurring in the later stages.[28] Siponimod has recently demonstrated efficacy in SPMS.[1]

As a first step, the remyelinating potential of siponimod after toxic demyelination by cuprizone was investigated by magnetic resonance imaging (MRI) of the corpus callosum. MTR and T2-WSI measurements at one week after cuprizone withdrawal demonstrated significant beneficial effects of siponimod treatment on CC integrity. Other studies with the more unspecific S1P1 receptor modulator fingolimod reported a downregulation of S1PR1 brain levels, and fingolimod-treated mice presented more oligodendrocytes in the secondary motor cortex after three weeks of remyelination. However, no differences in remyelination or axonal damage were observed compared to placebo.[29] In a novel MS model, a combination of EAE and cuprizone intoxication, siponimod mitigated the extent of demyelination.[30]

To further assess the remyelinating potential of siponimod, we used an inducible experimental model developed in *Xenopus laevis*. After demyelination of the Xenopus tadpoles over 10 days, spontaneous remyelination occurred. However, remyelination was significantly accelerated by siponimod in a bell-shaped dose-response curve. We had previously shown that in both the mouse and Xenopus brain S1PR5 is only expressed by oligodendrocytes, and that the remyelinating potency of siponimod is lost upon deletion of S1PR5.[15,31] It is therefore likely that the mechanism of action of siponimod-induced remyelination is by activating the myelination program of oligodendrocyte through activation of S1PR5. In addition, as S1P1 is also expressed on microglia,[32] a cell population required during spontaneous remyelination,[33] we also investigated their regulation after siponimod treatment. An increased number of $IB4^+$ microglia was observed presenting an elongated morphology 3 days after recovery. In line with this hypothesis, recent observations suggest that, in contrast to the S1P1 receptor, the S1P5 receptor is not subject to agonist-induced down-modulation and that siponimod should be considered as a true S1P5-agonist.[34] In this case, a phenomenon such as S1P5-desensitization at supra-maximal stimulation could be suspected to explain the bell-shaped curve for the pro-myelination effect of siponimod.

After these promising results we then moved to mouse EAE models in order to investigate the effects in a more disease specific model with translational potential. Siponimod crosses the blood-brain barrier and targets different S1P receptor subtypes, associated with T-cell migration into the CNS, astrogliosis, repair mechanisms via modulation of S1PR5 on oligodendrocytes and cell survival.[35,36] Hence, the EAEON model in mice appears as a perfectly suited mechanistic tool to assess the impact of siponimod on all these central effects. In this model, a significant attenuation of the clinical EAE score with 2 and 6 mg/kg BW was observed, when the therapy was initiated at the day of immunization, in line with previous approaches, using various EAE models in mice and rats.[2,37–39] To explore effects of siponimod beyond its immunomodulatory capacity we not only used different dosing paradigms but also started the siponimod diet at prophylactic (d0) and early or late therapeutic (d14/d30) time points. Other studies addressing similar issues varied only one of these parameters and started treatment no later than 8 days after EAE immunization.[38] A significant beneficial effect on the EAE score was observed when treatment was started at day 14 and 30 after MOG immunization, but surprisingly only with the lower concentration (2 mg/kg BW), indicating a bell-shaped dose-effect curve. We already identified the same dose-dependency in a rat $MOG_{28–152}$ induced EAE in C57Bl/6J mice, where the same dosing (10 mg/kg food or 2 mg/kg BW) led to the most effective reduction of the EAE score of 72.5%[18,20] with

robust dose-proportional CNS penetration and distribution for siponimod.[18] As preclinical study designs with readouts directly transferable to clinical trials are of increasing interest and other preclinical studies on siponimod's central effects lack of these techniques, we included visual system measurements to evaluate the results. The IRL, consisting of the RNFL, GCL and IPL containing the axons of the optic nerve, ganglion cells and their dendritic arbor, is the ideal structure to study neuroprotection and retinal degeneration in MS,[6,9,40] as well as in preclinical EAEON studies.[10–12,17,41] As functional readout, the OMR is a suitable measure for the visual acuity in rodents.[17,23,42] While IRL degeneration was attenuated by a prophylactic and a therapeutic 2 mg/kg BW treatment starting 14 dpi, the visual function was even preserved by a therapeutic regimen starting at 30 dpi. This observation was mirrored by the number of RGCs, where the loss of these cells was significantly diminished by prophylactic, but also therapeutic siponimod therapy, mainly by the lower dose of 2 mg/kg BW, also observed in similar studies.[43–45]

The reduced number of circulating T-cells led to a decreased infiltration of $CD3^+$ cells into the optic nerve, if the intervention was started not later than d14. A therapy at d30 still reduced the circulating T-cells by a significant level, but the infiltration into the optic nerve, mainly occurring around day 11-14 at the peak of the EAEON,[41] could not be prevented. Anti-demyelinating effects, also observed by other researchers in mouse organotypic slice cultures,[36] were detected after prophylactic siponimod treatment at both doses and interestingly also after therapeutic treatment with 2 mg/kg BW. As S1P receptors, with the exception of S1P5, are also expressed on microglia cells,[32] we expected a reduced number of Iba1 positive cells in the optic nerve after siponimod treatment. However, this effect was only observed after prophylactic therapy, which can be explained by the fact, that microgliosis is already present as early as 7 dpi in EAEON.[41] We therefore extended the histological investigations, on genes associated to oligodendrocyte and microglia regulation. We found no transcriptional regulation of genes regulating oligodendrocyte maturation and myelination at the early time points of 21 and 35 dpi. On the other hand, histological stainings of the optic nerve revealed an improved Olig2+ cell survival at 35 dpi and a less pronounced demyelination at 21 and 35 dpi, measured by the MBP score, similar as at the endpoint of 90 dpi. Together with the result, that no regulation of PDGFR α positive cells by siponimod was found, this indicates an effect of the drug on mature oligodendrocytes rather than on OPCs. Furthermore, we observed significant upregulation of the microglia regenerative markers Ym1 and Arg-1 and a downregulation of the pro-inflammatory cytokine TNF-α on a transcriptional and translational level at 21 and 35 dpi after siponimod therapy in the optic nerve. In mice, Ym1 is highly expressed in inflammatory brain lesions during EAE and has been demonstrated to induce oligodendrogenesis.[46] Thus, it seems reasonable to assume that the observed beneficial effects of siponimod on myelin status observed at 90 dpi may, at least in part, be resulting from its effects on microglial cells, shifting them to a pro-myelinating phenotype. This is in line with the assumption that the beneficial effects of siponimod go beyond lymphocyte trafficking and rely on its interactions with other cells of the CNS, like astrocytes and neurons, as the drug crosses the blood-brain barrier and S1P receptors are expressed on almost all CNS cell types.[47]

In addition to the targeted investigations of oligodendroglial and microglial genes and proteins, we also applied an unbiased approach, analyzing the transcriptome of the optic nerve by bulk RNAseq. It was striking, that 129 and 106 genes were downregulated, while only one and no gene was upregulated after 2 and 6 mg/kg BW siponimod treatment in EAEON, respectively. Significantly downregulated genes potentially altering the disease progression were associated to inflammation. We decided to perform a bulk RNAseq of the whole optic nerve to receive a cell-unspecific, unbiased overview on DEGs after siponimod treatment of EAEON

mice. However, a more targeted approach sequencing single cells, such as oligodendrocytes, microglia or astrocytes, might have led to more homogeneous and conclusive results. As we focused our EAEON study on *in vivo* readouts of the visual system the histology and transcriptomic analyses were also focused on the optic nerve. We acknowledge that also investigating the spinal cord may have yielded additional information but this would have been beyond the focus of this study.

Taken together these observations suggest a beneficial effect of siponimod in the CNS by shifting microglia to a regenerative phenotype and protective effect on oligodendrocytes, in line with the pro-remyelination effects observed in the *Xenopus laevis* model.

In summary, siponimod demonstrated increased remyelination in CC in the cuprizone demyelination model, pro-remyelination potential in the Xenopus model and strong prophylactic and therapeutic effects in the mouse EAEON, as revealed by visual (functional and structural) readouts. Having used three experimental models in two different animal species strengthens our results in favor of a remyelinating potential for siponimod in MS.

Funding

This work was supported by grants to PA from Novartis Pharma GmbH, the charitable Ilselore-Lückow Stiftung and the charitable Dr.-Robert-Pfleger Stiftung. The study was partially funded by a research grant from Novartis to BZ and the European Union's Horizon 2020 Research and Innovation Programme ENDpoiNTs project Grant Agreement number: 825759 and grant BRECOMY funded jointly by DFG and ANR to BZ..

Disclosures

MD received speaker honoraria from Merck. MG has received honoraria for speaking/consultation from Bayer Healthcare, Boehringer Ingelheim and a research grant from B. Braun, outside the submitted work. BS has received compensation for boards and/or lectures from Biogen, Sanofi-Genzyme, Novartis and Teva, and research grants from Merck, Roche, and Sanofi-Genzyme. CL has participated to advisory boards for Vertex, Roche, Biogen, Novartis, Genzyme, Merck, and speaking honoraria from Ipsen and Biogen. PG performed consultancy work for GeNeuro and received support from the Research Commission of the medical faculty of the Heinrich Heine University. HPH has received fees for serving on steering and data monitoring committees from Bayer Healthcare, Biogen, Celgene BMS, CSL Behring, GeNeuro, MedImmune, Merck, Novartis, Octapharma, Roche, Sanofi Genzyme, TG Therapeutic sand Viela Bio; fees for serving on advisory boards from Biogen, Sanofi Genzyme, Merck, Novartis, Octapharma, and Roche; and lecture fees from Biogen, Celgene BMS, Merck, Novartis, Roche, Sanofi Genzyme. PK performed consultancy work for GeNeuro and received support from Sanofi Genzyme, French societies ARSEP and AFM, Deutsche Forschungsgemeinschaft (DFG; grants KU1934/2_1, KU1934/5-1), Stifterverband/Novartisstiftung and from James and Elisabeth Cloppenburg, Peek and Cloppenburg Düsseldorf Stiftung. SGM received honoraria for lecturing and travel expenses for attending meetings from Almirall, Amicus Therapeutics Germany, Bayer Health Care, Biogen, Celgene, Diamed, Genzyme, MedDay Pharmaceuticals, Merck Serono, Novartis, Novo Nordisk, ONO Pharma, Roche, Sanofi-Aventis, Chugai Pharma, QuintilesIMS, and Teva. His research is funded by the German Ministry for Education and Research (BMBF), Deutsche Forschungsgemeinschaft (DFG), Else Kröner Fresenius Foundation, German Academic Exchange Service, Hertie Foundation, Interdisciplinary Center for Clinical Studies (IZKF) Muenster, German Foundation Neurology, and by Almirall,

Amicus Therapeutics Germany, Biogen, Diamed, Fresenius Medical Care, Genzyme, Merck Serono, Novartis, ONO Pharma, Roche, and Teva. BZ received research support from Novartis and Merck and travel grant from Merck. PA received compensation for serving on Scientific Advisory Boards for Ipsen, Novartis, Biogen; he received speaker honoraria and travel support from Novartis, Teva, Biogen, Merz Pharmaceuticals, Ipsen, Allergan, Bayer Healthcare, Esai, UCB and Glaxo Smith Kline; he received research support from Novartis, Biogen, Teva, Merz Pharmaceuticals, Ipsen, and Roche. PR, CB, ST, NB, DS and MB are employees of the Novartis Institutes for BioMedical Research. The other authors report no disclosures.

Acknowledgments

France: We thank ARSEP foundation, FRM (Fondation pour la Recherche Médicale), Bouvet-Labruyere Family, INSERM-DHOS, APHP (Assistance Publique des Hôpitaux de Paris), the program “Investissements d’Avenir” ANR-10-IAIHU-06, NeurATRIS, ANR grant BRECOMY to B.Z. and NRJ foundation for their precious support related to basic and clinical research on remyelination in Paris. Novartis: We thank Claire Moebs, Catherine Afatsawo, Desrayaud Sandrine, Hager Claude, Neuhaus Anna, Lang Meike, Perrot Ludovic, Rudin Stefan, Wipfli Peter and Zurbruegg Stefan for their key scientific and operational support.
Germany: Computational support of the Zentrum für Informations- und Medientechnologie, especially the HPC team (High Performance Computing) at the Heinrich-Heine University is acknowledged. We also thank Thorsten Wachtmeister for technical support and Zippora Kohne for technical assistance.

References

1. Kappos L, Bar-Or A, Cree BAC, et al. Siponimod versus placebo in secondary progressive multiple sclerosis (EXPAND): A double-blind, randomised, phase 3 study. *Lancet*. 2018;391(10127):1263–1273.
2. Gentile A, Musella A, Bullitta S, et al. Siponimod (BAF312) prevents synaptic neurodegeneration in experimental multiple sclerosis. *J. Neuroinflammation*. 2016;13(1):207.
3. Lubetzki C, Zalc B, Williams A, Stadelmann C, Stankoff B. Remyelination in multiple sclerosis: from basic science to clinical translation. *Lancet Neurol.* 2020;19(8):678–688.
4. Franklin RJM, Ffrench-Constant C. Regenerating CNS myelin - from mechanisms to experimental medicines. *Nat. Rev. Neurosci.* 2017;18(12):753–769.
5. Zhan J, Mann T, Joost S, Behrangi N, Frank M, Kipp M. The Cuprizone Model: Dos and Do Nots. *Cells*. 2020;9(4).
6. Albrecht P, Ringelstein M, Muller AK, et al. Degeneration of retinal layers in multiple sclerosis subtypes quantified by optical coherence tomography. *Mult. Scler.* 2012;18(10):1422–1429.
7. Gabilondo I, Martinez-Lapiscina EH, Martinez-Heras E, et al. Trans-synaptic axonal degeneration in the visual pathway in multiple sclerosis. *Ann. Neurol.* 2014;75(1):98–107.
8. Saidha S, Al-Louzi O, Ratchford JN, et al. Optical coherence tomography reflects brain atrophy in multiple sclerosis: A four-year study. *Ann Neurol*. 2015;78(5):801–813.
9. Albrecht P, Fröhlich R, Hartung H-P, Kieseier BC, Methner A. Optical coherence tomography measures axonal loss in multiple sclerosis independently of optic neuritis. *J. Neurol.* 2007;254(11):1595–1596.
10. Dietrich M, Koska V, Hecker C, et al. Protective effects of 4-aminopyridine in experimental optic neuritis and multiple sclerosis. *Brain*. 2020;143(4):1127–1142.
11. Cruz-Herranz A, Dietrich M, Hilla AM, et al. Monitoring retinal changes with optical coherence tomography predicts neuronal loss in experimental autoimmune encephalomyelitis. *J. Neuroinflammation*. 2019;16(1):203.
12. Knier B, Rothhammer V, Heink S, et al. Neutralizing IL-17 protects the optic nerve from autoimmune pathology and prevents retinal nerve fiber layer atrophy during experimental autoimmune encephalomyelitis. *J. Autoimmun.* 2014;56:34–44.
13. Diem R, Molnar F, Beisse F, et al. Treatment of optic neuritis with erythropoietin (TONE): A randomised, double-blind, placebo-controlled trial-study protocol. *BMJ Open*. 2016;6(3):e010956.
14. Kaya F, Mannioui A, Chesneau A, et al. Live imaging of targeted cell ablation in Xenopus: A new model to study demyelination and repair. *J. Neurosci.* 2012;32(37):12885–12895.
15. Mannioui A, Vauzanges Q, Fini JB, et al. The Xenopus tadpole: An in vivo model to screen drugs favoring remyelination. *Mult. Scler.* 2018;24(11):1421–1432.
16. Martin E, Aigrot M-S, Grenningloh R, et al. Bruton's Tyrosine Kinase Inhibition Promotes Myelin Repair. *Brain Plast*. 2020;5(2):123–133.
17. Dietrich M, Helling N, Hilla A, et al. Early alpha-lipoic acid therapy protects from degeneration of the inner retinal layers and vision loss in an experimental autoimmune encephalomyelitis-optic neuritis model. *J. Neuroinflammation*. 2018;15(1):71.
18. Bigaud M, Rudolph B, Briard E, et al. Siponimod (BAF312) penetrates, distributes, and acts in the central nervous system: Preclinical insights. *Mult Scler J Exp Transl Clin*. 2021;7(4):20552173211049168.

19. Bachmanov AA, Reed DR, Beauchamp GK, Tordoff MG. Food intake, water intake, and drinking spout side preference of 28 mouse strains. *Behav. Genet.* 2002;32(6):435–443.
20. Bigaud M, Perdoux J, Ramseier P, Tisserand S, Urban B, Beerli C. Pharmacokinetic/Pharmacodynamic Characterization of Siponimod (BAF312) in Blood versus Brain in Experimental Autoimmune Encephalomyelitis Mice (P2.2-066). *Neurology*. 2019;92:15 Supplement. https://n.neurology.org/content/92/15_Supplement/P2.2-066.
21. Bigaud M, Tisserand S, Ramseier P, et al. Differentiated pharmacokinetic/pharmacodynamic (PK/PD) profiles for Siponimod (BAF312) versus Fingolimod. Poster (P622) presented at: 35th Congress of the European Committee for Treatment and Research in Multiple Sclerosis, September 11-13, 2019, Stockholm, Sweden.
22. Dietrich M, Cruz-Herranz A, Yiu H, et al. Whole-body positional manipulators for ocular imaging of anaesthetised mice and rats: A do-it-yourself guide. *BMJ Open Ophthalmol.* 2017;1(1):e000008.
23. Dietrich M, Hecker C, Hilla A, et al. Using Optical Coherence Tomography and Optokinetic Response As Structural and Functional Visual System Readouts in Mice and Rats. *J. Vis. Exp.* 2019;143.
24. Cruz-Herranz A, Balk LJ, Oberwahrenbrock T, et al. The APOSTEL recommendations for reporting quantitative optical coherence tomography studies. *Neurology*. 2016;86(24):2303–2309.
25. Prusky GT, Alam NM, Beekman S, Douglas RM. Rapid quantification of adult and developing mouse spatial vision using a virtual optomotor system. *Invest. Ophthalmol. Vis. Sci.* 2004;45(12):4611–4616.
26. Lewerenz J, Albrecht P, Tien M-LT, et al. Induction of Nrf2 and xCT are involved in the action of the neuroprotective antibiotic ceftriaxone in vitro. *J. Neurochem.* 2009;111(2):332–343.
27. Beckmann N, Giorgetti E, Neuhaus A, et al. Brain region-specific enhancement of remyelination and prevention of demyelination by the CSF1R kinase inhibitor BLZ945. *Acta Neuropathol. Commun.* 2018;6(1):9.
28. Vargas DL, Tyor WR. Update on disease-modifying therapies for multiple sclerosis. *J. Investig. Med.* 2017;65(5):883–891.
29. Nystad AE, Lereim RR, Wergeland S, et al. Fingolimod downregulates brain sphingosine-1-phosphate receptor 1 levels but does not promote remyelination or neuroprotection in the cuprizone model. *J. Neuroimmunol.* 2020;339:577091.
30. Behrangi N, Atanasova D, Kipp M. Siponimod ameliorates inflammation and axonal injury in a novel multiple sclerosis model. 2019. Poster (P512) presented at: 35th Congress of the European Committee for Treatment and Research in Multiple Sclerosis, September 11-13, 2019, Stockholm, Sweden.
31. Jaillard C, Harrison S, Stankoff B, et al. Edg8/S1P5: An oligodendroglial receptor with dual function on process retraction and cell survival. *J. Neurosci.* 2005;25(6):1459–1469. Available at: https://pubmed.ncbi.nlm.nih.gov/15703400.
32. Tham C-S, Lin F-F, Rao TS, Yu N, Webb M. Microglial activation state and lysophospholipid acid receptor expression. *Int. J. Dev. Neurosci.* 2003;21(8):431–443.
33. Miron VE, Boyd A, Zhao J-W, et al. M2 microglia and macrophages drive oligodendrocyte differentiation during CNS remyelination. *Nat. Neurosci.* 2013;16(9):1211–1218.
34. Bigaud M, Tisserand S, Fuchs-Loesle P, Guerini D. The S1P5 receptor is not down-modulated in response to selective agonists. 2018. Poster (EP1617) presented at: 34th Congress of the European Committee for Treatment and Research in Multiple Sclerosis, October 10-12, 2019; Berlin, Germany.

35. Bigaud M, Guerini D, Billich A, Bassilana F, Brinkmann V. Second generation S1P pathway modulators: Research strategies and clinical developments. *Biochim. Biophys. Acta*. 2014;1841(5):745–758.
36. O'Sullivan C, Schubart A, Mir AK, Dev KK. The dual S1PR1/S1PR5 drug BAF312 (Siponimod) attenuates demyelination in organotypic slice cultures. *J. Neuroinflammation*. 2016;13:31.
37. Gergely P, Nuesslein-Hildesheim B, Guerini D, et al. The selective sphingosine 1-phosphate receptor modulator BAF312 redirects lymphocyte distribution and has species-specific effects on heart rate. *Br. J. Pharmacol.* 2012;167(5):1035–1047.
38. Ward LA, Lee DS, Sharma A, et al. Siponimod therapy implicates Th17 cells in a preclinical model of subpial cortical injury. *JCI Insight*. 2020;5(1).
39. Hundehege P, Cerina M, Eichler S, et al. The next-generation sphingosine-1 receptor modulator BAF312 (siponimod) improves cortical network functionality in focal autoimmune encephalomyelitis. *Neural Regen. Res.* 2019;14(11):1950–1960.
40. Dietrich M, Aktas O, Hartung H-P, Albrecht P. Assessing the anterior visual pathway in optic neuritis: Recent experimental and clinical aspects. *Curr. Opin. Neurol.* 2019;32(1):346–357.
41. Manogaran P, Samardzija M, Schad AN, et al. Retinal pathology in experimental optic neuritis is characterized by retrograde degeneration and gliosis. *Acta Neuropathol. Commun.* 2019;7(1):116.
42. Hecker C, Dietrich M, Issberner A, Hartung H-P, Albrecht P. Comparison of different optomotor response readouts for visual testing in experimental autoimmune encephalomyelitis-optic neuritis. *J. Neuroinflammation*. 2020;17(1):216.
43. McDougald DS, Dine KE, Zezulin AU, Bennett J, Shindler KS. SIRT1 and NRF2 Gene Transfer Mediate Distinct Neuroprotective Effects Upon Retinal Ganglion Cell Survival and Function in Experimental Optic Neuritis. *Invest. Ophthalmol. Vis. Sci.* 2018;59(3):1212–1220.
44. Smith AW, Rohrer B, Wheless L, et al. Calpain inhibition reduces structural and functional impairment of retinal ganglion cells in experimental optic neuritis. *J. Neurochem.* 2016;139(2):270–284.
45. Larabee CM, Desai S, Agasing A, et al. Loss of Nrf2 exacerbates the visual deficits and optic neuritis elicited by experimental autoimmune encephalomyelitis. *Mol. Vis.* 2016;22:1503–1513.
46. Starossom SC, Campo Garcia J, Woelfle T, et al. Chi3l3 induces oligodendrogenesis in an experimental model of autoimmune neuroinflammation. *Nat. Commun.* 2019;10(1):217.
47. Behrangi N, Fischbach F, Kipp M. Mechanism of Siponimod: Anti-Inflammatory and Neuroprotective Mode of Action. *Cells*. 2019;8(1):24.

Appendix

Supplementary Methods

Histological examination and analysis of cuprizone-treated mice

All mice were sacrificed on the last day of week 7 and intra-cardially perfused with PBS (3 min 4-5 ml/min) and 4% PFA (4 min 4-5 ml/min) and the brains were removed. The whole forebrains were put in 4% PFA for 48 h at 4°C. After fixation brains were processed for paraffin embedding by dehydration through increasing ethanol series. Automated immunohistochemistry of paraffin sections was performed on 3 µm paraffin sections mounted on SuperFrost+ slides (Thermo Fisher Scientific) and automatically immuno-stained using the Discovery XT technology (Ventana, Roche Diagnostics). Sections were de-paraffinized, re-hydrated, subjected to antigen retrieval by heating with CC1 cell conditioning buffer for 28–68 min according to the antibody, incubated for 1–3 h depending on the antibody at room temperature with the primary antibody diluted in antibody diluent (Ventana), incubated with the respective biotinylated secondary antibody diluted in antibody diluent, reacted with the DAB- Mab kit and counterstained with Hematoxylin II and Bluing reagent (Ventana). Slides were washed with soap in hot tap water and rinsed under cold running tap water to remove the soap, then dehydrated and embedded with Pertex.

For LFB staining, slides were de-paraffinized and rehydrated with 95% ethanol. Slides were then incubated in LFB solution (Solvent Blue 38 (Sigma S3382) in 95% ethanol and 10% acetic acid (Sigma 695092)) overnight at 60 °C, rinsed in 95% ethanol for 1 min, then in distilled water for 2 min and in 0.05% lithium carbonate for 5 s. Subsequently, slides were rinsed in 70% ethanol twice for 10 s, then in distilled water for 2 min. The rinsing was repeated in 0.05% lithium carbonate (Merck 105680) prepared freshly, 70% ethanol and distilled water until there was a sharp contrast between the blue of the white matter (myelin) and the colorless grey- matter. Finally, slides were dehydrated starting with 95% ethanol and mounted in Pertex.

The primary antibody was a rabbit anti-mouse GST-π (MBL 312) 1:500. Secondary detection antibody: Goat anti-rabbit IgG biotinylated (Jackson ImmunoResearch 111–065-144; Jackson ImmunoResearch Europe Ltd, Ely, UK) 1:1000.

Xenopus laevis demyelination model and metronidazole preparation

In this model, myelinating oligodendrocytes selectively express both the GFP reporter and the bacterial nitroreductase (NTR) enzyme, under the control of a portion of mouse *Mbp* regulatory sequence.[1] The NTR enzyme converts the nitro radical of prodrugs, such as metronidazole (MTZ), to a highly cytotoxic hydroxylamine derivative; therefore, introduction of MTZ into the swimming water of transgenic *Mbp:GFP-NTR* tadpoles provokes an oligodendrocyte cell-death.[1,2] Xenopus tadpoles were staged according to Nieuwkoop and Faber.[3] Transgenic tadpoles were treated between stages NF 50 and 55, corresponding to pre-metamorphosis, a stage of ongoing myelination.

MTZ (Fluka) was dissolved in filtered tap water containing 0.1% DMSO (Sigma Aldrich). MTZ was used at a concentration of 10 mM with an exposure length of 10 days. Transgenic or non-transgenic sibling tadpoles were maintained in 600 ml of MTZ solution (maximum 10 tadpoles/600 ml) at 20˚C in complete darkness (MTZ is light-sensitive) and the solution was changed daily throughout the duration of treatment. For regeneration experiments, MTZ-exposed animals were allowed to recover for 3 days in either normal water (control) or water containing siponimod at increasing concentrations in ambient laboratory lighting (12 h light/12 h dark).

Pharmacokinetics study in C57Bl/6J mice

Female, 6-weeks old C57Bl/6J mice (Janvier Labs, Le Genest-Saint-Isle, France) were treated for two weeks with siponimod (BAF312) at 0.3, 1.5 or 3 mg/kg BW, or vehicle (DMSO:H_2O, 1:20), via drinking water or were fed over four weeks with siponimod-loaded pellets at 0.03, 0.1 and 0.2 g/kg of food for the concentration analysis and 0.3, 0.1, 0.03, and 0.01 g/kg of food for a second concentration analysis and the lymphocyte counts. Siponimod-loaded pellets were prepared as previously described.[4] Briefly, dry powdered food (~500 g) for rodents (Provimi Kliba SA, Switzerland) was mixed with siponimod at the final concentrations. The whole mixing procedure was conducted in a fume cupboard as a safety precaution to avoid dust inhalation. Whilst still mixing, 250 ml water was gradually added and final mixture was loaded into a custom-built extruder for compression into a long cylinder of food mixture (~ 1.5 cm in diameter) which was broken by hand in pieces of approximately 2 to 4 cm in length. These food-pellets were left to dry on a metal grid overnight, at 35 °C, in a food-dehydrator (Excalibur®). Drug-free pellets were prepared similarly for controls. All pellets were stored at room temperature and prepared fresh every 2 weeks.

Blood samples were collected (via tail nick) in short intervals and at termination to assess blood siponimod levels by LC/MS/MS (explained below) and lymphocytes counts using Vet ABC™ (scil animal care, Germany) or ADVIA™ hematology analyzers (Siemens Healthineers, Germany).

Results were analyzed by using one-way Anova Holm-Sidak's multiple comparisons test (GraphPad Prism Software Inc., San Diego, California, USA). A value of $p < 0.05$ was considered significant.

Tissues sampling for measurements of siponimod exposures in Xenopus tadpoles

At end of studies, i.e. 3 days after stopping MTZ, tadpoles were euthanized, put on ice and cut in two, separating the head (mainly brain) from the rest of the body. The “Body” parts were weighed (approx. 1 g each), distributed to individual Eppendorf tubes and snap-frozen in liquid N2. Concerning the “Brain” parts, due to their very small size (≤3 mg), they were mixed in one single Eppendorf tube, according to treatment groups, before snap-freezing. All samples were then stored at -80°C until further processing for measuring siponimod levels by liquid chromatography/tandem mass spectrometry (LC/MS/MS), explained in detail see § “Measurements of siponimod levels in blood/tissues samples of Xenopus tadpoles and mice” below.

OCT and OMR in mice

The measurements of retinal layers were performed using a Spectralis™ HRA+OCT device (Heidelberg Engineering, Germany) under ambient light conditions. The OCT device was equipped with several adaptions for rodents described elsewhere[5] and the scanning protocol was executed as previously described.[6,7] We report the methodology in line with the APOSTEL recommendations.[8] Automated segmentation was carried out by the Heidelberg Eye Explorer™ software version 1.9.10.0 followed by manual correction of an investigator, blinded for the experimental groups. We calculated the thickness of the inner retinal layers (IRL), consisting of the retinal nerve fibre layer (RNFL), ganglion cell layer (GCL) and inner plexiform layer (IPL) as described elsewhere.[6] High-resolution mode was used; only scans with a quality of at least 20 decibels were included.

The visual function analysis was carried out with a testing chamber and the OptoMotry™ software from CerebralMechanics™, Canada. The mice were positioned on a platform in a virtual cylinder with a moving grid and the head movements (tracking) were evaluated by an investigator blinded on the experimental groups. As

a measure for visual acuity, we used the threshold of the highest spatial frequency at 100% contrast. As tracking of the mice is performed exclusively from temporal to nasal direction, left and right eye tracking can be distinguished.

Cuprizone-preparation and randomization of C57Bl/6J mice

Cuprizone (Bis(cyclohexanone) oxaldihydrazone, Sigma-Aldrich, Buchs, Switzerland) was mixed into rodent food pellets (0.2% w/w) by Provimi Kliba AG (Kaiseraugst, Switzerland). Siponimod-loaded pellets (10 mg/kg food) and sham pellets were prepared in-house as previously described.[4] Mice were randomized in 3 study groups (n=7 each), with similar mean baseline bodyweight in each group (20.6 ± 0.3 g; 20.5 ± 0.3 g; 20.8 ± 0.4 g). Mice were regularly monitored via visual inspection and bodyweight. MRI measurements were performed at week 5, 6 and 7 as described below.

Wholemount of Xenopus optic nerve and analysis

Tadpoles were fixed by immersion in 4% paraformaldehyde for 1h at room temperature. Fixed optic nerves were carefully dissected out before being rinsed in PBS (1x) and incubated in methanol-acetone (1:1 v:v) for 10 min at 4 °C, then blocked in 10% normal goat serum (NGS-Thermo-Fisher 50062Z) containing 0.3% Triton X-100® overnight at 4 °C. Optic nerves were incubated in anti-GFP for 3 days at 4 °C in blocking solution (PBS-Triton X-100 0.3%-NGS 1%). Samples were then rinsed in PBS/0.1% Tween-20 and secondary antibody added overnight at 4 °C in blocking solution. After extensive washes in PBS, optic nerves were mounted on glass slide with an anti-fade mounting medium (Vectashield vibrance, Eurobio).

Z-series using the Olympus FV-1200 upright confocal microscope were performed at 0.3 µm increment and maximum orthogonal projection of images was carried out using Fiji software (NIH, Bethesda, Maryland). Serial images were collected and the number of GFP+ cells counted on the whole optic nerve. We used chicken anti-GFP (1:1000, Aves Lab, USA), and goat anti-chicken Alexa Fluor 488, (1:600, InVitrogen) as secondary antibody.

Microglial cells were stained with *Bandeiraea Simplicifolia isolectin* B4 (IB4) on wholemount optic nerves prepared as above. Samples were incubated for 48h at 4°C with Alexa Fluor 594-conjugated IB4 (1:1000, Invitrogen) in PBT 0,1% supplemented with 1mM calcium under gentle shaking, and then washed in blocking solution before exposures to antibodies, as described above. Counting of $IB4^+$ cells per optic nerve was performed on collected serial images obtained on a Nikon A1R-HD25 confocal microscope.

Electron microscopy of Xenopus tadpole optic nerve

Xenopus larvae were fixed in a mixture of 2% paraformaldehyde, 2% glutaraldehyde, in 0.1 M cacodylate buffer pH 7.4 and 0.002% calcium chloride overnight at 4 °C, washed in 0.1 M cacodylate buffer, and postfixed in 1% osmium tetroxide, 1% potassium ferricyanide in 0.1 M cacodylate buffer. After washing in cacodylate buffer and water, larvae were incubated in 2% uranyl acetate aqueous solution at 4 °C overnight. After rinsing twice in water, larvae were dehydrated in increasing concentrations of ethanol, final dehydration was in 100% acetone (twice 10 min each). Samples were infiltrated with 50% acetone 50% Epon for 2 h, followed by pure Epon for 1 h (EMBed 812, Electron Microscopy Sciences Cat 14120). Blocks were then embedded in a new batch of Epon and heated at 56 °C for 48 h. Semi-thin (0.5 µm thick) and ultra-thin (70 nm thick) sections were cut with an ultramicrotome (UC7, Leica Microsystems). Semi-thin sections were stained with 0.5% toluidine

blue in 1% borax buffer and examined under a conventional microscope, objective X63 (Eclipse TiE, Nikon). Ultrathin sections were contrasted with Reynold's lead citrate solution[9] and mounted on 200 mesh copper grids (Electron microscopy science cat# EMS200-Cu).

Wholemounts and histological optic nerve analysis of C57Bl/6J EAEON mice

After 21, 35 or 90 days of EAEON, mice were sacrificed with an overdose of Isofluran (Piramal Critical Care). Ketamine (50 mg/kg, i.p.) was administered for analgesia before cardiac perfusion was performed with cold phosphate-buffered saline (PBS). Eyes were extracted, retinae were isolated and fixed in 4% paraformaldehyde (PFA) for 30 min and wholemounts were stained with anti-Bnr3a (1:200, Santa Cruz Biotechnology, USA).

Optic nerves were snap frozen in liquid nitrogen and stored at -80°C for qPCR or RNA sequencing (RNAseq) or fixed in 4% PFA over night at 4 °C and dehydrated in sucrose solutions with increasing concentrations. After embedding in O.C.T. compound (Sakura Finetek, The Netherlands), longitudinal sections of 5 µm were cut for immunohistological analysis

Iba1 and GFAP staining of the mouse eye cross-sections

At 90 days after immunization, mice were sacrificed with an overdose of Isofluran (Piramal Critical Care). Ketamine (50 mg/kg, i.p.) was administered for analgesia before cardiac perfusion was performed with cold phosphate-buffered saline (PBS). Eyes were isolated and fixated in 4 % PFA over night at 4 °C and dehydrated in ethanol solutions with increasing concentrations. After embedding in paraffin (Paraplast, Leica, Germany), longitudinal sections of 5 µm were cut for immunohistological analysis. Slices of the retinae were incubated with an Iba1 antibody (1:500, Wako chemicals) and Glial fibrillary acidic protein (GFAP) antibody. (1:500, Sigma Aldrich). Cy3 anti-rat (1:500, Millipore) was used as secondary antibody. Fluorescence stained longitudinal optic nerve sections were acquired with a Leica HyD detector attached to a Leica DMi8 confocal microscope (63x objective lens magnification). Microglia (Iba1) and actrocyte (GFAP) number was counted in three eye sections per group in a blinded manner.

Cultivation and treatment of BV2 cells

Microglial BV2 cells were cultivated in DMEM GlutaMAX (Invitrogen Corporation, Carlsbad, CA, USA) containing 10% fetal calf serum (FCS; Lonza, Basel, Switzerland) and 50 U/ml penicillin/streptomycin (Invitrogen, Carlsbad, USA) in T75-flasks at 37°C in a humidified atmosphere of 5% CO2.

For siponimod stimulation experiments, confluent BV2 microglia were washed once with 10 ml PBS, detached by adding 5 ml Trypsin EDTA and a 5 min incubation at 37°C. Afterwards, Trypsin reaction was stopped by adding 10 ml BV2-medium. The cell suspension was collected in a centrifuge tube and spun down at 300 x g for 5 min at 4°C. Supernatant was discarded, the cell pellet resuspended in 5 ml fresh BV2-media and cell viability and numbers were quantified using trypan blue staining.

25.000 cells were seeded into 24-well plates containing 1 ml DMEM glutaMAX (Invitrogen Corporation, Carlsbad, CA, USA) supplemented with 2% FCS (Lonza, Basel, Switzerland)), 50 U/ml penicillin/streptomycin (Invitrogen, Carlsbad, USA). Stimulation was performed 24h after cells were seeded with respective Siponimod or DMSO concentrations. Cells were lysed 24h after stimulation using RLT buffer – β-mercaptoethanol mixture (1:100) according to the manufacturer’s protocol (RNAeasy Mini Kit, Qiagen, Germany). RNA isolation, reverse

transcription, and quantitative real-time PCR was performed as previously described.[10] GAPDH served as endogenous control genes. Primer sequences can be found in eTable 1.

eTable 1. Oligonucleotides used in this study

Gene ID	Gene name	Primer	Sequence (5'-3')
BCAS1	Breast carcinoma-amplified sequence 1	Forward	agaaagctctttaggcacaagg
		Reverse	tggctttgtccgacttgag
CD206	Cluster of differentiation 206	Forward	ccacagcattgaggagtttg
		Reverse	acagctcatcatttggctca
CNPase	2',3'-Cyclic-nucleotide 3'-phosphodiesterase	Forward	cgctggggcagaagaatac
		Reverse	aaggccttgccatacgatct
Galc	Galactocerebrosidase	Forward	ttttgggtgccaagcattat
		Reverse	cggcctttcattccaaatc
Iba1	Ionized calcium-binding adapter molecule 1	Forward	ggatttgcagggaggaaaa
		Reverse	tgggatcatcgaggaattg
MBP	Myelin basic protein	Forward	agccctctgccctctcat
		Reverse	ggtagttctcgtgtgtgagtcct
MD-1	Lymphocyte antigen 86	Forward	attctgaactactcctatccccttt
		Reverse	ggccggcatagtatatctgttct
MOG	Myelin oligodendrocyte glycoprotein	Forward	gaatctccatcggacttttga
		Reverse	ggtccaagaacaggcacaat
NG2	Neuron-glial antigen 2	Forward	cagaggaggtcttggtgaactt
		Reverse	cagaggacatctcgtgctca
PDGFR-α	Platelet-derived growth factor receptor A	Forward	aagacctgggcaagaggaac
		Reverse	gaacctgtctcgatggcact
TMEM 119	Transmembrane Protein 119	Forward	gtcactccatcccagtttcac
		Reverse	ggaccatgttgagctatggaa
Chi3l3/Ym1	Chitinase 3-like-3	Forward	ggtctgaaagacaagaacactgag
		Reverse	gagaccatggcactgaacg
Arg-1	Arginase-1	Forward	cattgtccttaagccgttcc
		Reverse	cagccaacatccccacat
TNF-α	Tumor necrosis factor alpha	Forward	ctgtagcccacgtcgtagc
		Reverse	ttgagatccatgccgttg

Measurements of siponimod levels in blood/tissues samples of Xenopus tadpoles and mice

Xenopus tadpole tissue: Tissues samples from xenopus-tadpoles (brains and bodies) and mouse blood samples were processed for assessing siponimod concentrations using a specific LC/MS/MS bioanalytical method using an Agilent 1290 Infinity UHPLC system coupled to an Agilent 6490 triple quadrupole mass spectrometer, controlled by a MassHunter Workstation software. Briefly, siponimod was extracted by a two-step protein precipitation using a mixture of acetonitrile/methanol/trichloromethane (40/30/30%). Aliquots of 5 µL of the calibration, Quality Control (QC), recovery control and unknown samples were directly injected on an

Agilent Eclipse Plus RRHD C18 2.1x50 mm column, filled with 1.8 µm particles and maintained at 40 °C. Chromatographic separation was performed applying a linear gradient from 20% to 100% B within 1.9 min at a flow rate of 500 µL/min. Solvent A was 0.2% formic acid and solvent B acetonitrile containing 0.2% formic acid. The column flow was guided to the AP-ESI JetStream source of the mass spectrometer run in positive mode (all source parameters were optimized for the siponimod). A structure related compound was used as internal standard. Both siponimod and internal standard were detected as positive ions. For calculation, the siponimod/internal standard ratio of the quantifier ion signals was used applying a polynomial regression with origin included and 1/x weighed regression over 8 calibration points. The regression coefficient was R2 = 0.99990. All calculations and data evaluation were done with MassHunter software and final reporting was done with MS Excel. The accuracy of individually prepared calibration samples between 40 and 80000 pg/sample was better than ±15.0%. The limit of quantification was measured to be 40 pg/sample and the precision, assessed with the help of QC samples was better than 3.1% relative standard deviation. The recovery was found to be 78.9%.

C57Bl/6J mouse blood: To 10 µl of blood samples 20 µl of 1EDTA solution were precipitated with 100 µl acetonitrile and centrifuged at 4 °C and 3000 g for at least 15 min. Approximately 50 µl of supernatant were transferred into a micro¬titer¬ plate and 400 µl of water/acetonitrile (1/1; v/v) was added. An aliquot of each sample was injected into the LC-MS/MS system for analysis as described above.

C57Bl/6J sample preparation brain: After addition of 5 parts of methanol/water (2/8; v/v) to the pre-weighed samples, a homogenization step was performed using a Gentle MACS Dissociator (Miltenyi Biotec GmbH, Bergisch Gladbach, Germany).

To 10 µl of brain homogenate samples 20 µl of a 2blood-EDTA mix were added followed by precipitation with 100 µl acetonitrile and centrifugation at 4 °C and 3000 g for at least 15 min. Approximately 50 µl of supernatant were transferred into a micro-titer¬ plate and 400 µl of water/acetonitrile (1/1; v/v) was added. An aliquot of each sample was injected into the LC-MS/MS system for analysis with a blood calibration curve as described above.

Magnetic resonance imaging (MRI), magnetization transfer ratio (MTR) and T2-weighted signal intensity (T2-WSI)

MRI measurements, with analysis for magnetization transfer ratio (MTR) and T2-weighted signal intensity (T2-WSI), were performed at week-5 (end of the cuprizone-intoxication phase), at week-6 and week-7 (treatment phase). MTR values at week 5 were used to randomize cuprizone-challenged mice into two groups at week 5, before initiation of vehicle or siponimod treatment. Measurements were performed with a Biospec 70/30 spectrometer (Bruker Medical Systems, Ettlingen, Germany) operating at 7 T. The operational software of the scanner was ParaVision 5.1 (Bruker). Images were acquired from anesthetized, spontaneously breathing animals using a mouse brain circularly polarized coil (Bruker, Model 1P T20063 V3; internal diameter 23 mm) for radiofrequency excitation and detection. Neither cardiac nor respiratory triggering was applied. Following a short period of introduction in a box, animals were maintained in anesthesia with 1.5% isoflurane (Abbott, Cham, Switzerland) in oxygen, administered via a nose cone. During MRI signal acquisitions, animals were placed in prone position in a cradle made of Plexiglas, the body temperature was kept at 37 ± 1 °C using a heating pad, and the respiration was monitored. A T2-weighted, two-dimensional multi slice RARE (Rapid Acquisition with Relaxation Enhancement) sequence[11] was used for determining the anatomical orientation

and for evaluating signal intensities. This was followed by a two- dimensional multi slice gradient-recalled FLASH (Fast Low-Angle Shot) acquisition[12] for assessment of MTR. As both sequences had the same anatomical parameters, the choice of the regions-of-interest for evaluations was performed on the RARE images and then transferred to the FLASH images. MRI images were analyzed using the ParaVision software. The parameters of the acquisitions were the following: (a) RARE sequence: effective echo time 80 ms, repetition time 3280 ms, RARE factor 16, 12 averages, field of view 20 × 18 mm, matrix size 213 × 192, pixel size 0.094 × 0.094 mm, slice thickness 0.5 mm, 15 adjacent slices. Hermite pulses of duration/bandwidth 1 ms/5400 Hz and 0.64 ms/5344 Hz were used for radiofrequency excitation and refocusing, respectively. Fat suppression was achieved by a gauss512 pulse of 2.61 ms/1051 Hz duration/bandwidth followed by a 2-ms-long gradient spoiler. The total acquisition time was of 7 min 52.3 s; (b) FLASH sequence: echo time 2.8 ms, repetition time 252.8 ms, 4 averages, field of view 20 × 18 mm, matrix size 213 × 192, pixel size 0.094 × 0.094 mm, slice thickness 0.5 mm, 15 adjacent slices. A hermite pulse of 0.9 ms/ 6000 Hz duration/bandwidth and flip angle 30° was used for radiofrequency excitation. MTR contrast was introduced by a gauss pulse of 15 ms/182.7 Hz duration/bandwidth applied with a radiofrequency peak amplitude of 7.5 µT and an irradiation offset of 2500 Hz. The acquisition was then repeated with the same parameters but without the introduction of the MTR contrast. MTR was then computed using the formula MTR= $(S_0\text{-}S_{MTR})/S_0$ where S_0 and S_{MTR} represent respectively the signal intensities in the FLASH acquisitions without and with the introduction of the MTR contrast. The total acquisition time for both data sets was of 6 min 31.6 s.

Signal intensities in T2-weighted images, T2-WSI and MTR were determined in different brain regions, including the Corpus Callosum (CC) at the level of the commissure of fornix. Data acquisition and analysis were performed by an experimenter blinded to the treatment.

Supplementary Results

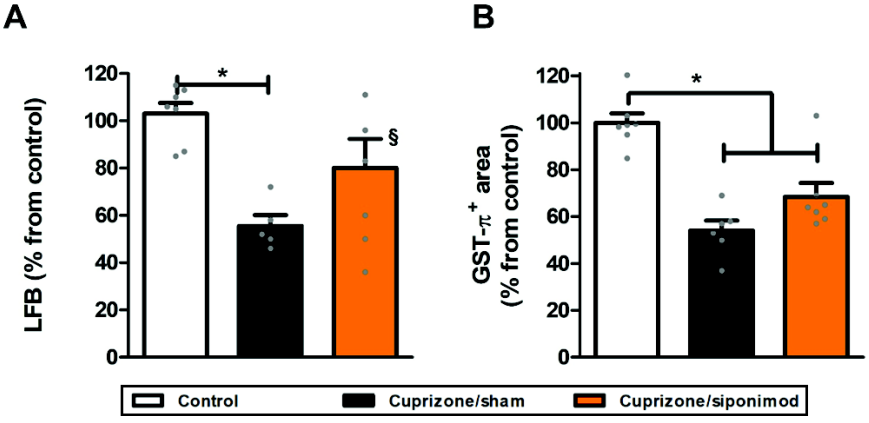

eFigure 1. Siponimod therapy trends to promote remyelination after toxic demyelination by cuprizone. Terminal qIHC for changes vs control in myelin density by LFB staining (and in oligodendrocyte numbers, assessed by GSTπ+ cells (in the CC (of siponimod treated or untreated mice Changes are expressed as meanmean±SEM (7 animals per group), grey dots show individual data points ..* 0 05 by ANOVA with Dunnett's post hoc test §One data points out of axis limits.

Conditional oligodendrocyte ablation and demyelination followed by spontaneous remyelination in the *Mbp:GFP-NTR* Xenopus laevis.

Thanks to the GFP reporter myelin forming oligodendrocytes sending their processes to nearby axons are easily observed in the optic nerve of transgenic *Mbp:GFP-NTR* tadpoles (D0; eFigure 2A). Exposure to metronidazole (MTZ) for 10 days induced a nearly complete ablation of GFP+ oligodendrocytes (D10; eFigure

2A). At the end of the MTZ treatment, animals recovered rapidly as observed already after 3 days (R3; eFigure 2A) and recovery is about complete at 8 days (R8; eFigure 2A). We expected that ablation of GFP+ cells should lead to demyelination. This was indeed the case as shown on transversal semi-thin sections stained with toluidine blue (eFigure 2B, compare D0 and D10) or on ultra-thin sections observed at the electron microscope (EM) (eFigure 2C). Demyelination was quantified on semi-thin sections showing that at the end of MTZ exposure the number of myelinated axons per optic nerve had decreased from 81.7 ± 7.2 down to 25.6 ± 7.3 (mean ± SEM; n= 3 or 4) (eFigure 2D). On EM of D10 samples, there was a drastic rarefaction of myelinated axons, surrounded with myelin debris as well as some axons undergoing demyelination (inset at D10) (eFigure 2C). As soon as exposure to MTZ was interrupted and tadpoles returned to normal water, spontaneous generation of new GFP+ oligodendrocytes (R3 eFigure 2A) and solid remyelination occurred already after only 3 days (R3; eFigure 2B and C). At R8 myelin recovery was complete and the number of myelinated axons was even double compared to D0 (eFigure 2D). This could be explained by the fact that 18 days occurred between the beginning of the experiment (i.e., D0) and R8, which means that tadpoles went from stage 50 to stage 55, i.e., a developmental stage with a higher number of myelinated axons.

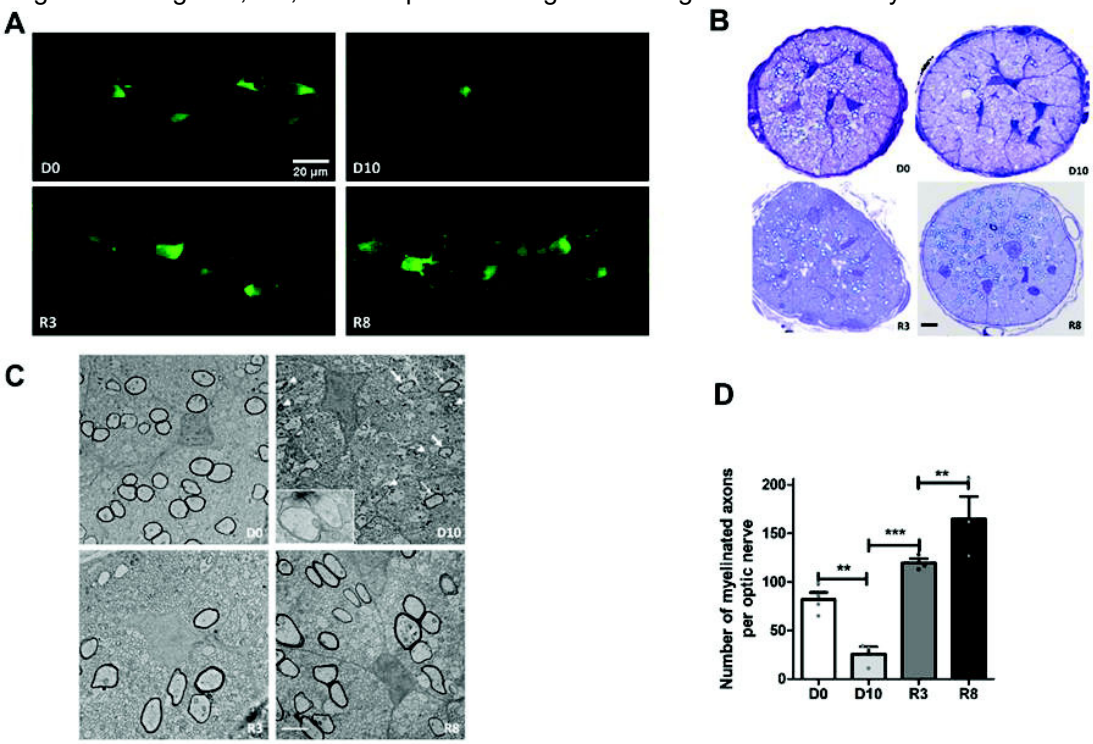

eFigure 2. Confocal and electron microscopic illustration of conditional demyelination and spontaneous remyelination of *Mbp:GFP-NTR* transgenic Xenopus laevis.
(A) *Mbp:GFP-NTR* Xenopus laevis (stage 50 tadpole) before (D0), at the end of metronidazole exposure (D10) and after 3 days (R3) and 8 days (R8) spontaneous recovery, scale bar=20 µm. (B) Semi-thin transversal sections stained with toluidine blue (C) and electron micrographs of transversal ultrathin sections of optic nerve of transgenic *Mbp:GFP-NTR* Xenopus laevis tadpole before (D0), at the end of metronidazole exposure (D10) and after 3 days (R3) and 8 days (R8) of spontaneous recovery, scale bar=2 µm. (D) Quantification of the number of myelinated axons of the semi-thin section between D0 and R8. Data are expressed as mean ± SEM, grey dots show individual data points (n = 3-4 tadpoles per group), with **p<0.01 and ***p<0.001 calculated using an unpaired two-tailed Student's t-test between two groups with a 95% confidence interval.

Pharmacokinetics study in mice shows pellet food is superior over supply via drinking water.

We performed a pharmacokinetics study to evaluate the best-suited formulation for oral administration and to assess the bioavailability and the effect of siponimod on the circulating blood lymphocytes. The treatments via drinking water achieved dose-dependent blood concentrations of siponimod, with 0.1, 0.4 and 0.6 µM ranges obtained with 0.3, 1.5 and 3 mg/kg bodyweight (BW), respectively. These results indicate a poor dose-

proportionality of siponimod blood levels and a large, time-dependent variability (eFigure 3A). A reduction in blood lymphocytes counts of about 20% was observed in all treatment groups (eFigure 3B). Using siponimod-loaded pellets, dose-dependent blood levels of siponimod were observed together with a dose-related reduction in lymphocyte counts. Pellets loaded at 0.03, 0.1 and 0.2 g/kg of food achieved siponimod blood levels within the 1, 4 and 8 µM ranges with good stability over time and low intra- and inter-individual variability (eFigure 3C). In mice fed with pellets loaded with 0.3, 0.1, 0.03, and 0.01 g/kg of food, circulating lymphocytes were reduced by 81, 56, 50 and 39% respectively (eFigure 3D). We therefore chose pellet-derived siponimod treatment at 0.03 and 0.01 g/kg food for all following experiments.

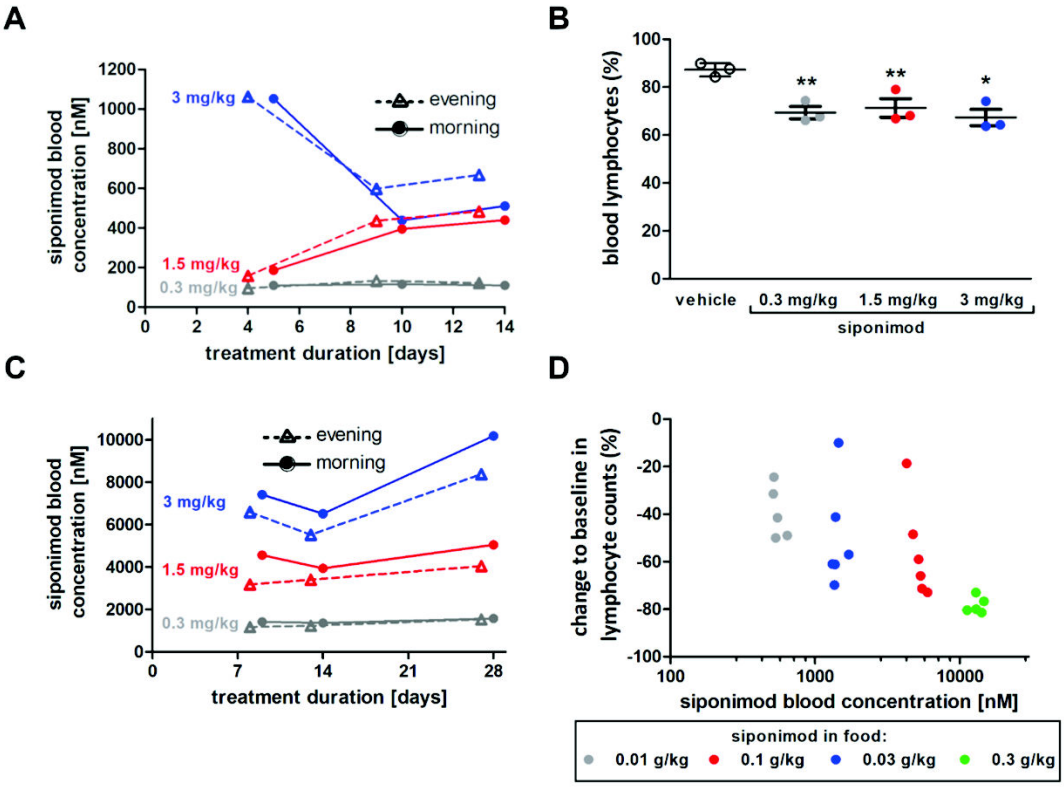

eFigure 3. Longitudinal changes of siponimod blood concentrations and lymphocyte counts in C57Bl/6J mice.
(A) Siponimod blood concentrations over 14 days and (B) lymphocyte counts after 14 days in mice during continuous siponimod treatment via drinking water (n=3 per group, concentrations in mg/kg BW). (C) Siponimod concentration over 28 days and (D) lymphocyte counts in blood after 28 days in mice, fed continuously with siponimod-loaded food pellets (n=5-6 per group, concentrations in g/kg of food). All graphs represent the pooled mean ± SEM with *p<0.05; **p<0.01; ***p<0.001, area under the curve compared by ANOVA with Dunnett's post hoc test for time courses and with *p<0.05, **p<0.01, by ANOVA with Dunnett's post hoc test for scatter plots compared to control untreated mice.

Flow-cytometry analysis of the circulating blood cells and siponimod blood concentrations in EAE animals.

As siponimod alters the lymphocyte profile in the periphery by modulation of S1P1/5 receptors, we investigated the effects on the circulating blood cells of EAEON mice. The $CD3^+$ T-cell population, pregated for lymphocytes (by forward- and side scatter) and $CD45^+$ (leukocyte) cells, was increased in MOG EAE mice 90 days after immunization. The siponimod therapy reduced the circulating $CD3^+$ cells by approximately 90% at 2 and 6 mg/kg BW, regardless when the treatment was started (eFigure 4A and B). Of note, the CD45+/$CD3^{low}$ population was decreased in EAEON mice, which was reversed by siponimod therapy, even showing a higher $CD3^{low}$ population compared to sham untreated mice (eFigure 4A). When the blood samples of the animals were analyzed for siponimod, dose dependent concentrations between 300-400 nM and 700-900 nM were

detected in mice treated at 2 or 6 mg/kg BW, respectively. No significant difference was measurable between the different treatment starting time points, confirming a robust stability of the substance over the time course (eFigure 4C).

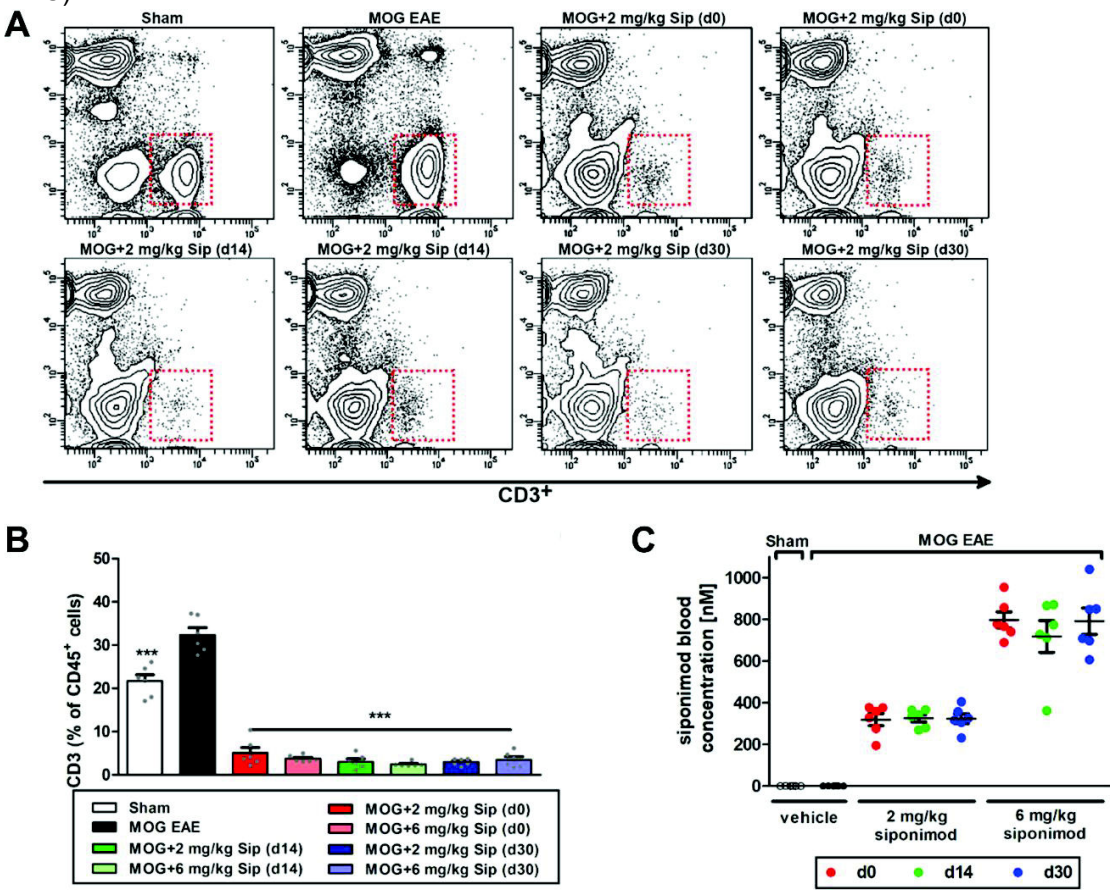

eFigure 4. Siponimod reduces the circulating CD3+ lymphocytes and shows dose dependent blood concentrations.
(A) Leucocytes were isolated 90 days after Sham injection or EAE immunization and directly analyzed. The cell population was gated and percentages of CD45+ (leukocyte) cells were analyzed for CD3+ cells. (B) Quantitative analysis of the flow-cytometry measurement. (C) Siponimod blood concentration 90 days after EAE Immunization. All graphs represent the pooled mean ± SEM, grey dots show individual data points (out of two independent experiments each with n = 6 animals per group) with ***p<0.001, by ANOVA with Dunnett's post hoc test compared to MOG EAE untreated mice.

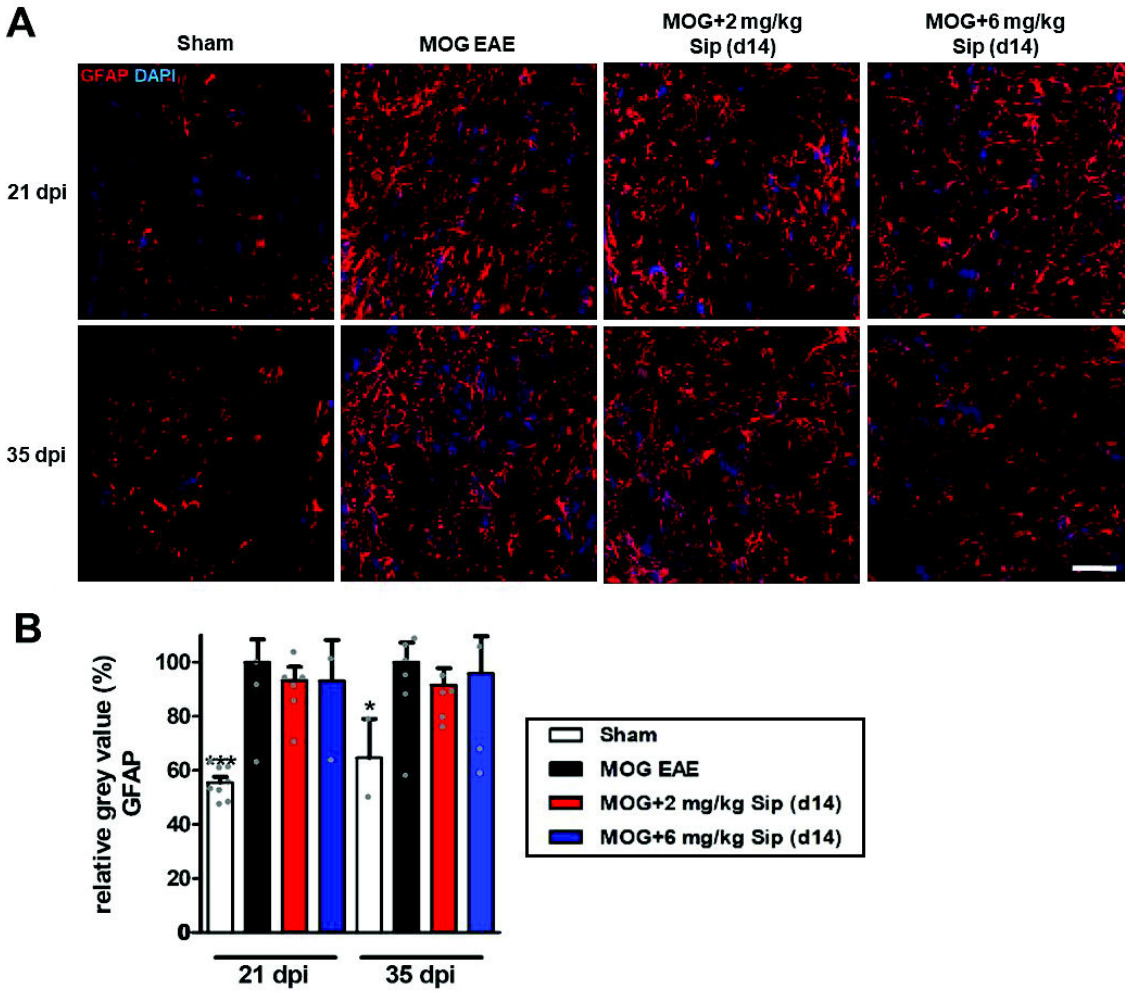

eFigure 5. Histological analysis of GFAP in the optic nerve at 21 and 35 dpi.
Optic nerves were stained for GFAP at 21 and 35 days after MOG 35 55 immunization, scale bar= 50 µm. (B) Quantitative analysis of longitudinal sections of optic nerves of C57Bl/6J mice. One optic nerve per mouse was included for histological examination. Graph represents the pooled mean ± SEM. Grey dots show individual data points (n=6 animals per group), with *p<0.05 ,***p<0.001 by ANOVA with Dunnett's post hoc test compared to untreated MOG EAE

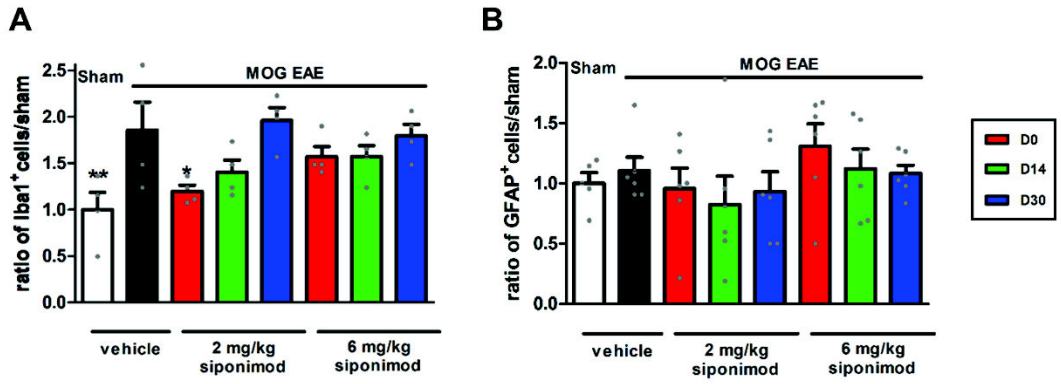

eFigure 6. Histological analysis of retinal cross sections of EAEON mice after siponimod treatment.
(A) Analysis of microglia number (Iba1+) and (B) number of GFAP+ cells (astrocytes and Mueller cells) 90 days after MOG immunization in the retinal cross sections. One eye per mouse was included. All graphs represent the pooled mean ± SEM, (n = 4-6 animals per group) with *p<0.05, **p<0.01 by ANOVA with Dunnett's post hoc test compared to MOG untreated mice.

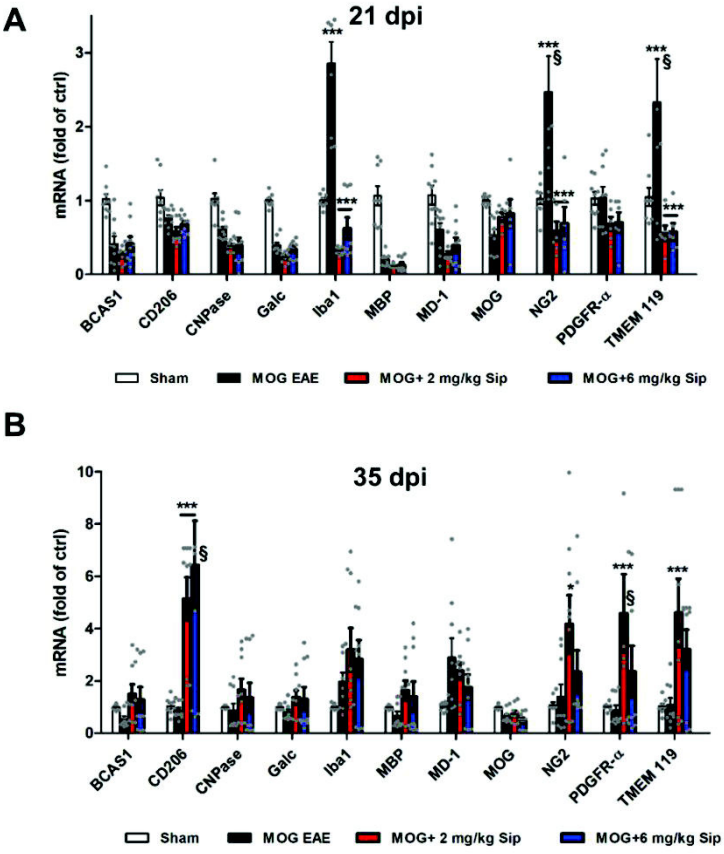

eFigure 7. qPCR analysis of optic nerve of EAEON mice after siponimod treatment.
Therapy was started at day 14 after immunization and tissue was analyzed at (A) 21 dpi and (B) 35 dpi. Graph represent the pooled mean ± SEM. (n=6 out of two separate experiments), with *p<0.05, **p<0.01, ***p<0.001 by ANOVA with Dunnett's post hoc test compared to MOG EAE.§Few data points out of axis limits. BCAS1: Breast carcinoma-amplified sequence 1; CD206: Cluster of differentiation 206; CNPase: 2',3'-Cyclic-nucleotide 3'-phosphodiesterase; Galc: Galactocerebroside C; Iba1: Ionized calcium-binding adapter molecule 1; MBP: Myelin basic protein; MD-1: Lymphocyte antigen 86; MOG: Myelin oligodendrocyte glycoprotein; NG2: Neuron-glial antigen 2, PDGFR-α: platelet-derived growth factor receptor A; TMEM 119: Transmembrane Protein 119

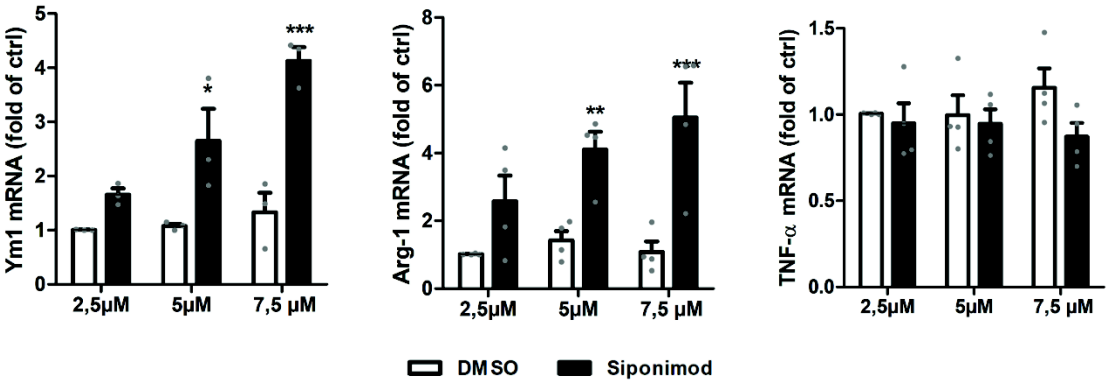

eFigure 8. qPCR analysis of BV2 cells after siponimod treatment.
The mRNA levels of Ym1, Arg-1 and TNF-α after siponimod treatment were analyzed. Graphs represent the pooled mean ± SEM. (n=3), with *p<0.05, **p<0.01, ***p<0.001 by two-way ANOVA with Bonferroni post hoc test compared to the DMSO control.

eTable 2. Top five downregulated genes of optic nerve linked to immune response from EAEON mice after siponimod therapy.

Feature ID	Description	MGI ID	Fold change		P-value[A]	
Siponimod treatment dose			2 mg/kg	6 mg/kg	2 mg/kg	6 mg/kg
Krt1	negative regulation of inflammatory response	96698	-1,532.92	-767.67	3.99E-03	8.81E-03
Muc4	negative regulation of T cell mediated cytotoxicity directed against tumor cell target	2153525	-378.65	-302.62	4.01E-03	8.81E-03
Serpinb3a	protection from natural killer cell mediated cytotoxicity	3573933	-7,252.07	-10,372.70	9.69E-03	9.18E-03
Elf3	inflammatory response	1101781	-51.48	-63.88	2.78E-02	2.57E-02
Pglyrp1	negative regulation of interferon-gamma production	1345092	-8.84	3.75E-02	-6.09	n. s.

[A] P-values (FDR corrected) compared to untreated MOG EAE.

Supplementary References

1. Kaya F, Mannioui A, Chesneau A, et al. Live imaging of targeted cell ablation in Xenopus: A new model to study demyelination and repair. J. Neurosci. 2012;32(37):12885–12895.
2. Mannioui A, Vauzanges Q, Fini JB, et al. The Xenopus tadpole: An in vivo model to screen drugs favoring remyelination. Mult. Scler. 2018;24(11):1421–1432.
3. Nieuwkoop PD, Faber J. Normal Table of Xenopus laevis (Daudin): Garland Publishing Inc, New York 1994.
4. Stringer R, Cordier V, Afatsawo C, et al. Utility of food pellets containing 1-aminobenzotriazole for longer term in vivo inhibition of cytochrome P450 in mice. Xenobiotica 2019;49(1):13–21.
5. Dietrich M, Cruz-Herranz A, Yiu H, et al. Whole-body positional manipulators for ocular imaging of anaesthetised mice and rats: A do-it-yourself guide. BMJ Open Ophthalmol. 2017;1(1):e000008.
6. Dietrich M, Hecker C, Hilla A, et al. Using Optical Coherence Tomography and Optokinetic Response As Structural and Functional Visual System Readouts in Mice and Rats. J. Vis. Exp. 2019;143.
7. Cruz-Herranz A, Dietrich M, Hilla AM, et al. Monitoring retinal changes with optical coherence tomography predicts neuronal loss in experimental autoimmune encephalomyelitis. J. Neuroinflammation 2019;16(1):203.
8. Cruz-Herranz A, Balk LJ, Oberwahrenbrock T, et al. The APOSTEL recommendations for reporting quantitative optical coherence tomography studies. Neurology 2016;86(24):2303–2309.
9. Reynolds ES. The use of lead citrate at high pH as an electron-opaque stain in electron microscopy. J. Cell Biol. 1963;17(1):208–212. Available at: https://pubmed.ncbi.nlm.nih.gov/13986422.
10. Kremer D, Gruchot J, Weyers V, et al. pHERV-W envelope protein fuels microglial cell-dependent damage of myelinated axons in multiple sclerosis. Proc. Natl. Acad. Sci. U. S. A. 2019;116(30):15216–15225.
11. Hennig J, Nauerth A, Friedburg H. RARE imaging: a fast imaging method for clinical MR. Magn. Reson. Med. 1986;3(6):823–833.
12. Haase A, Matthaei D, Hänicke W, Frahm J. Dynamic digital subtraction imaging using fast low-angle shot MR movie sequence. Radiology 1986;160(2):537–541.

4 Summary and Discussion

Neuronal degeneration is the crucial mechanism for the chronically progression of patients suffering from neurological diseases like MS. Despite decades of research, mainly immunomodulatory therapies are available, but no effective treatment to stop neuronal degeneration. MS, ON and potential new treatment options can be investigated in the animal model of EAE, which mimics the key pathological features of MS. Functional and structural changes of the retina and anterior visual pathway due to inflammation, demyelination and neuronal degeneration can be examined, amongst others, by OCT and OMR analysis.

4.1 Comparison of different optomotor response readouts for visual testing in experimental autoimmune encephalomyelitis- opticus neuritis

A former study of our group revealed optimized settings for OCT measurements in EAE mice (Cruz-Herranz et al., 2019). Although OMR was already used for visual testing in rodents, the most reliable and sensitive OMR parameters were not well established. Therefore, in this study, we examined two different readouts for optomotor response analysis in EAE mice and analyzed which protocol delivers the most consistent and reproducible results. Overall, we concluded that spatial frequency measurements are better suited than contrast sensitivity measurements. Since different strains show diverse responses to visual stimuli the study only offers insight limited to the tested C57BL/6J mice under EAE conditions. Mice with an albino background are for example rather poorly suited for OMR analysis. Our experience with albino NOD/ShiLtJ mice (unpublished data) and studies with the albino strains BALB/c and CD1 showed that those mice are unresponsive to OMR stimuli (Abdeljalil et al., 2005; Braha et al., 2021). There are several other methods to test visual function in rodents, such as behavioral tests relying on operant training, where mice are put in mazes or touchscreen-based systems are used. Since training of mice for those tests requires days or weeks and some mice are practically not trainable, those methods are time consuming and inefficient for high throughput studies (Prusky and Douglas, 2008; Storchi et al., 2019). Besides the visual water test and OMR, other techniques using instinctive behaviors are the eye blink response test, visual placing test or the visual cliff test (Leinonen and Tanila, 2018). Some of those have the disadvantage that they only test whether mice can see, but are unable to measure the degree of visual acuity, making them rather weak tools for visual function analysis (Prusky and Douglas, 2008). Although with the visual water test the degree of visual function can be determined it is not

well suited for our interest of MS research, as impairment of motor function would make it impossible for EAE mice to perform the swimming involved in the test (Prusky et al., 2000). Additionally, to OMR analysis, Braha et al. also analyzed spatial resolution of C57BL/6J and BALB/c mice with the electrophysiological vision tests, pattern electroretinogram (PERG) and pattern visual evoked potential (PVEP) (Braha et al., 2021). PERG is a relative noninvasive technique to measure electrical signals from the corneal surface generated by the retina and can be used to test retinal visual acuity, contrast threshold and temporal resolution (Leinonen and Tanila, 2018). PVEP is an rather invasive technique where the activation of the brain upon photic stimulation is recorded either from the skulls surface overlying the primary visual cortex (V1) (by subcutaneous electrodes), from the cortical surface (by screw electrodes) or inside the V1 (by local field potential electrodes) (Leinonen, 2016; Marenna et al., 2019). For PERG and PVEP analysis virtually the same protocols can be used to perform the measurements in humans and mice, making the techniques interesting for translational research. In studies with different strains, it was shown that in C57BL/6J mice PERG, PVEP and OMR acuities are all in the same range, while in BALB/c mice PERG und PVEP acuities were in a similar range and in CD1 mice normal ERG values were measured, but in both strains OMR acuity could not be determined (Abdeljalil et al., 2005; Braha et al., 2021). This implies that OMR may require better visual function to obtain meaningful results than the electrophysiological tests. PERG may allow a more precise localization of the lesion within the visual pathway, as it focusses on retinal activation while PVEP and OMR assess the entire visual pathway (Leinonen, 2016; Mafei and Fiorentini, 1981). The complicated preparations of the electrodes on the animals, make the electrophysiological techniques rather complex and elaborate for some research questions and OMR seems more feasible as functional visual readout.

As mice are nocturnal animals their vision is specialized for motion and contrast detection at night under scotopic conditions. Their retina inhabits a low number (3%) of cone photoreceptors and a high amount of the for scotopic conditions more sensitive rod photoreceptors (Jeon et al., 1998). Since most visual tests are performed under photopic conditions Abdeljalil et al performed a study to examine if OMR is also a reliable tool to analyze visual function under scotopic conditions. Their results show that in general both conditions are suitable to perform OMR analysis although the visual acuity was lower in scotopic than in photopic conditions. This suggests that lightning conditions might be another critical factor that should be kept in mind when performing OMR testing (Abdeljalil et al., 2005).

4.2 Increased remyelination and pro-regenerative microglia under siponimod therapy in mechanistic models

While immunomodulatory therapies are able to effectively prevent or mitigate early disease progression in MS, effective treatments to attenuate or inhibit the degeneration in later disease stages and support remyelination are still needed. In the second study in this thesis, we analyzed the effect of siponimod therapy on remyelination and microglia in several mechanistic models. Siponimod is a selective S1P1/5 modulator approved for treatment of SPMS, showing significant reduction of disability progression, cognitive decline and total brain volume loss in SPMS patients (Kappos et al., 2018). First, to analyze siponimods potential on remyelination, the cuprizone-induced demyelination in mice was used. Those experiments were performed by our cooperation partners at Novartis. In this model demyelination is induced by administration of cuprizone-containing chow, causing the mature oligodendrocytes to die, thereby leading to demyelination in the central nervous system, especially in the corpus callosum (CC) (Matsushima and Morell, 2001). Magnetic resonance imaging of the CC was performed and significant beneficial effects of siponimod treatment on CC integrity was found.

Additionally, in the lab of Boris Zalc, remyelination under Siponimod treatment was evaluated using an inducible model developed in *Xenopus laevis* where siponimod significantly promoted remyelination. As oligodendrocytes are the only cells in the brains of Xenopus and mice that express S1PR5 and the remyelinating potential of siponimod is lost upon deletion of S1PR5 (Jaillard et al., 2005; Mannioui et al., 2018), it was concluded that siponimod may activate the myelination program in oligodendrocytes by activation of S1PR5. Additional to S1PR5, siponimod also works as S1PR1 modulator. S1PR1 is expressed on microglia amongst others and seems upregulated during the reactive state of the cells and neuroinflammation (Roggeri et al., 2020). Since microglia are needed during spontaneous remyelination (Miron et al., 2013), Xenopus larvae were also analyzed regarding IB4+ microglia cells and an increased number of IB4+ microglia was observed, possibly also contributing to the remyelination process.

We performed an EAE study in C57BL/6J mice to analyze the effects of siponimod in a more disease specific model with translational potential. Other groups already showed that prophylactic treatment with siponimod significantly ameliorates EAE in rodents (Gentile et al., 2016; Gergely et al., 2012; Hundehege et al., 2019; Ward et al., 2020). Additionally, we were able to show that siponimod ameliorates EAE when the treatment starts at an early (day 14 after immunization) or late (day 30 after immunization) therapeutic time point,

indicating effects of siponimod beyond immunomodulation. Since translational research is of growing interest, and visual system analysis like OCT and OMR are easy transferable, the visual system of EAE mice was studied. OCT revealed amelioration by prophylactic and early therapeutic treatment, in OMR analysis also late therapeutic treatment preserved the visual function. Histological studies of retinal wholemounts showed that siponimod can protect against retinal ganglion cell loss not only with prophylactic but also with early therapeutic intervention. In addition, the optic nerves of EAE mice were examined histologically and by qPCR. We found reduced microgliosis in optic nerves, which is in line with findings of Gentile er al, who found reduced microgliosis in striatum of EAE mice (Gentile et al., 2016). Because microglia play an important role in EAE and they can have both negative and positive influences on the disease, depending on their reactive state (Plastini et al., 2020), histological studies were extended to proteins related to microglia regulation. By analyzing earlier timepoints than the endpoint (90 days post immunization) of EAE we found significant upregulation of the microglia regenerative markers Ym1 and Arg-1 and a downregulation of the pro-inflammatory cytokine TNF-α. This led to the assumption that the beneficial effect of siponimod was at least partly due to the shift to a pro-myelinating microglia phenotype. To identify other genes that could be regulated by siponimod therapy the optic nerve was analyzed by bulk RNAseq. Results of optic nerves treated with siponimod showed a downregulation of several genes that are associated with inflammation, thereby potentially altering the disease progression. However, a more targeted approach using single cell sequencing of oligodendrocytes or microglia may lead to more accurate and clean cut results. Jordão et al for example identified at least four disease-associated microglia subsets by single cell RNA sequencing of CNS compartments of EAE mice (Jordão et al., 2019). In further studies it could therefore be interesting to examine if those subsets are also found in optic nerve and if siponimod treatment has an influence on their expression level.

In conclusion, siponimod showed increased remyelination in the CC of mice in the cuprizone demyelination model, pro-myelinating potential in the Xenopus model, and potent prophylactic and therapeutic effects in mouse EAEON.

To further analyze the effect of siponimod on microglia, $Cx3cr1^{GFP}$ mice could be used for EAE and Cuprizone experiments. $Cx3cr1^{GFP}$ mice are heterozygous mice of the strain B6.129P2(Cg).$Cx3cr1^{tm1Litt}$/J (Jackson Laboratory, Stock No: 005582), expressing green fluorescent protein (GFP) under control of the endogenous CX3C chemokine receptor 1 (Cx3cr1). In the CNS Cx3cr1 is expressed exclusively by microglia and perivascular

macrophages (Cardona et al., 2006) making those mice a good tool to study the role of those cells. We already developed a semi-automated protocol to analyze microglial activation in EAE mice from the Cx3cr1^{GFP}-strain using confocal scanning laser ophthalmoscopy (Frenger et al., 2021). Others also used the strain to show that innate immune response in EAE takes place in two distinct waves; an early microglial response, associated with subsequent neuroaxonal damage and characterized by a pathogen response profile, and a later response characterized by a more neuroprotective profile (Cruz-Herranz et al., 2021). In addition to EAE experiments Cx3cr1^{GFP}-mice would be interesting to analyze in the demyelinating cuprizone model. Lampron et al examined remyelination in Cx3cr1-deficient (Cx3cr1$^{-/-}$) mice using the cuprizone model and showed that although inflammatory responses are not affected by the knockout, there is a clear deficit in microglial phagocytic processes leading to persistence of myelin debris (Lampron et al., 2015). For future studies it would, therefore, be very interesting to utilize Cx3cr1^{GFP}-mice for studies with siponimod and to longitudinally study the impact of siponimod on microglia cell populations *in vivo*.

5 Publications as co-author

Ingwersen, J., De Santi, L., Wingerath, B., Graf, J., Koop, B., Schneider, R., **Hecker, C.**, Schröter, F., Bayer, M., Engelke, A. D., Dietrich, M., Albrecht, P., Hartung, H. P., Annunziata, P., Aktas, O., & Prozorovski, T. (2018). ***Nimodipine confers clinical improvement in two models of experimental autoimmune encephalomyelitis.*** Journal of neurochemistry, 10.1111/jnc.14324. Advance online publication.

Contribution:

- Execution and analysis of the following methods: histological analysis (25%), Western blot analysis (50%)

Dietrich, M., **Hecker, C.**, Hilla, A., Cruz-Herranz, A., Hartung, H. P., Fischer, D., Green, A., & Albrecht, P. (2019). ***Using Optical Coherence Tomography and Optokinetic Response as Structural and Functional Visual System Readouts in Mice and Rats.*** Journal of visualized experiments: JoVE, (143), 10.3791/58571.

Contribution:

- Execution and analysis of the following methods: OCT measurements (75%), OMR measurements (75%)
- Writing of the Manuscript (20%)

Cruz-Herranz, A., Dietrich, M., Hilla, A. M., Yiu, H. H., Levin, M. H., **Hecker, C.**, Issberner, A., Hallenberger, A., Cordano, C., Lehmann-Horn, K., Balk, L. J., Aktas, O., Ingwersen, J., von Gall, C., Hartung, H. P., Zamvil, S. S., Fischer, D., Albrecht, P., & Green, A. J. (2019). ***Monitoring retinal changes with optical coherence tomography predicts neuronal loss in experimental autoimmune encephalomyelitis.*** Journal of neuroinflammation, 16(1), 203.

Contribution:

- Execution, analysis, and statistics of the following methods: OCT measurements (75 %), OMR measurements (75 %), MOG EAE in C57Bl/6J mice (50 %), histology of optic nerve (40 %) and retina (30 %), electron microscopy of optic nerve (30 %)

Dietrich, M., Koska, V., **Hecker, C.**, Göttle, P., Hilla, A. M., Heskamp, A., Lepka, K., Issberner, A., Hallenberger, A., Baksmeier, C., Steckel, J., Balk, L., Knier, B., Korn, T., Havla, J., Martínez-Lapiscina, E. H., Solà-Valls, N., Manogaran, P., Olbert, E. D., Schippling, S., … Albrecht, P. (2020***). Protective effects of 4-aminopyridine in experimental optic neuritis and multiple sclerosis.*** Brain: a journal of neurology, 143(4), 1127–1142.

Contribution:

- Execution, analysis, and statistics of the following methods: MOG EAE in C57Bl/6J mice (50 %), OCT measurements of mice (75 %), OMR measurements (75 %), preparation and cultivation of mouse oligodendrocyte precursor cells (100%), NFAT translocation assay with mouse oligodendrocyte precursor cells (100%)

Dietrich, M., **Hecker, C.**, Nasiri, M., Samsam, S., Issberner, A., Kohne, Z., Hartung, H. P., & Albrecht, P. (2021). ***Neuroprotective Properties of Dimethyl Fumarate Measured by Optical Coherence Tomography in Non-inflammatory Animal Models.*** Frontiers in neurology, 11, 601628.

Contribution:

- Execution, analysis, and statistics of the following methods: Li-PRL in C57Bl/6J mice (75 %), OCT measurements of mice (100%)

Frenger, M. J., **Hecker, C.**, Sindi, M., Issberner, A., Hartung, H. P., Meuth, S. G., Dietrich, M., & Albrecht, P. (2021). **Semi-Automated Live Tracking of Microglial Activation in CX3CR1GFP Mice During Experimental Autoimmune Encephalomyelitis by Confocal Scanning Laser Ophthalmoscopy.** Frontiers in immunology, 12, 761776.

Contribution:

- Execution, analysis, and statistics of the following methods: OCT measurements (50%), MOG EAE in C57Bl/6J mice (50%)

Fleischer, V., Gonzalez-Escamilla, G., Ciolac, D., Albrecht, P., Küry, P., Gruchot, J., Dietrich, M., **Hecker, C.**, Müntefering, T., Bock, S., Oshaghi, M., Radetz, A., Cerina, M., Krämer, J., Wachsmuth, L., Faber, C., Lassmann, H., Ruck, T., Meuth, S. G., Muthuraman, M., … Groppa, S. (2021). ***Translational value of choroid plexus imaging for tracking neuroinflammation in mice and humans.*** Proceedings of the National Academy of Sciences of the United States of America, 118(36), e2025000118.

Contribution:

- Execution of the following methods: MOG EAE in C57Bl/6J mice (30%)

6 Bibliography

Abdeljalil, J., Hamid, M., Abdel-Mouttalib, O., Stéphane, R., Raymond, R., Johan, A., José, S., Pierre, C., Serge, P., 2005. The optomotor response: a robust first-line visual screening method for mice. Vision Res. 45, 1439–1446. https://doi.org/10.1016/j.visres.2004.12.015

Aktas, O., Albrecht, P., Hartung, H.-P., 2016. Optic neuritis as a phase 2 paradigm for neuroprotection therapies of multiple sclerosis: update on current trials and perspectives. Curr. Opin. Neurol. 29, 199–204. https://doi.org/10.1097/WCO.0000000000000327

Albrecht, P., Fröhlich, R., Hartung, H.-P., Kieseier, B.C., Methner, A., 2007. Optical coherence tomography measures axonal loss in multiple sclerosis independently of optic neuritis. J. Neurol. 254, 1595–1596. https://doi.org/10.1007/s00415-007-0538-3

Albrecht, P., Ringelstein, M., Müller, A.K., Keser, N., Dietlein, T., Lappas, A., Foerster, A., Hartung, H.P., Aktas, O., Methner, A., 2012. Degeneration of retinal layers in multiple sclerosis subtypes quantified by optical coherence tomography. Mult. Scler. Houndmills Basingstoke Engl. 18, 1422–1429. https://doi.org/10.1177/1352458512439237

Al-Salama, Z.T., 2019. Siponimod: First Global Approval. Drugs 79, 1009–1015. https://doi.org/10.1007/s40265-019-01140-x

Beitz, J.M., 2014. Parkinson's disease: a review. Front. Biosci. Sch. Ed. 6, 65–74. https://doi.org/10.2741/s415

Bennett, J.L., 2019. Optic Neuritis. Contin. Minneap. Minn 25, 1236–1264. https://doi.org/10.1212/CON.0000000000000768

Bjelobaba, I., Begovic-Kupresanin, V., Pekovic, S., Lavrnja, I., 2018. Animal models of multiple sclerosis: Focus on experimental autoimmune encephalomyelitis. J. Neurosci. Res. 96, 1021–1042. https://doi.org/10.1002/jnr.24224

Braha, M., Porciatti, V., Chou, T.-H., 2021. Retinal and cortical visual acuity in a common inbred albino mouse. PloS One 16, e0242394. https://doi.org/10.1371/journal.pone.0242394

Brinkmann, V., Billich, A., Baumruker, T., Heining, P., Schmouder, R., Francis, G., Aradhye, S., Burtin, P., 2010. Fingolimod (FTY720): discovery and development of an oral drug to treat multiple sclerosis. Nat. Rev. Drug Discov. 9, 883–897. https://doi.org/10.1038/nrd3248

Bryan, A.M., Del Poeta, M., 2018. Sphingosine-1-phosphate receptors and innate immunity. Cell. Microbiol. 20, e12836. https://doi.org/10.1111/cmi.12836

Cardona, A.E., Pioro, E.P., Sasse, M.E., Kostenko, V., Cardona, S.M., Dijkstra, I.M., Huang, D., Kidd, G., Dombrowski, S., Dutta, R., Lee, J.-C., Cook, D.N., Jung, S., Lira, S.A., Littman, D.R., Ransohoff, R.M., 2006. Control of microglial neurotoxicity by the fractalkine receptor. Nat. Neurosci. 9, 917–924. https://doi.org/10.1038/nn1715

Cartier, A., Hla, T., 2019. Sphingosine 1-phosphate: Lipid signaling in pathology and therapy. Science 366. https://doi.org/10.1126/science.aar5551

Chiba, K., 2005. FTY720, a new class of immunomodulator, inhibits lymphocyte egress from secondary lymphoid tissues and thymus by agonistic activity at sphingosine 1-phosphate receptors. Pharmacol. Ther. 108, 308–319. https://doi.org/10.1016/j.pharmthera.2005.05.002

Constantinescu, C.S., Farooqi, N., O'Brien, K., Gran, B., 2011. Experimental autoimmune encephalomyelitis (EAE) as a model for multiple sclerosis (MS). Br. J. Pharmacol. 164, 1079–1106. https://doi.org/10.1111/j.1476-5381.2011.01302.x

Constantinescu, C.S., Hilliard, B.A., 2005. Adjuvants in EAE, in: Lavi, E., Constantinescu, C.S. (Eds.), Experimental Models of Multiple Sclerosis. Springer US, Boston, MA, pp. 73–84. https://doi.org/10.1007/0-387-25518-4_5

Cruz-Herranz, A., Dietrich, M., Hilla, A.M., Yiu, H.H., Levin, M.H., Hecker, C., Issberner, A., Hallenberger, A., Cordano, C., Lehmann-Horn, K., Balk, L.J., Aktas, O., Ingwersen, J., von Gall, C., Hartung, H.-P., Zamvil, S.S., Fischer, D., Albrecht, P., Green, A.J., 2019. Monitoring retinal changes with optical coherence tomography predicts neuronal loss in experimental autoimmune encephalomyelitis. J. Neuroinflammation 16, 203. https://doi.org/10.1186/s12974-019-1583-4

Cruz-Herranz, A., Oertel, F.C., Kim, K., Cantó, E., Timmons, G., Sin, J.H., Devereux, M., Baker, N., Michel, B., Schubert, R.D., Rani, L., Cordano, C., Baranzini, S.E., Green, A.J., 2021. Distinctive waves of innate immune response in the retina in experimental autoimmune encephalomyelitis. JCI Insight 6, 149228. https://doi.org/10.1172/jci.insight.149228

Dietrich, M., Aktas, O., Hartung, H.-P., Albrecht, P., 2019a. Assessing the anterior visual pathway in optic neuritis: recent experimental and clinical aspects. Curr. Opin. Neurol. 32, 346–357. https://doi.org/10.1097/WCO.0000000000000675

Dietrich, M., Cruz-Herranz, A., Yiu, H., Aktas, O., Brandt, A.U., Hartung, H.-P., Green, A., Albrecht, P., 2017. Whole-body positional manipulators for ocular imaging of anaesthetised mice and rats: a do-it-yourself guide. BMJ Open Ophthalmol. 1, e000008. https://doi.org/10.1136/bmjophth-2016-000008

Dietrich, M., Hecker, C., Hilla, A., Cruz-Herranz, A., Hartung, H.-P., Fischer, D., Green, A., Albrecht, P., 2019b. Using Optical Coherence Tomography and Optokinetic Response As Structural and Functional Visual System Readouts in Mice and Rats. J. Vis. Exp. JoVE. https://doi.org/10.3791/58571

Dietrich, M., Helling, N., Hilla, A., Heskamp, A., Issberner, A., Hildebrandt, T., Kohne, Z., Küry, P., Berndt, C., Aktas, O., Fischer, D., Hartung, H.-P., Albrecht, P., 2018. Early alpha-lipoic acid therapy protects from degeneration of the inner retinal layers and vision loss in an experimental autoimmune encephalomyelitis-optic neuritis model. J. Neuroinflammation 15, 71. https://doi.org/10.1186/s12974-018-1111-y

Dobson, R., Giovannoni, G., 2019. Multiple sclerosis - a review. Eur. J. Neurol. 26, 27–40. https://doi.org/10.1111/ene.13819

Douglas, R.M., Alam, N.M., Silver, B.D., McGill, T.J., Tschetter, W.W., Prusky, G.T., 2005. Independent visual threshold measurements in the two eyes of freely moving rats and mice using a virtual-reality optokinetic system. Vis. Neurosci. 22, 677–684. https://doi.org/10.1017/S0952523805225166

Fischer, M.D., Huber, G., Beck, S.C., Tanimoto, N., Muehlfriedel, R., Fahl, E., Grimm, C., Wenzel, A., Remé, C.E., van de Pavert, S.A., Wijnholds, J., Pacal, M., Bremner, R., Seeliger, M.W., 2009. Noninvasive, in vivo assessment of mouse retinal structure using optical coherence tomography. PloS One 4, e7507. https://doi.org/10.1371/journal.pone.0007507

Fisher, J.B., Jacobs, D.A., Markowitz, C.E., Galetta, S.L., Volpe, N.J., Nano-Schiavi, M.L., Baier, M.L., Frohman, E.M., Winslow, H., Frohman, T.C., Calabresi, P.A., Maguire, M.G., Cutter, G.R., Balcer, L.J., 2006. Relation of visual function to retinal nerve fiber layer thickness in multiple sclerosis. Ophthalmology 113, 324–332. https://doi.org/10.1016/j.ophtha.2005.10.040

Frenger, M.J., Hecker, C., Sindi, M., Issberner, A., Hartung, H.-P., Meuth, S.G., Dietrich, M., Albrecht, P., 2021. Semi-Automated Live Tracking of Microglial Activation in CX3CR1GFP Mice During Experimental Autoimmune Encephalomyelitis by Confocal Scanning Laser Ophthalmoscopy. Front. Immunol. 12, 761776. https://doi.org/10.3389/fimmu.2021.761776

Frohman, E.M., Fujimoto, J.G., Frohman, T.C., Calabresi, P.A., Cutter, G., Balcer, L.J., 2008. Optical coherence tomography: a window into the mechanisms of multiple sclerosis. Nat. Clin. Pract. Neurol. 4, 664–675. https://doi.org/10.1038/ncpneuro0950

Galetta, K.M., Calabresi, P.A., Frohman, E.M., Balcer, L.J., 2011. Optical coherence tomography (OCT): imaging the visual pathway as a model for neurodegeneration. Neurother. J. Am. Soc. Exp. Neurother. 8, 117–132. https://doi.org/10.1007/s13311-010-0005-1

Gentile, A., Musella, A., Bullitta, S., Fresegna, D., De Vito, F., Fantozzi, R., Piras, E., Gargano, F., Borsellino, G., Battistini, L., Schubart, A., Mandolesi, G., Centonze, D., 2016. Siponimod (BAF312) prevents synaptic neurodegeneration in experimental multiple sclerosis. J. Neuroinflammation 13, 207. https://doi.org/10.1186/s12974-016-0686-4

Gergely, P., Nuesslein-Hildesheim, B., Guerini, D., Brinkmann, V., Traebert, M., Bruns, C., Pan, S., Gray, N.S., Hinterding, K., Cooke, N.G., Groenewegen, A., Vitaliti, A., Sing, T., Luttringer, O., Yang, J., Gardin, A., Wang, N., Crumb, W.J., Saltzman, M., Rosenberg, M., Wallström, E., 2012. The selective sphingosine 1-phosphate receptor modulator BAF312 redirects lymphocyte distribution and has species-specific effects on heart rate. Br. J. Pharmacol. 167, 1035–1047. https://doi.org/10.1111/j.1476-5381.2012.02061.x

Graf, J., Mares, J., Barnett, M., Aktas, O., Albrecht, P., Zamvil, S.S., Hartung, H.-P., 2021. Targeting B Cells to Modify MS, NMOSD, and MOGAD: Part 1. Neurol. Neuroimmunol. Neuroinflammation 8, e918. https://doi.org/10.1212/NXI.0000000000000918

Hauser, S.L., Bar-Or, A., Cohen, J.A., Comi, G., Correale, J., Coyle, P.K., Cross, A.H., de Seze, J., Leppert, D., Montalban, X., Selmaj, K., Wiendl, H., Kerloeguen, C., Willi, R., Li, B., Kakarieka, A., Tomic, D., Goodyear, A., Pingili, R., Häring, D.A., Ramanathan, K., Merschhemke, M., Kappos, L., ASCLEPIOS I and ASCLEPIOS II Trial Groups, 2020. Ofatumumab versus Teriflunomide in Multiple Sclerosis. N. Engl. J. Med. 383, 546–557. https://doi.org/10.1056/NEJMoa1917246

Huang, D., Swanson, E.A., Lin, C.P., Schuman, J.S., Stinson, W.G., Chang, W., Hee, M.R., Flotte, T., Gregory, K., Puliafito, C.A., 1991. Optical coherence tomography. Science 254, 1178–1181. https://doi.org/10.1126/science.1957169

Hundehege, P., Cerina, M., Eichler, S., Thomas, C., Herrmann, A.M., Göbel, K., Müntefering, T., Fernandez-Orth, J., Bock, S., Narayanan, V., Budde, T., Speckmann, E.-J., Wiendl, H., Schubart, A., Ruck, T., Meuth, S.G., 2019. The next-generation sphingosine-1 receptor modulator BAF312 (siponimod) improves cortical network functionality in focal autoimmune encephalomyelitis. Neural Regen. Res. 14, 1950–1960. https://doi.org/10.4103/1673-5374.259622

Jaillard, C., Harrison, S., Stankoff, B., Aigrot, M.S., Calver, A.R., Duddy, G., Walsh, F.S., Pangalos, M.N., Arimura, N., Kaibuchi, K., Zalc, B., Lubetzki, C., 2005. Edg8/S1P5: an oligodendroglial receptor with dual function on process retraction and cell survival. J. Neurosci. Off. J. Soc. Neurosci. 25, 1459–1469. https://doi.org/10.1523/JNEUROSCI.4645-04.2005

Jeon, C.J., Strettoi, E., Masland, R.H., 1998. The major cell populations of the mouse retina. J. Neurosci. Off. J. Soc. Neurosci. 18, 8936–8946.

Jordão, M.J.C., Sankowski, R., Brendecke, S.M., Sagar, null, Locatelli, G., Tai, Y.-H., Tay, T.L., Schramm, E., Armbruster, S., Hagemeyer, N., Groß, O., Mai, D., Çiçek, Ö., Falk, T., Kerschensteiner, M., Grün, D., Prinz, M., 2019. Single-cell profiling identifies myeloid cell subsets with distinct fates during neuroinflammation. Science 363, eaat7554. https://doi.org/10.1126/science.aat7554

Kappos, L., Bar-Or, A., Cree, B.A.C., Fox, R.J., Giovannoni, G., Gold, R., Vermersch, P., Arnold, D.L., Arnould, S., Scherz, T., Wolf, C., Wallström, E., Dahlke, F., EXPAND Clinical Investigators, 2018. Siponimod versus placebo in secondary progressive multiple sclerosis (EXPAND): a double-blind, randomised, phase 3 study. Lancet Lond. Engl. 391, 1263–1273. https://doi.org/10.1016/S0140-6736(18)30475-6

Kretschmer, F., Tariq, M., Chatila, W., Wu, B., Badea, T.C., 2017. Comparison of optomotor and optokinetic reflexes in mice. J. Neurophysiol. 118, 300–316. https://doi.org/10.1152/jn.00055.2017

Lampron, A., Larochelle, A., Laflamme, N., Préfontaine, P., Plante, M.-M., Sánchez, M.G., Yong, V.W., Stys, P.K., Tremblay, M.-È., Rivest, S., 2015. Inefficient clearance of myelin debris by microglia impairs remyelinating processes. J. Exp. Med. 212, 481–495. https://doi.org/10.1084/jem.20141656

Lassmann, H., Bradl, M., 2017. Multiple sclerosis: experimental models and reality. Acta Neuropathol. (Berl.) 133, 223–244. https://doi.org/10.1007/s00401-016-1631-4

Leinonen, H., 2016. Electrophysiology of visual pathways as a screening tool for neurodegenerative diseases: evidence from mouse disease models.

Leinonen, H., Tanila, H., 2018. Vision in laboratory rodents-Tools to measure it and implications for behavioral research. Behav. Brain Res. 352, 172–182. https://doi.org/10.1016/j.bbr.2017.07.040

London, A., Benhar, I., Schwartz, M., 2013. The retina as a window to the brain-from eye research to CNS disorders. Nat. Rev. Neurol. 9, 44–53. https://doi.org/10.1038/nrneurol.2012.227

Lublin, F.D., 2014. New multiple sclerosis phenotypic classification. Eur. Neurol. 72 Suppl 1, 1–5. https://doi.org/10.1159/000367614

Mafei, L., Fiorentini, A., 1981. Electroretinographic responses to alternating gratings before and after section of the optic nerve. Science 211, 953–955. https://doi.org/10.1126/science.7466369

Mannioui, A., Vauzanges, Q., Fini, J.B., Henriet, E., Sekizar, S., Azoyan, L., Thomas, J.L., Pasquier, D.D., Giovannangeli, C., Demeneix, B., Lubetzki, C., Zalc, B., 2018. The Xenopus tadpole: An in vivo model to screen drugs favoring remyelination. Mult. Scler. Houndmills Basingstoke Engl. 24, 1421–1432. https://doi.org/10.1177/1352458517721355

Marenna, S., Castoldi, V., d'Isa, R., Marco, C., Comi, G., Leocani, L., 2019. Semi-invasive and non-invasive recording of visual evoked potentials in mice. Doc. Ophthalmol. Adv. Ophthalmol. 138, 169–179. https://doi.org/10.1007/s10633-019-09680-z

Martin, E., Aigrot, M.-S., Grenningloh, R., Stankoff, B., Lubetzki, C., Boschert, U., Zalc, B., 2020. Bruton's Tyrosine Kinase Inhibition Promotes Myelin Repair. Brain Plast. Amst. Neth. 5, 123–133. https://doi.org/10.3233/BPL-200100

Martínez-Morales, J.C., Romero-Ávila, M.T., Reyes-Cruz, G., García-Sáinz, J.A., 2018. S1P1 receptor phosphorylation, internalization, and interaction with Rab proteins: effects of sphingosine 1-phosphate, FTY720-P, phorbol esters, and paroxetine. Biosci. Rep. 38. https://doi.org/10.1042/BSR20181612

Matsushima, G.K., Morell, P., 2001. The neurotoxicant, cuprizone, as a model to study demyelination and remyelination in the central nervous system. Brain Pathol. Zurich Switz. 11, 107–116. https://doi.org/10.1111/j.1750-3639.2001.tb00385.x

Miron, V.E., Boyd, A., Zhao, J.-W., Yuen, T.J., Ruckh, J.M., Shadrach, J.L., van Wijngaarden, P., Wagers, A.J., Williams, A., Franklin, R.J.M., Ffrench-Constant, C., 2013. M2 microglia and macrophages drive oligodendrocyte differentiation during CNS remyelination. Nat. Neurosci. 16, 1211–1218. https://doi.org/10.1038/nn.3469

Montalban, X., Arnold, D.L., Weber, M.S., Staikov, I., Piasecka-Stryczynska, K., Willmer, J., Martin, E.C., Dangond, F., Syed, S., Wolinsky, J.S., Evobrutinib Phase 2 Study

Group, 2019. Placebo-Controlled Trial of an Oral BTK Inhibitor in Multiple Sclerosis. N. Engl. J. Med. 380, 2406–2417. https://doi.org/10.1056/NEJMoa1901981
Montalban, X., Hauser, S.L., Kappos, L., Arnold, D.L., Bar-Or, A., Comi, G., de Seze, J., Giovannoni, G., Hartung, H.-P., Hemmer, B., Lublin, F., Rammohan, K.W., Selmaj, K., Traboulsee, A., Sauter, A., Masterman, D., Fontoura, P., Belachew, S., Garren, H., Mairon, N., Chin, P., Wolinsky, J.S., ORATORIO Clinical Investigators, 2017. Ocrelizumab versus Placebo in Primary Progressive Multiple Sclerosis. N. Engl. J. Med. 376, 209–220. https://doi.org/10.1056/NEJMoa1606468
Olsson, T., Barcellos, L.F., Alfredsson, L., 2017. Interactions between genetic, lifestyle and environmental risk factors for multiple sclerosis. Nat. Rev. Neurol. 13, 25–36. https://doi.org/10.1038/nrneurol.2016.187
O'Sullivan, C., Schubart, A., Mir, A.K., Dev, K.K., 2016. The dual S1PR1/S1PR5 drug BAF312 (Siponimod) attenuates demyelination in organotypic slice cultures. J. Neuroinflammation 13, 31. https://doi.org/10.1186/s12974-016-0494-x
Piguet, F., Alves, S., Cartier, N., 2017. Clinical Gene Therapy for Neurodegenerative Diseases: Past, Present, and Future. Hum. Gene Ther. 28, 988–1003. https://doi.org/10.1089/hum.2017.160
Plastini, M.J., Desu, H.L., Brambilla, R., 2020. Dynamic Responses of Microglia in Animal Models of Multiple Sclerosis. Front. Cell. Neurosci. 14, 269. https://doi.org/10.3389/fncel.2020.00269
Prineas, J.W., Kwon, E.E., Cho, E.S., Sharer, L.R., Barnett, M.H., Oleszak, E.L., Hoffman, B., Morgan, B.P., 2001. Immunopathology of secondary-progressive multiple sclerosis. Ann. Neurol. 50, 646–657. https://doi.org/10.1002/ana.1255
Proia, R.L., Hla, T., 2015. Emerging biology of sphingosine-1-phosphate: its role in pathogenesis and therapy. J. Clin. Invest. 125, 1379–1387. https://doi.org/10.1172/JCI76369
Prusky, G.T., Alam, N.M., Beekman, S., Douglas, R.M., 2004. Rapid quantification of adult and developing mouse spatial vision using a virtual optomotor system. Invest. Ophthalmol. Vis. Sci. 45, 4611–4616. https://doi.org/10.1167/iovs.04-0541
Prusky, G.T., Douglas, R.M., 2008. Measuring vision in the awake behaving mouse. Eye Retina Vis. Syst. Mouse Chalupa LM Williams RL Eds Pp 107–117.
Prusky, G.T., West, P.W., Douglas, R.M., 2000. Behavioral assessment of visual acuity in mice and rats. Vision Res. 40, 2201–2209. https://doi.org/10.1016/s0042-6989(00)00081-x
Roggeri, A., Schepers, M., Tiane, A., Rombaut, B., van Veggel, L., Hellings, N., Prickaerts, J., Pittaluga, A., Vanmierlo, T., 2020. Sphingosine-1-Phosphate Receptor Modulators and Oligodendroglial Cells: Beyond Immunomodulation. Int. J. Mol. Sci. 21. https://doi.org/10.3390/ijms21207537
Schwartz, M., Belkin, M., Yoles, E., Solomon, A., 1996. Potential treatment modalities for glaucomatous neuropathy: neuroprotection and neuroregeneration. J. Glaucoma 5, 427–432.
Shao, H., Huang, Z., Sun, S.L., Kaplan, H.J., Sun, D., 2004. Myelin/oligodendrocyte glycoprotein-specific T-cells induce severe optic neuritis in the C57BL/6 mouse. Invest. Ophthalmol. Vis. Sci. 45, 4060–4065. https://doi.org/10.1167/iovs.04-0554
Soria Lopez, J.A., González, H.M., Léger, G.C., 2019. Alzheimer's disease. Handb. Clin. Neurol. 167, 231–255. https://doi.org/10.1016/B978-0-12-804766-8.00013-3
Storchi, R., Rodgers, J., Gracey, M., Martial, F.P., Wynne, J., Ryan, S., Twining, C.J., Cootes, T.F., Killick, R., Lucas, R.J., 2019. Measuring vision using innate behaviours in mice with intact and impaired retina function. Sci. Rep. 9, 10396. https://doi.org/10.1038/s41598-019-46836-y

Thompson, A.J., Baranzini, S.E., Geurts, J., Hemmer, B., Ciccarelli, O., 2018. Multiple sclerosis. Lancet Lond. Engl. 391, 1622–1636. https://doi.org/10.1016/S0140-6736(18)30481-1

Toosy, A.T., Mason, D.F., Miller, D.H., 2014. Optic neuritis. Lancet Neurol. 13, 83–99. https://doi.org/10.1016/S1474-4422(13)70259-X

Ward, L.A., Lee, D.S., Sharma, A., Wang, A., Naouar, I., Ma, X.I., Pikor, N., Nuesslein-Hildesheim, B., Ramaglia, V., Gommerman, J.L., 2020. Siponimod therapy implicates Th17 cells in a preclinical model of subpial cortical injury. JCI Insight 5, 132522. https://doi.org/10.1172/jci.insight.132522

Wingerchuk, D.M., Carter, J.L., 2014. Multiple sclerosis: current and emerging disease-modifying therapies and treatment strategies. Mayo Clin. Proc. 89, 225–240. https://doi.org/10.1016/j.mayocp.2013.11.002

7 Appendix

7.1 List of abbreviations

BBB	Blood-brain barrier
BTK	Bruton tyrosine kinase
CC	Corpus callosum
CFA	Complete Freund´s Adjuvant
CNS	Central nervous system
Cx3cr1	CX3C chemokine receptor 1
EAE	Experimental autoimmune encephalomyelitis
GFP	Green fluorescent protein
MOG	Myelin oligodendrocyte glycoprotein
MS	Multiple Sclerosis
OCT	Optical coherence tomography
OMR	Optomotor response
ON	Optic neuritis
PERG	Pattern electroretinogram
PPMS	Primary progressive MS
PVEP	Pattern visual evoked potential
RGC	Retinal ganglion cell
S1P	Sphingosine-1-phosphate
S1PR1/5	Sphingosine-1-phosphate receptor 1/5
SPMS	Secondary progressive MS
V1	Primary visual cortex

7.2 Acknowledgement/Danksagung

Zuallererst möchte ich mich gerne bei Philipp Albrecht bedanken, der mir die Möglichkeit gegeben hat diese Arbeit unter seiner Leitung anzufertigen. Vielen Dank für kompetente Gespräche, viele spannende Projekte, Optimismus, konstruktive Kritik und Lob. Ich habe in der Zeit vieles gelernt und bin dankbar für die angenehme Arbeitsatmosphäre.

Des Weiteren möchte ich mich gerne bei Frau Prof. Dr. von Gall bedanken, die als Mentorin für diese Arbeit zur Verfügung steht. Vielen Dank für das Lesen und Begutachten dieser Arbeit!

Ebenso möchte ich mich gerne bei allen Mitgliedern der Arbeitsgruppe bedanken, vor allem bei Michael Dietrich und Andrea Issberner, die mir immer mit Rat und Tat beiseite standen und die gemeinsame Zeit im Life Science Center sehr angenehm gestaltet haben. Ich habe sehr gerne mit euch zusammengearbeitet! Ein weiterer Dank geht an die Kollegen der anderen Arbeitsgruppen am LSC sowie die Kooperationspartner und Koautoren.

Besonders möchte ich mich bei Christina Wilms bedanken, die mit mir gemeinsam Studium, Abschlussarbeiten und schließlich auch die Promotion mit allen Höhen und Tiefen durchgestanden hat. Vielen Dank dafür, ohne dich hätte das alles bestimmt nicht so gut funktioniert. Ich freue mich, dass du inzwischen auch offiziell Teil der Familie bist und wünsche euch für die Zukunft nur das Beste!

Last but not least, möchte ich mich noch bei meiner Familie und meinen Freunden bedanken. Danke, dass ihr immer an meiner Seite seid und mich unterstützt. Es ist schön zu wissen, dass ihr, selbst wenn man sich mal nicht sehen kann, nur eine Nachricht oder einen Anruf entfernt seid. Ich habe euch lieb!

7.3 Declaration/ Erklärung

Ich versichere an Eides Statt, dass die Dissertation von mir selbständig und ohne unzulässige fremde Hilfe unter der Beachtung der “Grundsätze zur Sicherung guter wissenschaftlicher Praxis an der Heinrich-Heine-Universität Düsseldorf” erstellt worden ist. Diese Dissertation wurde bei keiner anderen Institution in dieser oder ähnlicher Form eingereicht und es wurden keine erfolglosen Promotionsversuche unternommen.

Düsseldorf, den 18.01.2022

_____

Christina Hecker